Integrated Optics
- Sensors, Sensing Structures and Methods
20th Jubilee IOS 2026

PROGRAMME
and
ABSTRACTS

Organizers of IOS 2026

Photonics Society of Poland

Committee of Electronics
and Telecommunications
of the Polish Academy of Sciences

Association of Polish Electrical Engineers
Polish Committee of Optoelectronics

Upper Silesian Division
of Polish Acoustical Society

in cooperation with
Department of Optoelectronics
at Silesian University of Technology

9th to 13th February 2026
Hotel "META"
Szczyrk - Beskidy Mountains, POLAND

https://ios-conference.pl

Dear Participants of 20th Jubilee Conference:
INTEGRATED OPTICS - Sensors, Sensing Structures and Methods, IOS 2026

Organizers welcome All of You very cordially in Szczyrk in the beautiful scenery of the Beskidy Mountains.

Honorary auspices of the Conference are taken over by Professor Wiesław Woliński – Full Member of the Polish Academy of Sciences.

We wish all Participants of the Conference IOS 2026 plenty of scientific satisfactions and many professional and social impressions.

Organizers

President of the Conference:	Prof. T. Pustelny
Secretary of the Conference:	Dr S. Drewniak
Treasurer of the Conference:	Dr hab. K. Barczak
Members:	Dr A. Olszewska
	Dr hab. P. Struk
	Dr B. Pustelny
	Dr M. Procek
	Dr P. Kałużyński

Scientific Committee

prof. Wiesław Woliński (The Honorary Patronage on the IOS)
prof. Tadeusz Pustelny (Chairman of the Scientific Committee)
prof. Krzysztof Abramski
dr hab. Kamil Barczak
prof. Zbigniew Bielecki
prof. Ryszard Buczyński
prof. Daumantas Ciplis (Lituania)
prof. Carlos Dominguez (Spain)
prof. Dominik Dorosz
prof. Jan Dorosz
prof. Wojciech Gawlik
prof. Christophe Gorecki (France)
prof. Jiri Homola (Czech Republic)
dr Jan Z. Jakubczyk (Canada)
prof. Zdzisław Jankiewicz
prof. Leszek R. Jaroszewicz
prof. Mirosław Karpierz
prof. Małgorzata Kujawińska
prof. Paul Lambeck (Netherland)
prof. Wiesław Królikowski (Australia)
prof. Erwin Maciak
prof. Piotr Martyniuk
prof. Paweł Mergo
prof. Zygmunt Mierczyk
prof. Risto Myllyla (Finland)
dr Aneta Olszewska
prof. Szymon Pustelny
prof. Ryszard Piramidowicz
dr Bartosz Sakowicz
prof. Giancarlo Rigini (Italy)
prof. Antoni Rogalski
prof. Ryszard Romaniuk
prof. Wolfgang Sohler (Germany)
prof. Przemysław Struk
prof. Małgorzata Szczerska
prof. Jan Szmidt
prof. Tomasz Szoplik
prof. Hugo Thienpoint (Belgium)
prof. Wacław Urbańczyk
prof. Tomasz R. Woliński

PROGRAMME
of the IOS 2026 Conference -
Integrated Optics - Sensors, Sensing Structures and Methods
Szczyrk, 09 – 13 February 2026

09.02.2026 Monday	
13.30	***Lunch***
15.00 – 15.10	**OPENING CEREMONY of the Conferences** **20th IOS 2026** **53rd WSEAV** **54th WSWQA**
15.10 – 16.20	**20th Integrated Optics - Sensors, Sensing Structures and Methods** **JUBILEE SESSION**
15.10 – 15.30	**20th JUBILEE of IOS Conference** T. PUSTELNY
15.30 – 16.00	***Plenary Lecture*** **Stabilization of laser frequency to atomic reference** W. GAWLIK
16.00 – 16.20	***Plenary Lecture*** **Tunable photonic fiber microstructures enhanced with gold nanoparticle-doped liquid crystals** T. R. WOLIŃSKI
16.20 – 17.00	***Coffee Break***
17.00 – 18.00	**Jubilee of the 50th Anniversary of Scientific Research and Academic Activity and the 75th Birthday of Professor Tadeusz Pustelny (*in Polish*)**
18.00 – 19.00	***Supper***
19.15 – 20.00	**MUSIC GLANCE**

10.02.2026 Tuesday	
7.00 – 10.00	***Breakfast***
13.00	***Lunch***
14.30 – 16.30	**Quantum Optics**
14.30 – 15.00	***Plenary Lecture*** **Searching for dark matter with optical sensor** S. PUSTELNY
15.00 – 15.20	**Spectroscopy of higher order states and valence band discontinuity in Ga-free type-II superlattices** M. RYGAŁA, J. ZANON, A. BADER, T. SMOŁKA, F. HARTMANN, S. HÖFLING, M. FLATTÉ, M. MOTYKA
15.20 – 15.40	**Beyond DBRs: high-contrast gratings, plasma enhanced DBRs, and fano resonance for mid-infrared VCSELs** T. SMOŁKA, A. SZERLING, B. ŚCIANA, S. HÖFLING, T. CZYSZANOWSKI, M. MOTYKA
15.40 – 16.30	**Optical Medicine**
15.40 – 16.10	***Plenary Lecture*** **Spatio-temporal optical coherence tomography - new method for in vivo structural and functional imaging** M. WOJTKOWSKI
16.10 – 16.30	**Optimization of MOEMS probe scanning properties for 3D optical coherence tomography imaging** P. STRUK, S. BARGIEL, M. JÓZWIK, B. MIRECKI, C. GORECKI, H. XIE, M. WOJTKOWSKI
16.30 – 17.00	***Coffee Break***

17.00 – 18.40	**Technologies for Photonics**
17.00 – 17.30	***Plenary Lecture*** **Polish perspective on integrated photonics - technologies, applications and challenges** R. PIRAMIDOWICZ, S. STOPIŃSKI, K. ANDERS, A. JUSZA, M. LELIT, A. POŁATYŃSKI, P. WIŚNIEWSKI, M. SŁOWIKOWSKI, M. JUCHNIEWICZ, J. OLSZEWSKI, R. CIECHAŃSKI, K. MACHAŁOWSKI, J. JUREŃCZYK, K. PIERŚCIŃSKI, D. PIERŚCIŃSKA
17.30 – 17.45	**FoSMoWater – development of an innovative photonic water resource monitoring system** J. KALWAS, A. JUSZA, F. ŁABAJ, P. MARCHEWKA, W. CHARAZIŃSKI, M. ABRAMOWICZ, K. MACHAŁOWSKI, R. STOJEK, R. CIECHAŃSKI, M. LIEBERT, T. MIRECKI, M. WINCEL, N. MATWIEJ, E. KIEDRZYŃSKA, A. BIENIEK-KACZOREK, Ł. KOZŁOWSKI, P. BORTNOWSKI, K. ANDERS, S. STOPIŃSKI, R. PIRAMIDOWICZ
17.45 – 18.00	**Thin-film technologies in optoelectronics** N. JĘDRZEJCZAK
18.00 – 18.15	**Temperature sensing with nickel-coated optical fibers** D. LIS
18.15 – 18.30	**Modern fusion splicing methods for multi-core and hollow-core optical fibers** M. ROMANOWICZ
18.30 – 18.40	**PhotonHub PHACTORY – A Gateway to Photonics Innovation** R. PIRAMIDOWICZ, A. SIEMION
20.00	***Festive Supper***

11.02.2026 Wednesday	
7.00 – 10.00	***Breakfast***
13.00	***Lunch***
14.30 – 16.30	**Photonic Sensors**
14.30 – 14.50	***Plenary Lecture*** **Sub-terahertz telecommunication link with a 3D-printed lens system for beam shaping** P. ZAGRAJEK, M. MACIEJEWSKI, P. KOMOROWSKI, N. PAŁKA
14.50 – 15.10	***Plenary Lecture*** **Topologically-protected edge states for intensity-selective and sensing THz photonic devices** B. JANASZEK, T. ŚMIAROWSKI, A. TYSZKA-ZAWADZKA, I. TSUKERMAN, P. SZCZEPAŃSKI
15.10 – 15.30	**Numerical and experimental exploration of nanostructured five-mode optical fibers** B. PAŁUBA, M. NAPIÓRKOWSKI, R. KASZTELANIC, R. BUCZYŃSKI
15.30 – 15.50	**An all-fiber optofluidic dye laser based on hollow-core anti-resonant fiber** K. RECHCIŃSKA, M. WINKOWSKI, M. ADAMOWSKA, B. PAŁUBA, A. FILIPKOWSKI, D. PYSZ, R. BUCZYŃSKI, T. STACEWICZ
15.50 – 16.10	**Design constraints for mid-infrared sensing waveguides: interaction-limited perspective** J. OLSZEWSKI, A. ŚLIPEK, T. MARTYNKIEN, K. ANDERS, S. STOPIŃSKI, R. PIRAMIDOWICZ
16.10 – 16.30	**How photonics and spectroscopy can shed light on cancer?** D. KAŁUŻYŃSKA
16.30 – 17.00	***Coffee Break***

17.00-19.00	**Optoelectronic Structures**
17.00 – 17.20	***Plenary Lecture*** **Variable wavelength interferometry for measuring phase and step-like objects-metrological aspects** D. LITWIN, K. RADZIAK, A. CZYŻEWSKI, J. GALAS, T. KRYSZCZYŃSKI, N. BŁOCKI, R. SZUMSKI, J. NIEDZIELA
17.20 – 17.40	**FDTD simulation for miniaturization** D. GOLEMBOWSKI
17.40 – 18.00	**When parts per trillion matter: emergent interfacial charge mediation governing ultra-low NO_2 sensing in hybrid nanocomposites** P. KAŁUŻYŃSKI, M. PROCEK, A. STOLARCZYK, K. GŁOSZ, T. JAROSZ
18.00 – 18.20	**Novel van der Waals materials for polarization-sensitive photodetection** A. TOŁŁOCZKO, J. ZIEMBICKI, S. J. ZELEWSKI, M. GRODZICKI, M. ROSMUS, R. KUDRAWIEC
18.20 – 18.40	**Practical implementation of Beer-Lambert law in gas detection** K. JABŁOŃSKI, T. KORZEC, M. BAŁECKI
18.40 – 19.00	**Biophotonic fiber optic measurement system as an advanced medical diagnostic tool increasing the safety of urological procedures** M. SŁADEK, M. PROCEK, K. BARCZAK, E. MACIAK
19.00 – 20.00	***Supper***
20:00 – 21.00	***Poster Session***

12.02.2026 Thursday	
7.00 – 10.00	***Breakfast***
13.00	***Lunch***
14:30 – 16:30	**Sensors and Nanostructures Systems**
14.30 – 15.00	***Plenary Lecture*** **Fabrication and applications of nonlinear soft-glass fiber and nanostructured elements based on 3D-printed preforms** P. WIENCŁAW, P. GOŁĘBIEWSKI, G. STĘPNIEWSKI, B. PAŁUBA, P. SOCHA, A. FILIPKOWSKI, D. PYSZ, W. LIU, A. BURGS, R. KASZTELANIC, R. BUCZYŃSKI
15.00 – 15.20	**A process design kit for mid-infrared photonic pilot line** S. STOPIŃSKI, J. OLSZEWSKI, A. ŚLIPEK, A. POŁATYŃSKI, M. LELIT, K. ANDERS, R. PIRAMIDOWICZ
15.20 – 15.40	**Use of broadband propagation in the metrology of waveguide layers** K. GUT
15.40 – 16.00	**Design of a mid-IR suspended GaAs/AlGaAs membrane waveguide gas sensor for CO_2 detection** A. ŚLIPEK, J. OLSZEWSKI, T. MARTYNKIEN, J. JUREŃCZYK, K. ANDERS, S. STOPIŃSKI, R. PIRAMIDOWICZ
16.00 – 16.15	**Optical transducers for measuring small temperature changes in aqueous environment caused by the absorption of high-energy radiation** C. TYSZKIEWICZ, M. ZIĘBA, P. KARASIŃSKI, Z. OPILSKI, K. BARCZAK
16.15 – 16.30	**DAS / DVS – principle of operation and overview of applications** J. KORYCIŃSKI
16.30 – 17.00	***Coffee Break***

17.00 – 18.00	**Application of Optoelectronic and Photonic Systems**
17.00 – 17.20	**Concept to produce next-generation low-loss ZBLAN optical fibers** A. DJORDJEVIC, T. UNGER, S. LEYER, H. A. MOSER, R. BUCZYŃSKI
17.20 – 17.40	**Design and performance of a home-built scalable projection micro-stereolithography platform** M. PTASZEK, S. ERTMAN
17.40 – 18.00	**Silica fiber with Nd:YAG nanocrystals: the influence of fiber drawing process on structure and emission properties of Nd^{3+} cations** M. ADAMOWSKA, B. PAŁUBA, A. MARKOVSKYI, L. SOJKA, A. FILIPKOWSKI, K. OLSZEWSKA, D. PYSZ, T. RUNKA, G. STĘPNIEWSKI, R. KASZTELANIC, S. SUJECKI, R. BUCZYŃSKI
18.30 – 19.30	***Supper***
19.30	**The State of Polish Photonics - Roundtable Discussion**

13.02.2026 Friday	
7.00 – 10.00	***Breakfast***

POSTER SESSION

1. A. BIENIEK-KACZOREK, S. STOPIŃSKI, A. JUSZA, K. ANDERS, R. PIRAMIDOWICZ
   Heart rate variability monitoring using a photonic integrated interrogator of fiber Bragg grating sensors

2. M. JANIK, T. GABLER, M. FICEK, M. PIERPAOLI, M. SAWCZAK, P. NIEDZIAŁKOWSKI, M. KOBA, M. ŚMIETANA, R. BOGDANOWICZ
   Nanodiamond- decorated optical fiber interferometric probes: dual-domain sensing with improved sensitivity

3. P. BORTNOWSKI, J. KALWAS, M. KOZUBAL, A. JUSZA, F. ŁABAJ, E. KIEDRZYŃSKA, R. PIRAMIDOWICZ
   Photonic system for monitoring nitrite and nitrate content in water

4. L. CZYŻEWSKA, M. GRZESIAK, M. GIL-KOWALCZYK, P. MERGO
   Correlation between deposition conditions and structural properties of palladium thin films

5. Ł. DREWNIAK, S. DREWNIAK, I. ZIMOCH, E. ŁOBOS-MOYSA, E. MACIAK
   Analysis of matrix effects on nitrate determination in surface waters using UVC spectrophotometry

6. S. DREWNIAK, Ł. DREWNIAK, E. MACIAK, K. MORACZEWSKA-MAJKU, W. K. NOCOŃ
   Modeling the effect of UV degradation on the raman spectrum of microplastics detected in drinking water

7. M. FICEK, A. OLEJNIK, M. BABIŃSKA, B. STONIO, M. PIERPAOLI, R. BOGDANOWICZ
   Periodically patterned boron-doped diamond nanostructures for enhanced opto-electrochemical transduction

8. M. GIL-KOWALCZYK, M. JÓZWICKI, P. MERGO
   Dye-assisted optical detection of trace water in diesel fuel

9. M. JUCHNIEWICZ, M. SŁOWIKOWSKI, D. DRECKA, M. JAROSIK
   Lithography methods in the fabrication of integrated photonics circuits

10. P. KAŁUŻYŃSKI, D. KAŁUŻYŃSKA
    When light prints more than objects: nanoscale waste, environmental persistence, and cytotoxicity in photopolymer manufacturing

11. Ł. KOZŁOWSKI, A. BIENIEK-KACZOREK, P. BORTNOWSKI, M. ZIELIŃSKA, K. ANDERS, S. STOPIŃSKI, A. JUSZA, J. KALWAS, R. PIRAMIDOWICZ
    Raman spectroscopy in water quality monitoring

12. K. KUCHTA, A. RYBCZYŃSKI, J. M. KUBICA
    Application of N,N-dimethyl-4,4’-azodianiline (DMADA) for UV fiber optic sensing

13. J. GALAS, D. LITWIN, K. RADZIAK, W. MAŁKIŃSKI, M. KARLIŃSKI, N. BŁOCKI, A. CZYŻEWSKI, M. KOZIELSKI, D. FOSZCZ, D. SARAMAK, S. LENCZOWSKI, E. KASIŃSKA-PILUT, R. PĘPKOWSKI, Ł. PAŁKA
    Flotation froth pattern recognition for the ore content estimation

14. J. ŁYŻWA, M. MIKA, M. ŻUK, B. SUDOŁ, A. AUGUSTOWSKI, A. OLSZEWSKI, K. BARCZAK, A. OLSZEWSKA
    Analysis of FBG signal transmission in optical fiber telecom networks

15. M. MAKARA, M. GRZESIAK, K. POTURAJ, G. WÓJCIK, A. WALEWSKI, M. JÓZWICKI, L. CZYŻEWSKA , Ł. BEDNARSKI, P. MERGO
    Use of low bend-loss optical fibers in distributed sensing

16. Z. OPILSKI, K. WERESZCZYŃSKI, A. DANIŁOWICZ, K. CYRAN, E. MACIAK
    Photonic two-qubit system for generation and characterization of entangled photon states

17. A. ORFINGER, B. FORTUNA, M. WINKOWSKI, P. KOMOROWSKI, R. KASZTELANIC, N. PAŁKA, R. BUCZYŃSKI
    3D-Printed structured optical fibers for terahertz applications

18. A. PAŹDZIOR, J. RZECZKOWSKI, P. MACIĄG, P. MERGO
    Applicability of commercial optical backscatter reflectometer LUNA OBR4600 to strain measurements in presence of vibrations

19. M. PROCEK, K. GŁOSZ, Ł. DREWNIAK, Z. OPILSKI, E. MACIAK, A. STOLARCZYK, T. JAROSZ
    From electronic sensor to optical sensor – concept of SPR hydrogen sensor based on polycarbazole receptor film

20. P. RADEK, K. BARCZAK, A. OLSZEWSKA
    PVDF as a potential receptor layer in fiber-optic sensors for PFAS pollutant detection

21. P. RADEK, K. RATAJCZYK, T. WOJNAR, K. PAŁUCHOWSKI, A. GARGULA, N. TOMANEK, E. MACIAK
    Optical fiber-based remote powering (POF) and sensing platform for environmental applications

22. A. PALECZEK , D. GROCHALA, S. KARCZ, M. KOCOŃ, A. RYDOSZ
    Advances in sensor technologies and machine learning for glyphosate and pesticide detection in water

23. M. KAŁUŻA, K. POGORZELEC, A. SIEMION, P. LESIAK
    Holographically designed diffractive optical element for efficient coupling into multicore fibers

24. M. SŁOWIKOWSKI, D. DRECKA, M. JUCHNIEWICZ, B. STONIO, M. GOLAS, M. FILIPIAK, M. LELIT, M. JAROSIK
    Passive integrated photonics platform for VIS spectral range

25. S.CIĘSZCZYK, D. HARASIM, K. SKORUPSKI, P.PANAS, J.KLIMEK
    Influence of polarization on demodulation methods for determining the SRI value for a single TFBG and an orthogonal grating system

26. P. WERAJTIS, J. IMAŃSKA, W. GILICKI, W. KOZŁOWSKI, V. STAWINOGA, K. BARCZAK, A. OLSZEWSKA
    Multi-pass measurement chamber as a tool for detection of trace substances in aqueous environment

27. K. WIDAJ, T. SMOŁKA, M. RYGAŁA, W. GŁOWADZKA, K. BOGDANOWICZ, M. EKIELSKI, M. MARCINIAK, M. ZADURA, P. ŚPIEWAK, M. KOWALSKI, M. GĘBSKI, M. KAŁUŻA, O. SADOWSKI, M. WASIAK, A. SZERLING, T. CZYSZANOWSKI, M. MOTYKA
    High contrast gratings for highly transparent and conductive mid-infrared electrodes

28. M. ZIĘBA, C. TYSZKIEWICZ, P. KARASIŃSKI
    Photocatalytic properties of oxide films obtained by the sol-gel method

SPONSORS:

INTERLAB®

INSTRUMENTY BADAWCZE & POMIAROWE

TECHNOLUTIONS

MONO SPEKTRA

ATEST GAZ

Niezawodne i Innowacyjne Systemy Bezpieczeństwa Gazowego

LECTURES

Stabilization of Laser Frequency to Atomic Reference

W. GAWLIK

Department of Photonics, Institute of Physics, Jagiellonian University,
ul. Prof. Łojasiewicza 11, 30-348 Kraków, Poland

e-mail address: gawlik@uj.edu.pl

In this talk, I will present the basics of laser frequency stabilization to stable atomic standards. I will discuss why stabilization is necessary and its main limitations. The topic of this presentation will focus on stabilizing diode lasers for high-resolution spectroscopy applications. I will present an example design of a stable diode laser. Methods for correlating laser radiation frequencies with reference standard frequencies, as well as modern methods using optical frequency combs, will be discussed in detail.

Tunable Photonic Fiber Microstructures Enhanced with Gold Nanoparticle-Doped Liquid Crystals

T. R. WOLIŃSKI

Warsaw University of Technology, Faculty of Physics, Koszykowa 75, 00-662 Warszawa, Poland

Selected tunable photonic microstructures doped with liquid crystal materials are discussed. Starting from early works on liquid crystalline-core optical fibers, the latest achievements in the field of liquid crystal-infiltrated photonic crystal fibers modified by using gold nanoparticles are presented. It has been demonstrated that photonic liquid crystal microstructures doped with gold nanoparticles can significantly lower threshold voltage and speed up response times due to the interaction of gold nanoparticles with liquid crystals, providing promising optical materials for realizing electro-optical modulation and switching, as well as tunable filter applications and sensing capabilities. Additionally, dual-refractive-index photonic crystal waveguides, fabricated by combining two-photon polymerization with a specially modified 3D nano printing system, enable reciprocal transitions between index-guiding and photonic bandgap-guiding.

FOS versus FOG – Remarks on Similarities and Differences

L. R. JAROSZEWICZ [1,2]

[1] Institute of Applied Physics/Military University of Technology, gen. S. Kaliskiego 2, 00-908 Warsaw, Poland
[2] ELPROMA Elektronika Sp. z o.o., Duńska 2A, 05-152 Czosnów, Poland

e-mail address: jarosz@wat.edu.pl

This year marks 42 years of my experience in the technical application of the fibre-optic loop interferometer, incorrectly referred to as the Sagnac interferometer (Fig. 1).

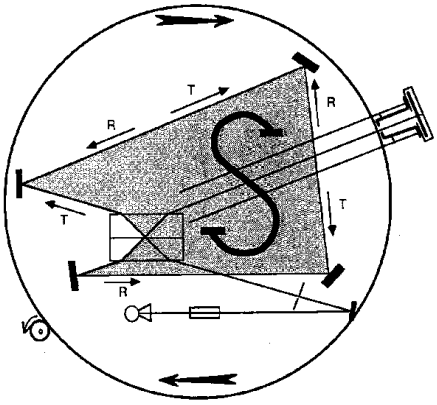

Fig. 1. Scheme of Sagnac experiment from 1913 [1].

This system has been used mainly in the construction of FOGs – Fibre-Optic Gyroscopes, especially for INS – Inertial Navigation System [2], (see Fig. 2), although other implementations, including as a FOSs - Fiber-Optic rotational Seismographs [3], are also intriguing.

Fig. 2. General view of FOG and INS prepared by iXblue.

While, from a physical point of view, both systems are clearly defined and understandable – we know how they should work and, what is more, they operate on the same principles (see Fig. 3) – their technical implementation poses many problems, resulting finally in completely different technical solutions.
I can repeat this again maliciously – a physicist knows how something should work, while a technical physicist knows how it works, and that is a huge difference.

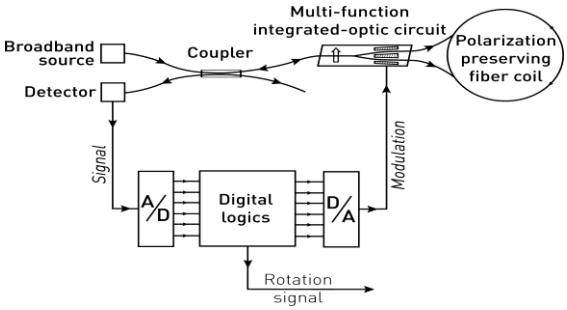

Fig. 3. Scheme of the Sagnac interferometer in so-called minimum configuration with closed-loop operation [2].

In 1988, I defended my doctoral thesis by constructing a model of an FOG, and although over the next few years I received an award for this solution at exhibitions in Nuremberg [4] and almost sold it to Iraq, I moved away from its practical implementation for many years, focusing mainly on an FORSs, bringing it today to the implementation stage (Fig. 4). I am currently returning to work on implementing FOG in INS. It seems to me that after 40 years, I know a little more about the differences and similarities between these systems, which is the subject of my immodest presentation.

Fig. 4. FOSREM as FOS By ELPROMA Elektronika.

Acknowledgments: This work was supported by grants from PARP – FENG.01.01-IP.02-1714/23 as well as COP Łódź - FELD-01.02-IP.02-0019/24.

References:

[1] Post, Review of Modern Physics, 39, (1967)
[2] H.C. Lefevre, The Fiber-Optic Gyroscope, 3rd Ed, Artech House, 2022
[3] Kurzych et. al., Sensors, 24, 7003 (2024)
[4] Bronze Medal at IENA'94, Nuremberg (1994)

Searching for Dark Matter with Optical Sensors

S. PUSTELNY [1,2]

[1] Institute of Physics, Jagiellonian University in Kraków, Łojasiewicza 11, 30-348, Kraków, Poland
[2] Department of Physics, Harvard University, 17 Oxford St., 02138, Cambridge, MA, USA

e-mail address: pustelny@uj.edu.pl

Dark matter remains one of the most significant unresolved problems in contemporary physics. Although its direct detection has not yet been achieved, a broad consensus regarding its existence is supported by compelling astrophysical and cosmological observations. The limited knowledge of its microscopic properties motivates a wide range of experimental searches exploring diverse theoretical scenarios.

One particularly well-motivated class of models involves ultralight dark matter, which may interact with ordinary matter through exotic, non-magnetic, spin-dependent couplings. Owing to their extremely low mass, such particles are expected to behave as coherently oscillating classical fields rather than as individual microscopic objects. This paradigm shift necessitates the development and implementation of novel experimental search strategies.

To address this challenge, we have developed and refined optical spin-based sensors designed to detect such interactions [1]. These sensors exhibit strongly suppressed sensitivity to conventional magnetic fields—one of the dominant noise sources in many dark matter searches—while maintaining exceptionally high sensitivity to non-magnetic spin couplings. This combination makes them particularly well suited for precision searches for ultralight dark matter.

In this contribution, we present the experimental techniques employed in these searches and review several recent measurements performed using our optical sensor platform [2–4]. We discuss the resulting constraints on ultralight dark matter models, highlighting the achieved sensitivities and excluded regions of parameter space. Finally, we outline future experimental strategies and technological improvements aimed at further extending the reach of spin-based searches for ultralight dark matter.

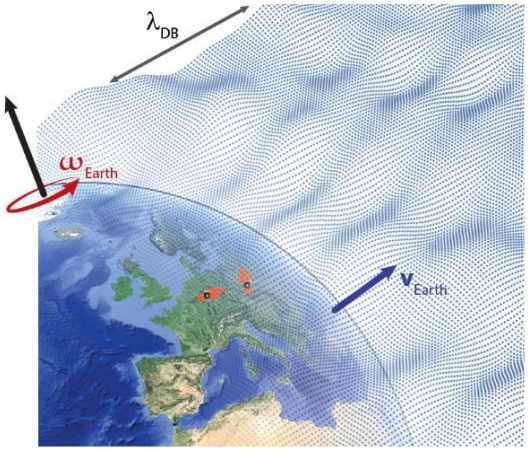

Fig. 1. Schematic diagram illustrating searches for stochastic dark matter. Adapted from Ref. [4]

Acknowledgments: This work was supported by the National Science Centre of Poland within the OPUS grant (grant No. 2019/34/E/ST2/00440). Sone of the presented results were obtained within the GNOME collaboration [5].

References:

[1] M. Padniuk et al., Physical Review Research 6, 013339 (2024).
[2] S. S. Khamis et al., Physical Review X 15, 031048 (2025).
[3] D. Gavilan-Martin et al., Nature Communications 16, 4953 (2025).
[4] Y. Wang et al., Nature (in press).
[5] https://budker.uni-mainz.de/gnome/

Spectroscopy of Higher Order States and Valence Band Discontinuity in Ga-Free Type-II Superlattices

M. RYGAŁA [1], J. ZANON [2], A. BADER[3], T. SMOŁKA[1],
F. HARTMANN[3], S. HÖFLING[3], M. E. FLATTÉ[2,4], M. MOTYKA[1]

[1] Department of Experimental Physics, Faculty of Fundamental Problems of Technology, Wrocław University of Science and Technology, wyb. S. Wyspiańskiego 27, 50-370, Wrocław, Poland
[2] Department of Applied Physics, Eindhoven University of Technology, P.O. Box 513, 5600 MB, Eindhoven, The Netherlands
[3] Julius-Maximilians-Universität Würzburg, Physikalisches Institut and Würzburg-Dresden Cluster of Excellence ct.qmat, Lehrstuhl für Technische Physik, Am Hubland, 97074 Würzburg, Germany
[4] Department of Physics and Astronomy, University of Iowa, Iowa City, Iowa 52242, USA

e-mail address: michal.rygala@pwr.edu.pl

In recent years, the search for efficient active regions for photodetectors designed for the mid- and longwave infrared spectral range has driven the growth technology of advanced semiconductor nanostructures, such as quantum cascade detectors and type-II superlattices (T2SLs). One of the superlattices considered is the gallium-free $InAs/InAsSb$, which is predicted to have optical properties worse than those of its Ga-rich counterparts but better electric properties. The latter has been related to the removal of mid-gap trap states caused by the gallium vacancies in the crystal lattice. [1]

In order to explore the $InAsSb$ material system, we have performed extensive experimental and theoretical study of the optical properties of $GaSb$ lattice-matched $InAs/InAs_{0.65}Sb_{0.35}$ T2SLs with different superlattice periods. By using photoluminescence and photoreflectance techniques, we were able to measure the optical response from the fundamental and higher-order optical states and later, identify the causes for the unusual behaviour of the emission at low-temperature regime. [2] In later steps, the energies of the optical features extracted from the experiment were used to fine-tune the numerical model of the confined states based on 14kp formalism. In order to reach the agreement between the refractive index curves calculated in the presence of photogenerated carriers and the photoreflectance spectra we explored different material parameters. The model was run against three structures with different periods with the response of three to four optical features. The agreement was reached for a small range of $InAsSb/InAs$ valence band offset (VBO) and $InAsSb$ bandgap for all the samples, revealing new information about the band discontinuity in this material system. Using the optimized bowing parameters we extracted the composition-dependence of VBO and the bandgap without the need for measuring the samples with different $InAsSb$ compositions.

This showed that conjoined optical-numerical study is a powerful tool to study advanced material systems.

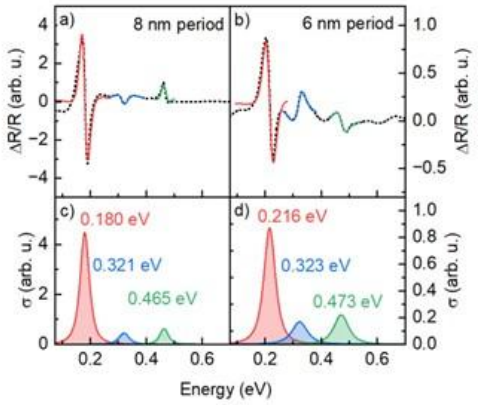

Fig. 1. Results of the photoreflectance experiment. Photoreflectance spectra and extracted moduli for the sample with 8 nm period (a, c) and 6 nm period (b,d).

Acknowledgments: This work has been funded by the German Federal Ministry of Research, Technology, and Space (BMFTR) within the joint research project RIBKD (13N16964). J.Z. was financially supported by Marie Sklodowska-Curie Grant No. 956548.

References:

[1] A. Jóźwikowska, et. al., Optical and Quantum Electronics, 51,7, (2019)
[2] K. Murawski, et. al., Journal of Electronic Materials, 52, 11 (2023)

Beyond DBRs: High-Contrast Gratings, Plasma Enhanced DBRs, and Fano Resonance for Mid-Infrared VCSELs

T. SMOŁKA [1], A. SZERLING[2], B. ŚCIANA[3], S. HÖFLING[4], T. CZYSZANOWSKI[5] AND M. MOTYKA[1]

[1] Laboratory for Optical Spectroscopy of Nanostructures, Department of Experimental Physics, Faculty of Fundamental Problems of Technology, Wrocław University of Science and Technology, Wybrzeże Wyspiańskiego 27, 50-370 Wrocław, Poland

[2] Łukasiewicz Research Network – Institute of Microelectronics and Photonics, al. Lotników 32/46, 02-668 Warsaw, Poland

[3] Department of Microelectronics and Nanotechnology, Faculty of Electronics, Photonics and Microsystems, Wrocław University of Science and Technology Janiszewskiego 11/17, 50-372 Wrocław, Poland

[4] Julius-Maximilians-Universität Würzburg, Physikalisches Institut, Lehrstuhl für Technische Physik, Am Hubland, 97074 Würzburg, Germany

[5]Photonics Group, Institute of Physics, Lodz University of Technology, ul. Wólczańska 219, 90-924 Łódź, Poland

e-mail address: tristan.smolka@pwr.edu.pl

Mid-infrared (MIR) vertical-cavity surface-emitting lasers (VCSELs) are promising light sources for sensing applications due to their compact footprint, low power consumption, and inherent single-mode operation. However, extending VCSEL operation into the MIR spectral range (3–5 µm and beyond) remains challenging, primarily because of limitations in available optical feedback structures. In this contribution, we review recent experimental and technological advances in mirror and cavity concepts that enable efficient MIR VCSEL operation, with particular emphasis on distributed Bragg reflectors (DBRs), monolithic high-contrast gratings (MHCGs), hybrid mirror configurations, and Fano-resonant structures.

Accurate optical design of MIR VCSEL cavities critically depends on reliable material parameters. Recent experimental determination of refractive indices for InP-, GaAs-, and related compound semiconductor systems across the MIR spectrum provides an essential foundation for mirror and cavity engineering [1]. Building on these data, semiconductor DBRs optimized for MIR wavelengths have been demonstrated, including monolithically grown plasmon-enabled Monolithic Bragg Reflectors [2]. Such approaches significantly relax material constraints and improve compatibility with MIR gain regions.

In parallel, subwavelength grating mirrors have emerged as an attractive alternative to conventional DBRs [3]. Monolithic high-contrast gratings fabricated in antimonide-based material systems exhibit high reflectivity over broad MIR bandwidths and for both polarizations, while offering reduced thickness and improved thermal properties [4]. Furthermore, resonant mirror concepts exploiting Fano interference enable strong wavelength selectivity and enhanced field confinement within compact vertical cavities [5].

Together, these developments establish a versatile toolbox for tailoring optical feedback in MIR VCSELs. The presented overview highlights experimentally demonstrated mirror technologies that pave the way toward compact, efficient, and spectrally selective MIR VCSEL sources for next generation sensing platforms.

Acknowledgments: This work was financially supported by the Swiss Contribution to reducing economic and social disparities in the EU and from the state budget through the National Centre for Research and Development, Call 2024/90/2025, project entitled “Quantum-cascade vertical cavity surface emitting laser for gas sensing” (QCVCSEL).

References:

[1] M. Mikulicz et al., Phys. Rev. Appl., vol. 21, no. 4, p. 44001, Apr. 2024

[2] M. Badura et al., Laser & Photonics Reviews - Submited (2026)

[3] M. Gębski et al., Opt. Express 23, 11674-11686 (2015)

[4] A. Schade et al., Opt. Express, vol. 31, no. 10, pp. 16025–16034, 2023

[5] M. Mikulicz et al., Opt. Express, vol. 31, no. 16, pp. 26898–26909, 2023

Optimization of MOEMS Probe Scanning Properties for 3D Optical Coherence Tomography Imaging

P. STRUK [1], S. BARGIEL [2], M. JÓZWIK [3], B. MIRECKI [3], C. GORECKI [4], H. XIE [5], M. WOJTKOWSKI [4]

[1] Department of Optoelectronics, Faculty of Electrical Engineering, Silesian University of Technology, 2 Krzywoustego Str., 44-100 Gliwice, Poland.
[2] FEMTO-ST Institute (UMR CNRS 6174, Université Bourgogne Franche-Comté), 15B Avenue des Montboucons, 25030 Besançon, France.
[3] Faculty of Mechatronics, Warsaw University of Technology, Faculty of Mechatronics of Warsaw University of Technology, ul. Św. Andrzeja Boboli 8, 02-525 Warsaw.
[4] Institute of Physical Chemistry, Polish Academy of Sciences, ul. Kasprzaka 44/52, Warsaw.
[5] University of Florida, P.O. Box 116200, Gainesville, Florida, USA.

e-mail address: przemyslaw.struk@polsl.pl

The authors present the numerical design and optimization, as well as experimental results, of a miniaturized endomicroscopy probe fabricated using Micro-Opto-Electro-Mechanical Systems (MOEMS) technology for three-dimensional (3D) optical coherence tomography (OCT) imaging. The main advantage of the proposed probe is its ability to operate in two distinct modes [1–4]:

- a forward-scanning mode, suitable for imaging samples located directly in front of the probe [2,3], and
- a transverse-scanning mode, used when the sample is located in confined or hard-to-reach regions [1,3].

The endomicroscopy probe consists of a GRIN lens integrated with a Mirau-type micro-interferometer and a two-axis electrothermal MEMS scanner. Owing to the compact size of the packaged probe (28.0 × 4.8 × 4.8 mm³, length × width × height), it is fully compatible with endomicroscopic applications.

A key challenge during the design phase was the optimization of the probe's geometric, optical, and scanning properties. This process required careful consideration of several factors, including the specific characteristics of MOEMS fabrication, the target optical resolution, scanner frequencies along the x and y axes, scanning speed, the spatial dimensions of the scanning area, and the coverage ratio associated with Lissajous scanning trajectories.

The presented endomicroscopy probe enables scanning with axial and transverse resolutions of 5 µm and 12 µm, respectively, at speeds of up to 5 fps and 10 fps, over a scanning area of 110 × 110 µm.

Acknowledgments:

The research was funded by projects: Labex Action program, ANR-11-LABX-0001-01, INSERM Plan Cancer program (ROBOT project), the French RENATECH network and its FEMTO-ST technological facility and by the Collegium SMYLE.

References:

[1] P. Struk et. al., IEEE Sensors Journal, Vol. 24, 9, 2024.
[2] P. Struk et. al., IEEE Sensors Journal, Vol. 15, 12, 2015.
[3] P. Struk et. al., Optics Letters, 43(19) (2018).
[4] F. Gracia-Ramirez et. al. Optics InfoBase Conference Papers, Vol. Part F180-OCT-(2020).

Polish Perspective on Integrated Photonics Technologies, Applications, and Challenges

R. PIRAMIDOWICZ [1,2,3], S. STOPIŃSKI[1,2,3], K. ANDERS[1,2,3], A. JUSZA[1,3], M. LELIT[1,4], A. POŁATYŃSKI[1,5], P. WIŚNIEWSKI[4], M. SŁOWIKOWSKI[4], M. JUCHNIEWICZ[4], J. OLSZEWSKI[1,2,6], R. CIECHAŃSKI[2], K. MACHAŁOWSKI[2], J. JUREŃCZYK[2], K. PIERŚCIŃSKI[7], D. PIERŚCIŃSKA[7]

[1]Warsaw University of Technology, Institute of Microelectronics and Optoelectronics, Koszykowa 75, 00-662 Warsaw, Poland
[2]VIGO Photonics, Poznańska 129/133, 05-850 Ożarów Mazowiecki, Poland
[3]LightHouse sp. z o.o., Stefczyka 34, 20-151 Lublin, Poland
[4]Warsaw University of Technology, Centre for Advanced Materials and Technologies CEZAMAT, Poleczki 19, 02-822 Warsaw, Poland
[5]VPIphotonics GmbH, Carnotstr. 6, 10587 Berlin, Germany
[6]Wrocław University of Science and Technology, Department of Optics and Photonics, Wyb. Wyspiańskiego 27, 50-370 Wrocław, Poland
[7]Łukasiewicz Research Network - Institute of Microelectronics and Photonics, Al. Lotników 32/46, 02-668 Warsaw, Poland

e-mail address: ryszard.piramidowicz@pw.edu.pl

The early decades of the 21st century have brought humanity into an entirely new era in which information, connectivity, and intelligence define not only technological progress but also the very foundations of modern civilization. From automated industry and robotics to the Internet of Things, smart cities, and artificial intelligence, global development is increasingly driven by our ability to generate, gather, process, transmit, and interpret data in real time. The technologies that underpin this transformation - electronics and photonics - have become the nervous system of the world. The microelectronic revolution of the second half of the 20th century established the foundation: compact, energy-efficient, and scalable integrated circuits that made computation ubiquitous. Today, an analogous revolution unfolds in the realm of light. Integrated photonics, which has been rapidly developing since the beginning of the 21st century, is emerging as the key enabler of next-generation communication, computation, and sensing systems. Photonic integrated circuits (PICs) are already at the heart of modern telecommunications and data centers [1], and their evolution now extends into new strategic domains, from distributed environmental and industrial sensing to biomedical and quantum technologies [2]. This expansion requires pushing the operational boundaries of photonic platforms beyond the traditional telecom wavelengths around 1.55 µm, toward visible or mid-infrared spectral ranges. In particular, the mid-IR spectral region offers unprecedented opportunities, providing access to the “molecular fingerprints” and enabling the detection and analysis of gases, liquids, and biological samples with unmatched selectivity and sensitivity [3].

The development of integrated photonics in Poland has followed a dynamic and increasingly mature trajectory. Since 2011, research at Warsaw University of Technology (WUT) has laid the foundation for the field through studies on the design and characterization of photonic components. A decade later, the establishment of the CEZAMAT research infrastructure enabled the development of dedicated technological platforms, while collaboration with VIGO Photonics and the Łukasiewicz Institute of Microelectronics and Photonics (Ł-IMiF) since 2021 has led to the development of the first Polish mid-IR PIC technology — MIRPIC [4]. This platform integrates passive germanium-on-silicon with advanced quantum-cascade lasers and superlattice type II antimonide photodetectors, marking a significant step toward establishing a complete domestic value chain for photonic integration.

The strategic importance of integrated photonics extends well beyond telecommunications. Future technologies - AI-assisted manufacturing and data processing, digital health, and IoT - increasingly rely on compact, energy-efficient, and scalable sensing and communication systems. Integrated photonics offers a pathway to such systems, combining unprecedented data throughput with low energy consumption and environmental sustainability. In the mid-IR range, it further unlocks applications in gas sensing, precision agriculture, industrial safety, and biomedical

diagnostics, aligning perfectly with global megatrends toward climate resilience, green transition, and digital sovereignty.

However, realizing this potential requires overcoming several interdependent scientific, technological, and systemic challenges. On the materials level, expanding the operational spectral range requires introducing new platforms, such as Ge-on-Si, SiN, and $LiNbO_3$, as well as hybrid integration with III-V compounds for active components. At the design level, accurate modeling of optical modes, coupling interfaces, and temperature dependencies is essential to ensure high yield and predictable performance. The next challenge is to develop reliable methods for hybrid and heterogeneous integration of lasers and detectors with passive circuits, while maintaining thermal stability and minimizing optical loss. Furthermore, scaling manufacturing from laboratory prototypes to pilot production requires investment in clean-room infrastructure, process automation, and metrology standards. Finally, at the ecosystem level, sustainable growth of the integrated photonics sector depends on coordinated collaboration among academia, industry, and government — fostering design ecosystems, accessible foundries, and cross-sector applications.

Poland's rapidly developing research and industrial landscape — with VIGO Photonics, WUT, and Ł-IMiF as core stakeholders — provides a solid foundation to address these challenges. Building on European initiatives such as IPCEI HyperPIC and PIXEurope, the national photonics community is now positioned to contribute meaningfully to Europe's technological sovereignty and to shape the future of mid-IR integrated photonics as a strategic enabler of digital and green transformation.

Acknowledgments: This work received support from the National Center for Research and Development through projects MIRPIC (TECHMATSTRATEG-III/0026/2019-00) and HyperPIC (FENG.02.10-IP.01-0005/23, IPCEI ME/CT). This work has received funding from the European Union's Horizon Europe under Grant Agreement #101213727, Chips Joint Undertaking (Chips JU).

References:

[1] X. Zhou, D. Yi, D.W.U. Chan, et al. Silicon photonics for high-speed communications and photonic signal processing, Nanophotonics 1, 27 (2024) https://doi.org/10.1038/s44310-024-00024-7

[2] M. Scholles et al. White Paper on Integrated Photonics (online: www.photonics21.org)

[3] M.A. Butt, M. Juchniewicz, M. Słowikowski, Ł. Kozłowski and R. Piramidowicz, "Mid-infrared photonic sensors: exploring fundamentals, advanced materials, and cutting-edge applications", Sensors 25 1102, 2025

[4] R. Piramidowicz, S. Stopiński, K. Anders, J. Jureńczyk, M. Liebert, J. Olszewski, A. Połatyński, M. Lelit, M. Słowikowski, M. Juchniewicz, P. Wiśniewski, D. Pierścińska and K, Pierściński, HyperPIC: on the road to mid-infrared photonic integrated circuits Proc. SPIE 13369 133690C, 2025

FoSMoWater – Development of an Innovative Photonic Water Resource Monitoring System

J. KALWAS[1,2], A. JUSZA[2], F. ŁABAJ[1,2], P. MARCHEWKA[1], W. CHARAZIŃSKI[1], M. ABRAMOWICZ[1], K. MACHAŁOWSKI[1], R. STOJEK[1], R. CIECHAŃSKI[1], M. LIEBERT[1], T. MIRECKI[1], M. WINCEL[1], N. MATWIEJ[3], E. KIEDRZYŃSKA[3], A. BIENIEK-KACZOREK[2], Ł. KOZŁOWSKI[2], P. BORTNOWSKI[2], K. ANDERS[1,2], S. STOPIŃSKI[1,2], R. PIRAMIDOWICZ[1,2]

[1] VIGO Photonics S.A., Poznańska 129/133, 05-850 Ożarów Mazowiecki
[2] Warsaw University of Technology, Institute of Microelectronics and Optoelectronics, Koszykowa 75, 00-662 Warsaw
[3] European Regional Centre for Ecohydrology of the Polish Academy of Sciences, Tylna 3, 90-364 Łódź

e-mail address: jkalwas@vigo.com.pl

Water resources, especially in the era of anthropogenic climate change and the current geopolitical situation, are crucial to public health, the economy, and the natural environment. Poland has some of the most limited freshwater resources in Europe, and these resources are also subject to significant pollution and increasing scarcity. For this reason, effective monitoring of freshwater resources is of strategic importance.

Surface waters in Poland are divided into over 4,000 areas, known as Uniform Water Parts. Their monitoring is supervised by the Chief Inspectorate for Environmental Protection.

Standard water quality assessment methods rely on laboratory techniques that use expensive equipment and hazardous chemical reagents. Moreover, the current national water quality monitoring system cannot identify threats on an ongoing basis. Nitrates, nitrites, phosphates, and ammonium compounds introduced into the environment as a result of human activity are the most common causes of adverse hydrobiological phenomena, leading to increasingly frequent ecological disasters.

The system of autonomous measuring probes developed within the FoSMoWater project is intended to enable online detection of the above-mentioned contaminants using newly developed, reagent-free photonic methods. The main research activities focused on evaluating the applicability of attenuated total internal reflection techniques in the mid-infrared range (FTIR-ATR/HATR), Raman spectroscopy techniques, and UV absorption spectroscopy for water quality monitoring. These techniques were selected for their potential for high sensitivity, selectivity, and miniaturization, which are essential for the development of compact, autonomous sensing devices capable of long-term operation in natural aquatic environments. Quantitative determination of the concentrations of all considered contaminants was achieved using the FTIR-HATR technique based on a multi-reflection horizontal ZnSe crystal cell. A key research outcome was the demonstration of the feasibility of both single- and multi-channel sensor architectures operating in the mid-infrared spectral range of 3–11 µm, representing a significant step toward fully integrated photonic sensing platforms.

The developed system employs miniature broadband mid-IR sources and laser sources, enabling flexible optimization of spectral coverage and system sensitivity. In parallel, Raman spectroscopy was used as a complementary technique to detect selected functional groups following controlled evaporation of water from samples with volumes below 1 µl. Additionally, UV absorption spectroscopy was investigated as a rapid and cost-effective method for measuring the concentrations of selected substances, further extending the versatility of the developed monitoring system. The above-mentioned methods were verified by validation procedures using laboratory measurements with chromatographic techniques and spectrophotometric reagent methods specified by standards.

Acknowledgments:
This work was supported by the National Centre for Research and Development through the project FoSMoWater (HYDROSTRATEG1/000E/2022).

Sub-Terahertz Telecommunication Link with a 3D-Printed Lens System for Beam Shaping

P. ZAGRAJEK[1], M. MACIEJEWSKI[1] , P. KOMOROWSKI[1], N. PAŁKA[1]

[1]Military University of Technology, 2 Kaliski Str., 00-908 Warsaw, Poland

e-mail address: norbert.palka@wat.edu.pl

Ubiquitous interest in the sub-terahertz frequency range has grown significantly in recent years, driven by the demand for higher data rates and robust wireless connectivity without relying on optical or infrared technologies. This part of the spectrum provides wide available bandwidth and maintains more advantageous propagation properties compared to optical systems.

Although sophisticated modulation schemes such as phase-shift keying (PSK) or quadrature amplitude modulation (QAM) can achieve very high data rates, amplitude modulation (AM) is often preferred in certain applications for its simpler implementation and lower hardware complexity.

Fig. 1. Measurement setup in the experimental hall

In the experimental setup (Fig. 1), the IMPATT diode source (Terasense, 100 GHz, 90 mW) was amplitude-modulated at frequencies up to 100 MHz. The broadband detector, equipped with a log-periodic antenna and mounted on an HR-Si lens, was connected to a voltage follower featuring a 108 MHz bandwidth.

Custom 3D-printed diffractive lenses (60 cm diameter, 100 cm focal length) were developed to provide precise beam shaping and efficient signal focusing.

The data generation and acquisition system was implemented using National Instruments PXI hardware. An NI PXI-6552 Digital I/O module was used to generate pseudo-random bit sequences, while an NI PXI-5160 oscilloscope facilitated signal detection and subsequent analysis.

Using this configuration, we successfully demonstrated a communication link in the sub-THz frequency band. Error-free data transmission was achieved over distances of up to 50 m between the transmitter and receiver, supporting data rates of up to 50 Mbit/s (Fig. 2)

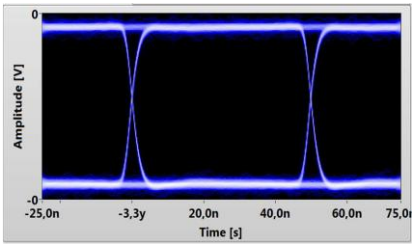

Fig. 2. Eye diagram at 20 Mbit/

Topologically-Protected Edge States for Intensity-Selective and Sensing THz Photonic Devices

B. JANASZEK [1,2], T. ŚMIAROWSKI[1,2], A. TYSZKA-ZAWADZKA[1], I. TSUKERMAN[3], P. SZCZEPAŃSKI [1,2]

[1]Warsaw University of Technology, Institute of Microelectronics and Optoelectronics, ul. Koszykowa 75, 00-662 Warsaw, Poland
[2]National Institute of Telecommunications, ul. Szachowa 1, 04-894 Warsaw, Poland
[3]The University of Akron, Department of Electrical and Computer Engineering, Akron, OH 44325, USA

e-mail address: bartosz.janaszek@pw.edu.pl

We present a planar photonic platform combining topological photonics, optical nonlinearity, and material sensitivity to external stimuli, enabling both intensity-selective operation and ultrasensitive gas detection in the terahertz (THz) spectral range. The investigated structure is a one-dimensional photonic crystal (1D PC) with a parametrized basic cell, terminated with a nonlinear graphene–spacer–graphene stack, see Fig 1. By employing a synthetic geometrical space composed of two independent structural parameters and a wavevector component, the photonic crystal is designed to emulate Weyl points and associated Fermi-arc states. These states map into real space as topologically protected edge states, in this case Tamm plasmon polaritons (TPPs) localized at the interface between the photonic crystal and graphene.

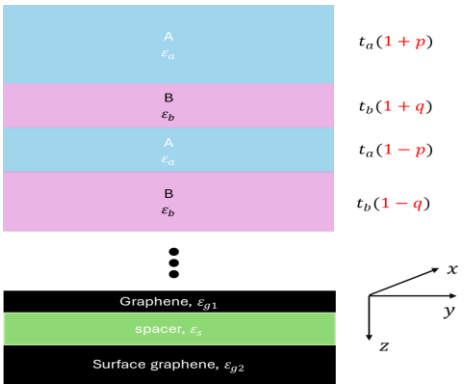

Fig. 1. Schematic of the considered 1D topological PC.

The topological origin of the interface states is confirmed by linear band degeneracies in the synthetic space and a vortex-like structure of the reflection phase, see Fig. 2, which guarantees the existence of surface modes independently of the specific properties of the terminating layer [1]. When graphene is used as the reflective termination, the resulting TPPs exhibit strong electromagnetic field confinement at the interface and inherit graphene's nonlinear and tunable optical response [2,3]. This combination enables a robust and controllable interaction between confined THz radiation and the graphene monolayer.

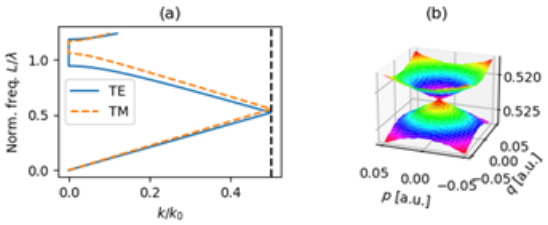

Fig. 2. The band dispersion of considered planar structure with 4-layer basic cell (a). Band dispersion in synthetic geometrical space (b))

In addition to its nonlinear optical response, graphene acts as an efficient gas-sensitive material whose carrier concentration and optical conductivity are modified upon adsorption of gas molecules such as NO_2. As demonstrated in our previous work [4], exposure to ultralow concentrations of NO_2 leads to measurable changes in graphene's permittivity and reflection phase. When coupled to topologically protected TPPs, these small material perturbations result in pronounced spectral shifts and amplitude changes of the interface resonance, enabling gas detection at the ppb level.

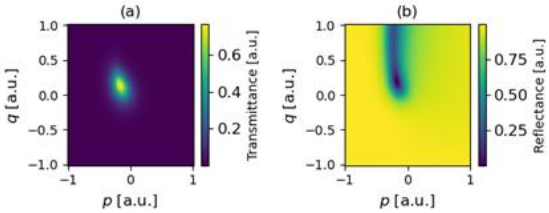

Fig. 3. Power transmission (a) and reflection (b) plotted in the pq space at frequency corresponding to the Weyl point of the first order, i.e., the contact point between 1st and 2nd band.

Numerical results show that the resulting optical properties, see Fig. 3, and related sensing (see Fig. 4) or optical limiting performance (see Fig. 5), are strongly enhanced by the appropriate selection of synthetic-space parameters corresponding to Fermi-arc states. Depending on the chosen parametrization, the device may operate in a reflection-, transmission-, or absorption-based sensing mode. In particular, sharp extrema in reflection or absorption spectra, originating from strong field localization at the graphene interface, provide well-defined spectral markers that can be tracked as a function of gas concentration. This approach yields a wide dynamic range, allowing for the quantitative determination of gas concentration, even for a single interface exposed to the analyte.

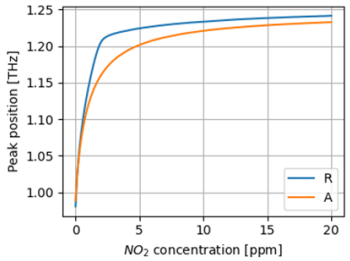

Fig. 4. Sample spectral shift characteristics illustrating gas sensing performance of the proposed 1D structure

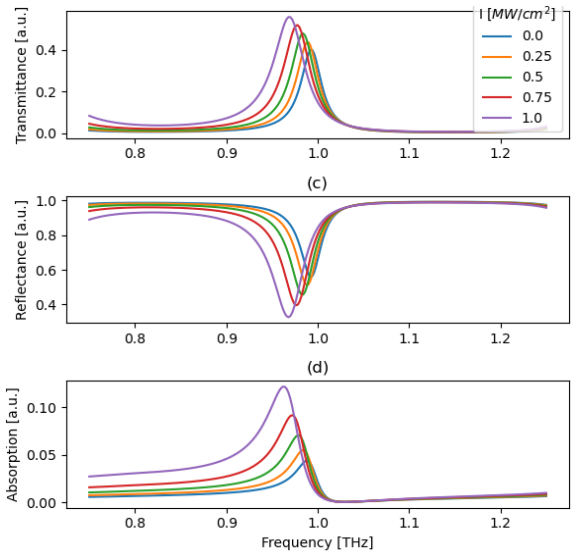

Fig. 5. Sample spectral shift of the TPP resonance in response to changing incident optical intensity, illustrating power limiting performance.

Beyond gas sensing and optical limiting, the underlying concept is applicable to a broader class of stimuli-responsive photonic devices. Any external factor capable of modifying the carrier concentration or conductivity of graphene or other two-dimensional materials—such as electrical gating, optical pumping, temperature variation, or adsorption of different chemical species—may be exploited to realize reconfigurable and multifunctional topological photonic components. This opens perspectives for tunable filters, switches, modulators, and adaptive devices operating in the THz regime.

Future work will focus on several complementary directions. First, the experimental realization of the proposed structures will be pursued, including the fabrication of parametrized 1D photonic crystals and their integration with high-quality graphene layers featuring controlled electrical biasing. Particular attention will be paid to verification of topological robustness and nonlinear response under realistic experimental conditions. Second, the development of efficient and scalable numerical methods will be undertaken to enable accurate modeling of nonlinear, nonlocal, and topological effects in large-area photonic structures. Such methods are essential for optimizing device performance and extending the concept toward more complex geometries.

Finally, a systematic investigation of the conditions required for the emergence of topologically protected nonlinear surface states will be conducted for both one-dimensional and two-dimensional photonic systems. Extending the synthetic-space approach to 2D photonic crystals and metasurfaces may enable the discovery of new classes of robust nonlinear interface modes with enhanced confinement and tunability. These studies are expected to provide general design rules for topology-enabled nonlinear photonic devices and to pave the way toward their practical implementation in next-generation THz photonic and sensing technologies.

Acknowledgments: This work was supported by WUT's AEEiTK Scientific Discipline Council grant.

References:

[1] Q. Wang et al., Physical Review X, 7(3), 031032, (2017).
[2] B. Janaszek et al., Micromachines MDPI, under review, (2026).
[3] B. Janaszek et al., Optica Open, (2024).
[4] B. Janaszek et al., Opt. Express 33, 51319-51334 (2025)

Numerical and Experimental Exploration of Nanostructured Five-Mode Optical Fibers

B. PAŁUBA[1], M. NAPIÓRKOWSKI[2], R. KASZTELANIC[1], R. BUCZYŃSKI[1]

[1] University of Warsaw, Faculty of Physics, Pasteura 5, 02-093, Warsaw, Poland.
[2] Wroclaw University of Science and Technology, Faculty of Fundamental Problems of Technology, Wybrzeze Wyspianskiego 27, 50-370, Wroclaw, Poland.

e-mail address: b.paluba@uw.edu.pl

Spatial division multiplexing (SDM) and mode division multiplexing (MDM) are actively developed approaches enabling a several-fold increase in telecommunication network bandwidth. These multiplexing schemes can be implemented using different optical fiber designs, including multicore fibers (MCFs) with coupled or independent cores, bundles of single-mode fibers, and strongly- or weakly-coupled few-mode fibers (FMFs) [1]. In our research, we are focused on the latter type of fibers which we develop based on nanostructuring technology, that is a method of optical fibers fabrication in which the fiber cores are composed of thousands of glass nanorods. With this approach one can obtain highly complex refractive index profiles, which, in the case of FMFs, may significantly increase separations of adjacent spatial modes [2,3]. The optical fiber is said to have weakly-coupled modes, if the lowest difference between their effective refractive indices, denoted as $\mathrm{Min}|\Delta n_{eff}|$, is greater than 1×10^{-3}.

Since the nanostructuring of fiber cores requires stacking thousands of rods of two or more types of glasses, usage of sophisticated numerical methods at the stage of fiber design is inevitable. Recently, we have been exploring the potential of neural networks in the context of FMFs structure optimization. Firstly, using the deep network of a simple, dense architecture, we obtained the five-mode fiber of $\mathrm{Min}|\Delta n_{eff}| = 9.73\times10^{-4}$ determined at a wavelength of 1550 nm. Its core was composed of pure silica glass rods and silica glass doped with 5% mol of germanium oxide. Afterwards, the designed fiber was fabricated in-house and characterized with scanning electron microscope (Fig. 1.). The diameters of the fiber and its core were ca. 128 µm and 19.3 µm, respectively.

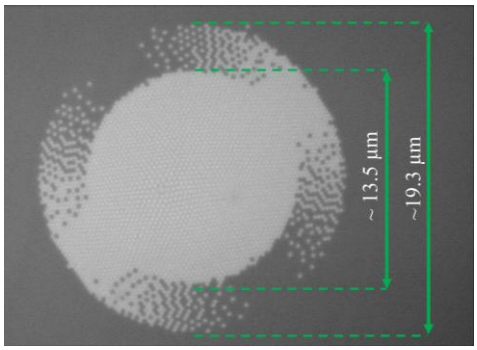

Fig. 1. Scanning electron microscope image of the fabricated nanostructured fiber designed to support five spatial modes. Lighter dots correspond to glass rods doped with GeO_2.

Furthermore, the obtained fiber was characterized to assess its potential for telecommunication applications. For instance, cross-talks and attenuation corresponding to supported spatial modes were determined. In Table 1. the crosstalk values between the LP_{01}, LP_{11a} and LP_{21a} modes at 1550 nm for a fiber segment length of 0.96 m are presented.

Tab. 1. The crosstalk values, expressed in dB, between selected spatial modes supported by the optical fiber shown in Fig. 1. of a length of 0.96 m.

		Input mode		
		LP_{01}	LP_{11a}	LP_{21a}
Output mode	LP_{01}	0	-0,06	-7,90
	LP_{11a}	-16,05	0	-6,58
	LP_{21a}	-11,97	-7,62	0

Gathered results indicated that several-meter-long segments of the designed nanostructured fiber can be used to guide selected spatial modes as independent telecommunication channels.

The next step of the research was to apply different neural network, based on convolutional layers. Instead of sequences of parameters describing the shape of the core as in the case of dense network used previously, convolutional neural networks operate with figures of fiber

cross-sections. Initially, simulations were carried out for the same chemical composition of glass rods (SiO_2 glass and SiO_2 glass doped with 5% mol GeO_2), to compare the utility of both types of neural networks. As expected, we were able to find a fiber of a completely different structure and of slightly greater separations with $\text{Min}|\Delta n_{eff}| = 1.05\times10^{-3}$ (Fig. 2.). To demonstrate that the new fiber still supported only five spatial modes, the bending losses of the fifth and sixth modes were additionally calculated for a loop of a radius of 5 cm.

$\text{Min}|\Delta n_{eff}| = 1.05\times10^{-3}$

Bending losses (r = 5 cm):

Max: **0.22 dB** (5th mode)

Min: **74.94 dB** (6th mode)

Fig. 2. The cross-section of the nanostructured five-mode fiber core (17,3 µm diameter) optimized using the convolutional neural network, along with the $\text{Min}|\Delta n_{eff}|$ and bending losses values. Black dots and white dots correspond to silica glass rods and silica glass rods doped with 5 % mol of GeO_2, respectively.

Since we aim to fabricate another nanostructured five-mode fiber, but using silica glass of higher GeO_2 concentration (6.1 % mol), the core structure was once again optimized using convolutional networks. In this case, the network was trained to find as many different structures of high $\text{Min}|\Delta n_{eff}|$ value as possible. As a result, we were able to design several promising fibers of significantly distinct rods distributions (Fig. 3.). However, the neural networks are very helpful with finding general, approximate patterns of rods, but not the most optimal solutions. Therefore, the selected structures were additionally optimized with Monte Carlo algorithm. In the case of examples shownin Fig. 3. the $\text{Min}|\Delta n_{eff}|$ values increased to 1.27×10^{-3} and 1.25×10^{-3}, respectively.

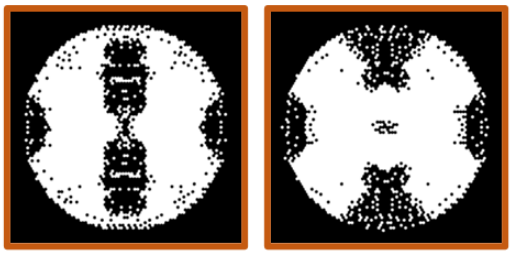

$\text{Min}|\Delta n_{eff}| = 1.24\times10^{-3}$ $\text{Min}|\Delta n_{eff}| = 1.18\times10^{-3}$

Fig. 3. Examples of cross-sections of five-mode nanostructured fiber cores (15 µm diameter) optimized using the convolutional neural network, along with the corresponding $\text{Min}|\Delta n_{eff}|$ values. Black and white dots represent silica glass rods and silica glass rods doped with 6.1 % mol of GeO_2, respectively.

To sum up, neural networks are a versatile tool that allows one to explore the set of fibers of highly complicated core structures composed of even thousands of nanometric glass rods, to extract those of desired properties. In the case of five-mode fibers, we designed different structures of mode separations exceeding 1×10^{-3} using pure silica glass rods and silica glass rods doped with 5 % or 6.1 % mol of GeO_2. One of the fibers have been fabricated recently and characterized in the context of telecommunication applications. Since complexity of the fibers, that may be fabricated using well-established fiber fabrication methods, is strongly limited, nanostructuring technology is a promising approach worth intense developing, both numerically and experimentally.

Acknowledgments: This work was financially supported by: the National Science Centre, Poland, grant Maestro 14, no. 2022/46/A/ST7/00238

References:

[1] D. J. Richardson et al., Nature Photonincs 7, 354–362 (2013).

[2] M. Napiórkowski et al. Engineering Applications of Artificial Intelligence 133, 107955 (2024).

[3] R. Kasztelanic et al. Optics Express 30, 41832 (2022).

An All-Fiber Optofluidic Dye Laser Based on Hollow-Core Anti-Resonant Fiber

K. RECHCIŃSKA [1,2], M. WINKOWSKI [1,2], M. ADAMOWSKA[3], B. PAŁUBA[2], A. FILIPKOWSKI[1], D. PYSZ[2], R. BUCZYŃSKI[1,2], T. STACEWICZ[2]

[1] Łukasiewicz Research Network – Institute of Microelectronics and Photonics, Photonics Materials Group, al. Lotników 32/46, 02-668 Warsaw, Poland
[2] University of Warsaw, Faculty of Physics, Pasteura 7, 02-093 Warsaw, Poland
[3] University of Warsaw, Faculty of Chemistry, Pasteura 1, 02-093 Warsaw, Poland

e-mail address: katarzyna.rechcinska@imif.lukasiewicz.gov.pl

Dye lasers offer broad tunability in the visible spectral range but are often limited by bulk optical setups and complex fluid handling systems. Integrating liquid gain media directly into optical fibers provides a compact and robust alternative. Recent advances in hollow-core fiber technology have enabled optofluidic platforms that overcome the limitations of solid-state dye lasers and earlier liquid-core fiber systems [1-4]. In particular, hollow-core anti-resonant fibers (HC-ARFs) enable efficient light–matter interaction within minimal liquid volumes [5].

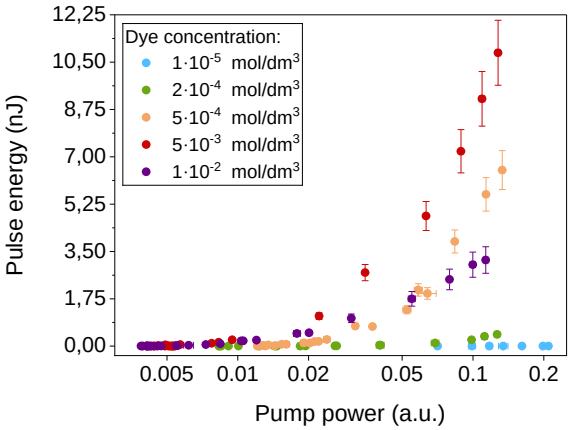

Fig. 1. Fiber dye laser pulse energy as a function of pump power for selected Rhodamine 6G concentrations.

We demonstrate an all-fiber optofluidic dye laser based on a Rhodamine 6G–filled HC-ARF pumped by a frequency-doubled Nd:YAG laser. The system integrates microfluidic dye delivery with standard fiber connectors, forming a compact, alignment-free, and mechanically robust laser module. Clear lasing threshold behavior is observed (Fig. 1), along with concentration-dependent tuning of the emission peak from 569 to 595 nm. Efficient laser operation is achieved for dye concentrations between $2 \cdot 10^{-4}$ and $1 \cdot 10^{-2}$ mol/dm³, with optimal performance at $5 \cdot 10^{-3}$ mol/dm³. Coherent laser emission is generated directly within the fiber core, establishing HC-ARFs as a promising platform for tunable optofluidic fiber lasers and integrated photonic applications.

Acknowledgments: This work was financially supported by National Science Centre, Poland, from CEUS-UNISONO 2020/02/Y/ST7/00136.

References:

[1] Vasdekis, A. E., Town, G. E., Turnbull, G. A., & Samuel, I. D. W. (2007). Fluidic fibre dye lasers. Optics express, 15(7), 3962-3967.
[2] Yu, J., Liu, Y., Wang, Y., Wang, Z., Zhang, X., Liu, X., ... & Wang, P. (2018). Optofluidic laser based on a hollow-core negative-curvature fiber. Nanophotonics, 7(7), 1307-1315.
[3] Anand Dewansingh et al (2025) Multimode emission of fluorinated ethylene propylene clad large diameter liquid-core lasers Laser Phys. Lett. 22 115101
[4] Chemnitz, M., Junaid, S., & Schmidt, M. A. (2023). Liquid-Core Optical Fibers-A Dynamic Platform for Nonlinear Photonics. Laser & Photonics Reviews, 17(9), 2300126.
[5] Rashid, Z., Jonáš, A., Buczyński, R., & Kiraz, A. (2018). Optofluidic dye lasers based on holey fibers: Modeling and performance analysis. *Journal of Lightwave Technology*, **36**(18), 4114-4122.

Design Constraints for Mid-Infrared Sensing Waveguides: Interaction-Limited Perspective

J. OLSZEWSKI [1,2,3], A. ŚLIPEK[1,2], T. MARTYNKIEN[2,3], K. ANDERS[1,2], S. STOPIŃSKI[1,2], R. PIRAMIDOWICZ[1,2]

[1]Warsaw University of Technology, Institute of Microelectronics and Optoelectronics, Koszykowa 75, 00-662 Warsaw, Poland
[2]VIGO Photonics S.A., Poznańska 129/133, 05-850 Ożarów Mazowiecki, Poland
[3]Wrocław University of Science and Technology, Department of Optics and Photonics, Wybrzeże Wyspiańskiego 27, 50-370 Wrocław, Poland

e-mail address: jacek.olszewski@pw.edu.pl

Integrated photonic waveguides operating in the mid-infrared (mid-IR) spectral range are essential for on-chip spectroscopic sensing, where molecular vibrational resonances provide strong and selective absorption signatures. The mid-IR region, conventionally spanning wavelengths from approximately 3 µm to 50 µm [1], is particularly valuable for environmental monitoring, industrial process control, and biomedical diagnostics. Unlike near-infrared photonic integrated circuits optimized primarily for data transmission, mid-IR sensing platforms are fundamentally governed by the trade-off between light–matter interaction strength and propagation loss. Consequently, design strategies directly inherited from telecom-band silicon photonics often fail to deliver optimal performance in the mid-IR [2, 3].

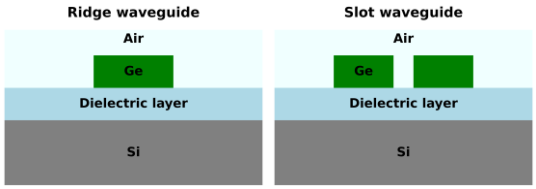

Fig. 1. Schematic representation of ridge and slot germanium-based waveguides.

In waveguide-based absorption sensing, the detected signal scales with the overlap between the guided optical mode and the surrounding analyte, while the transmitted optical power decays exponentially with propagation loss. This defines an interaction-limited operating regime in which an optimal waveguide length exists, determined by the inverse of the total loss coefficient. Beyond this length, further extension of the sensing path yields diminishing returns or degraded performance. As a result, minimizing propagation loss alone is insufficient; the relevant figure of merit becomes the ratio of analyte overlap to loss, which directly governs achievable sensitivity and limit-of-detection in integrated mid-IR sensors [4].

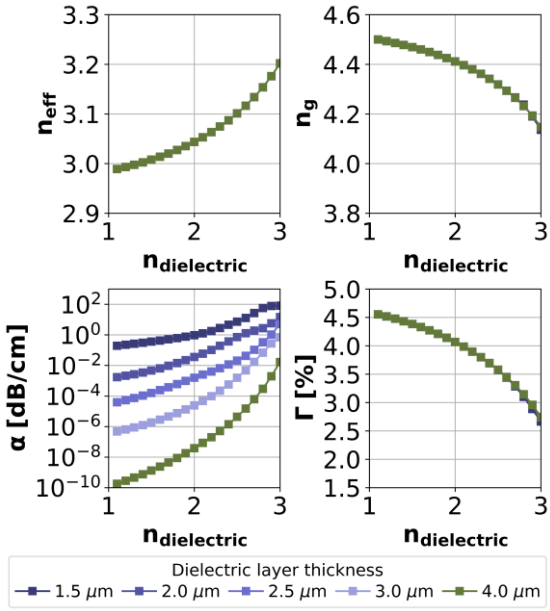

Fig. 2. Ridge waveguide (core height/width 1.0 µm/1.8 µm, λ = 4.25 µm) - calculated TE_0 mode phase (n_{eff}) and group (n_g) effective indices, confinement loss (α) and analyte-confinement factor (Γ) vs. refractive index of dielectric layer separating Ge core and Si substrate.

Numerical simulations of germanium-based ridge and slot waveguides (Fig. 1) reveal that attempts to enhance sensitivity by deliberately relaxing modal confinement must be approached cautiously. Modifying the refractive index of the bottom cladding (i.e., the dielectric layer), as shown in Fig. 2 and Fig. 3, can increase the evanescent field fraction but simultaneously induce rapid propagation-loss increase due to vertical radiation leakage into the bottom cladding (and possibly into the substrate). The resulting loss establishes a sharp boundary between low-loss and leakage-dominated regimes. Crucially, increased modal delocalization benefits sensing

performance only when the additional optical field redistributes into the analyte region; delocalization into lossy substrates or dielectric layers instead reduces overall performance. These observations demonstrate that vertical refractive-index engineering is a first-order design parameter in mid-IR waveguides [3, 5].

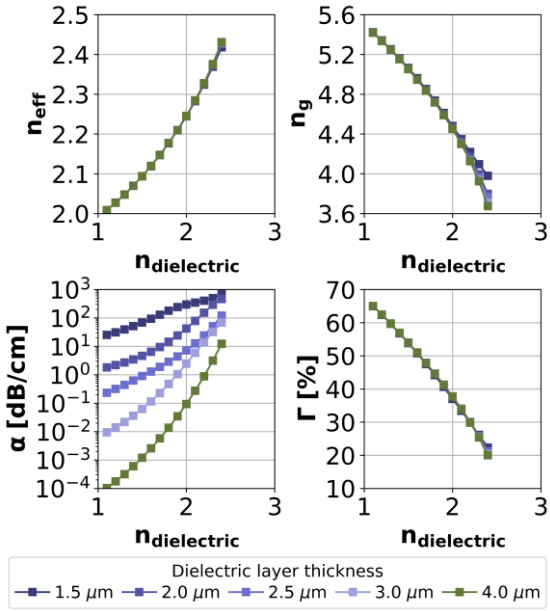

Fig. 3. Slot waveguide (core height/width 1.0 µm/1.8 µm, slot gap 0.2 µm, λ = 4.25 µm) - calculated TE_0 mode phase (n_{eff}) and group (n_g) effective indices, confinement loss (α) and analyte-confinement factor (Γ) vs. refractive index of dielectric layer separating Ge core and Si substrate.

Propagation loss in this spectral range is dominated by boundary-related mechanisms rather than bulk material absorption alone. Substrate leakage, absorption in buried dielectric layers, and surface-related loss play decisive roles as the wavelength increases and the modal fields extend further into the surrounding media [3]. While sidewalls remain important contributors to loss, recent studies indicate that sidewall-induced scattering cannot be adequately described by roughness amplitude alone. Instead, scattering is a process governed by the correlation of sidewall roughness and modal phase evolution along the propagation direction. In particular, roughness correlation lengths can produce phase-matched coherent scattering that persists even at long wavelengths [6, 7]. Consequently, fabrication processes that modify sidewall statistics without significantly changing roughness amplitude can lead to substantial variations in propagation loss [8].

Waveguide geometry must therefore be optimized specifically for mid-IR operation rather than scaled directly from near-infrared designs. Ridge and slot waveguides respond differently to vertical boundary conditions due to their distinct field distributions. Slot geometries can maintain high analyte overlap while suppressing substrate leakage owing to their inherently asymmetric modal profiles, whereas ridge waveguides are generally more susceptible to vertical leakage as confinement relaxes [5, 9]. However, the high confinement factors achievable in slot waveguides also increase sensitivity to boundary conditions and fabrication-induced imperfections, indicating that no single geometry universally maximizes performance. Polarization further serves as an active design variable, influencing confinement, leakage, and interaction strength [9, 10].

Overall, mid-IR sensing waveguides operate in an interaction-limited regime, where performance is governed by the balance between analyte overlap and boundary-dominated loss mechanisms. Vertical refractive-index engineering, control of coherent sidewall scattering, and geometry-specific optimization are therefore central to achieving low-loss, high-sensitivity operation. By emphasizing physical constraints rather than isolated design heuristics, this framework provides a robust foundation for comparing material platforms and guiding the development of next-generation mid-IR photonic integrated sensors.

Acknowledgments: This work received support from the National Center for Research and Development through projects MIRPIC (TECHMATSTRATEG-III/0026/2019-00) and HyperPIC (FENG.02.10-IP.01-0005/23, IPCEI ME/CT). This work has received funding from the European Union's Horizon Europe under Grant Agreement #101213727, Chips Joint Undertaking (Chips JU).

References:

[1] ISO 20473:2007, Optics and Photonics – Spectral Bands
[2] R. Soref, Nat. Photon. 4, 495–497 (2010)
[3] G. Z. Mashanovich et al., Opt. Mater. Express 8, 2276–2286 (2018)
[4] J. Lim et al., ACS Photon. 11, 4268–4278 (2024)
[5] J. Soler-Penadés et al., Opt. Express 24, 22908–22916 (2016)
[6] F. P. Payne et al., Opt. Quantum Electron. 26, 977–986 (1994)
[7] [8] S. M. Hörmann et al., J. Lightwave Technol. 41, 1503–1510 (2023)
[8] U. Griskeviciute et al., IEEE 16th International Conference on Group IV Photonics Proc., 1–2 (2019)
[9] D. M. Kita et al., Optica 5, 1046–1054 (2018)
[10] M. Vlk et al., Light Sci. Appl. 10, 26 (2021)

How Can Photonics and Spectroscopy Shed Light on Cancer?

D. KAŁUŻYŃSKA

Silesian University of Technology, Cathedral of Optoelectronics, Krzywoustego 2, 44-100 Gliwice, Poland

e-mail address: daria.kaluzynska@polsl.pl

Cancer remains one of the leading causes of mortality worldwide, driving the need for advanced diagnostic and therapeutic approaches that are both precise and minimally invasive. In recent years, photonics and optical techniques have emerged as innovative tools in cancer research, enabling non-invasive probing of biological tissues and targeted therapeutic interventions.

This work provides a concise overview of optical methods applied in cancer, with a particular focus on the interaction of light with both healthy and cancerous tissues.

Diagnostic techniques, including optical microscopy, multiphoton microscopy, Raman spectroscopy, light scattering, and Fourier transform infrared (FTIR) spectroscopy, are reviewed, highlighting their ability to detect and distinguish between healthy and cancerous cells and tissues. The role of endogenous fluorophores, extracellular matrix remodeling, and molecular fingerprints in cancer detection is emphasized.

In addition, selected photonic approaches for cancer treatment are outlined, including laser-based ablation, photothermal therapy, and photodynamic therapy, with particular attention to wavelength-dependent tissue interactions and underlying therapeutic mechanisms.

Variable Wavelength Interferometry for Measuring Phase and Step-Like Objects-Metrological Aspects

D. LITWIN[1], K. RADZIAK[1], A. CZYŻEWSKI[1], J. GALAS[1], T. KRYSZCZYŃSKI[1], N. BŁOCKI[1], R. SZUMSKI[2], J. NIEDZIELA[2]

[1]Łukasiewicz Research Network-Tele and Radio Research Institute,
11 Ratuszowa St, 03-450 Warsaw, Poland,
[2]Central Office of Measures, Time and Length Department
2 Elektoralna St., 00-139 Warsaw, Poland

e-mail address: dariusz.litwin@itr.lukasiewicz.gov.pl

Accurate measurements of different structures including phase and step-like objects need a suitable metrological technology. One of these is the Variable Wavelength Interferometry (VAWI)[1], which, depending on configuration, can be used for measuring both type of objects (including the retardance of waveplates). The interferometer's key element is a unique collection of Wollaston prisms that are built in a standard microscope. In the presented approach, the classical procedures based on finding coincidences and anti-coincidences of the object fringe pattern (Fig.1) with respect to the empty field pattern is replaced by continuous phase registration[2]. In addition, the work includes new algorithms and modified optical architecture of the interferometer. The conclusion includes comparative analysis of results, which provides new insight to the VAWI technology[3,4]. The system, being insensitive to environmental factors, is suitable for industrial applications, and the retardance can be measured across the visible spectrum with low uncertainty, which extends the field of applications.

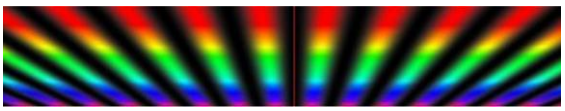

Fig.1. A typical fringe pattern in the VAWI measurement technology.

Acknowledgments: The project was funded by the Polish Ministry of Science and Higher Education, grant no. PM/SP/0046/2021/1, a part of the Programme "Polish Metrology".

References:

[1] M. Pluta, Advanced Light Microscopy, Vol. 3, PWN, Elsevier, Warszawa-Amsterdam-London-New York-Tokyo, 404-506 (1993).

[2] D. Litwin, K. Radziak, A. Czyżewski, J. Galas, T. Kryszczyński, N. Błocki, R. Szumski, J. Niedziela, "Multispectral interferometry for characterizing nano-objects", Proceedings Volume 12997, Optics and Photonics for Advanced Dimensional Metrology III; 129970F (2024) https://doi.org/10.1117/12.3017614, SPIE Photonics Europe, 2024, Strasbourg, France.

[3] D. Litwin, K. Radziak, A. Czyżewski, J. Galas, T. Kryszczyński, N. Błocki, R. Szumski, J. Niedziela, "A Reflected-Light-Mode Multiwavelength Interferometer for Measurement of Step Height Standards", Sensors 2024, 24(16), 5082; https://doi.org/10.3390/s24165082.

[4] D. Litwin, K. Radziak, A. Czyzewski, J. Galas, T. Kryszczyński, N. Błocki, R. Szumski, J. Niedziela, Waveplates retardance multispectral metrology with a Wollaston prism generated fringe field, Optical Measurement Systems for Industrial Inspection XIV, 13567, pp. 88-93, 2025/8/8, SPIE.

When Parts per Trillion Matter: Emergent Interfacial Charge Mediation Governing Ultra-Low NO_2 Sensing in Hybrid Nanocomposites

P. KAŁUŻYŃSKI [1], M. PROCEK [1], A. STOLARCZYK [2], K. GŁOSZ [2], T. JAROSZ [2]

1Department of Optoelectronics, Silesian University of Technology, Gliwice, Poland, Boleslawa Krzywoustego 2 Street, Gliwice, 44-100, Poland
2Department of Physical Chemistry and Technology of Polymers, Silesian University of Technology, Gliwice, Poland, ks. M. Strzody 9 Street, Gliwice, 44-100, Poland

e-mail address: pkaluzynski@polsl.pl

The pursuit of ultra-trace nitrogen dioxide detection at the parts-per-trillion level increasingly exposes the limitations of conventional chemoresistive sensing paradigms, where sensitivity gains are often achieved at the expense of signal stability and mechanistic clarity. Hybrid organic–inorganic nanocomposites offer a compelling alternative by enabling deliberate mediation between p- and n-type charge transport pathways; however, such systems are inherently prone to competing conductivity mechanisms that evolve over time and under environmental stimuli (Fig. 1).

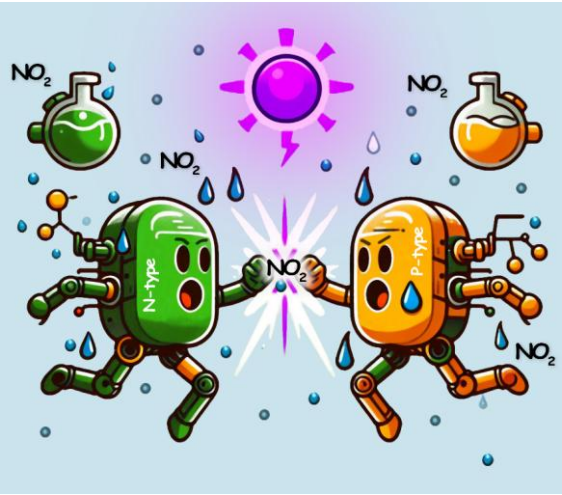

Fig. 1. Graphical abstract of p- and n-type mediated NO2 sensor response

Here, we report a systematic investigation of charge transport mediation in a ZnO/graft-copolymer nanocomposite engineered for room-temperature NO_2 sensing. By combining controlled variation of polymer fraction with ageing, humidity exposure, and ultraviolet activation, we demonstrate that sensor performance is governed not by a static p–n junction model, but by a dynamic balance between parallel and competing conduction channels. Freshly prepared receptor layers exhibit predominantly p-type behavior, which progressively transitions toward n-type conductivity upon ageing, a process markedly accelerated under humid conditions.

Electrochemical Impedance Spectroscopy (EIS) and Electron Paramagnetic Resonance (EPR) spectroscopy reveal that UV irradiation induces efficient photogeneration of charge carriers in the inorganic phase, while simultaneously activating interfacial charge transfer pathways mediated by the polymer matrix. Exposure to NO_2 introduces an additional level of complexity: depending on the relative contribution of p- and n-type domains, gas adsorption can either reinforce or counteract the prevailing conduction mechanism, directly impacting baseline resistance stability and sensor response linearity.

Crucially, we show that this apparent instability can be harnessed rather than suppressed. By precisely tuning the organic-to-inorganic ratio and exploiting controlled photodegradation processes, the competing charge transport pathways are driven toward a quasi-equilibrium state. This stabilization enables reproducible sensing responses and an exceptional limit of detection reaching 50 ppt NO_2 under UV-assisted operation at room temperature.

These results demonstrate that ppt-level gas detection is not merely a function of surface reactivity, but emerges from intentional control over multiscale charge mediation in hybrid nanocomposites. The presented framework establishes hybrid semiconductor mediation as a powerful design strategy for next-generation chemoresistive sensors, reconciling extreme sensitivity with long-term operational stability.

Novel van der Waals Materials for Polarization-Sensitive Photodetection

A. K. TOŁŁOCZKO [1], J. ZIEMBICKI[1], S. J. ZELEWSKI[1], M. GRODZICKI[1], M. ROSMUS[2], R. KUDRAWIEC[1]

[1] *Wrocław University of Science and Technology, Wybrzeże Wyspiańskiego 27, 50-370 Wrocław, Poland*
[2] *Solaris National Synchrotron Radiation Centre, Jagiellonian University, Czerwone Maki 98, 30-392 Kraków, Poland*

e-mail address: agata.tolloczko@pwr.edu.pl

Van der Waals (vdW) crystals constitute a versatile class of low-dimensional materials whose properties can be tailored through thickness control, interface engineering, and heterostructure design. Owing to their atomically sharp interfaces, mechanical flexibility, and strong light-matter interaction, vdW materials have become an important platform for optical and photonic systems [1].

Among them, group IV monochalcogenides (MX, where M = Ge, Sn and X = S, Se) are semiconducting vdW crystals that combine strong optical absorption, environmental stability, and composition based on earth-abundant, non-toxic elements [2]. A distinctive feature of MXs is their orthorhombic crystal structure, which gives rise to pronounced in-plane anisotropy of electronic and optical properties. This anisotropy results in intrinsic linear dichroism, making MX materials promising candidates for polarization-sensitive photodetectors. Such devices are capable of detecting changes in light polarization after propagation through birefringent media, including crystalline materials and biological systems, such as protein solutions. Importantly, the intrinsic polarization selectivity can significantly simplify device architectures compared to conventional approaches relying on multiple optical components.

We present a comprehensive investigation of the origins of linear dichroism in MXs [3,4] and demonstrate a polarization-sensitive Ag/GeSe Schottky barrier photodetector [5]. The device exhibits fast temporal response, high on/off ratio, and a strong dependence of the photocurrent on the polarization direction of the incident light near the optical absorption edge.

Additionally, photoemission spectroscopy was employed to determine the Fermi level position, ionization potential, and band edge energies of selected MXs. These parameters are crucial for designing heterostructures and prediction of the electrical contact character (ohmic or Schottky) formed with different metals. Particularly interesting is the possibility of integration of MXs with their chalcogen-rich phase, MX_2. Group IV monochalcogenides are intrinsically p-type due to native acceptor defects, whereas dichalcogenides exhibit intrinsic n-type conductivity arising from donor defects [6]. This natural complementarity enables the formation of p-n heterojunctions without intentional doping. Their shared elemental composition, differing only in stoichiometric ratio, may allow for clean synthesis of the MX/MX_2 structures, within a single growth environment by appropriate control of growth conditions.

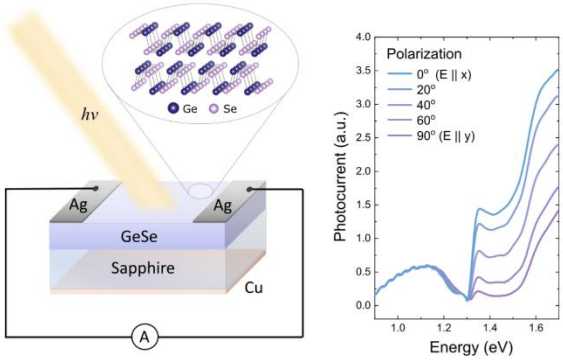

Fig. 1. Schematic illustration of the Ag/GeSe Schottky barrier photodetector and its polarization-depended spectral response.

References:

[1] K.S. Novoselov et al., Science, 353, 6298 (2016)
[2] L.C. Gomes, A. Carvalho, Phys. Rev. B, 92 (8), 085406 (2015)
[3] A.K. Tołłoczko et al., Adv. Optical Mater., 12, 2302049 (2024)
[4] A.K. Tołłoczko et al., Small, 21, 2410903, (2025)
[5] A.K. Tołłoczko et al., J. Mater. Chem. C, 9, 14838, (2021)
[6] A.K. Tołłoczko et al., J. Phys. Chem. C, 128, 16640−16651 (2024)

Practical Implementation of Beer-Lambert Law in Gas Detection

K. JABŁOŃSKI[1], T. KORZEC[1], M. BAŁECKI[1]

[1] Atest Gaz A. M. Pachole sp. j., ul. Spokojna 3, 44-109 Gliwice, Polska

e-mail address: k.jablonski@atestgaz.pl

In the context of electromagnetic radiation, transmittance means a material's ability to allow electromagnetic radiation to pass through.

$$T = \frac{I}{I_0}; \qquad (1)$$

where: I_0 is the intensity of radiation entering an absorbing body; I is the intensity of radiation after passing through the body.

Complementary quantity is called absorptance and is defined as:

$$ABT = 1 - \frac{I}{I_0}. \qquad (2)$$

Absorbance is a measure of the amount of electromagnetic radiation absorbed by a substance, expressed as a natural logarithm:

$$ABB = \ln\left(\frac{I_0}{I}\right). \qquad (3)$$

The absorption of electromagnetic radiation by a partially absorbing medium is described by the Lambert–Beer law. This law states that absorbance is directly proportional to the concentration of the absorbing substance and to the thickness of the layer through which the radiation passes, which can be expressed by the equation:

$$ABB = k \cdot L \cdot C; \qquad (4)$$

where: k is absorption coefficient, which is characteristic of a given substance and wavelength; L is length of optical path; C is concentration of absorbing substance.

After substituting (2) and (3) and transforming to calculate the concentration we get:

$$C = -\ln\frac{(1 - ABT)}{kL}. \qquad (5)$$

This law is widely used for measuring gas concentrations. One of the designs used for this purpose is the Non-Dispersive Infrared (NDIR) sensor. Its construction typically includes a broadband infrared source and a dual-channel detector. One of the channels, called the active channel, has an optical filter that allows observation of light intensity in a band where the measured gas strongly absorbs radiation, while the reference channel has a filter tuned to a band where the target substance absorbs weakly enough.

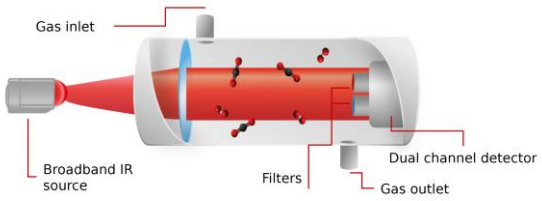

Fig. 1. Non-dispersive infrared sensor schematic.

Since we are only interested in changes in light intensity caused by the presence of the gas, and not by other factors such as source aging, optical contamination, or other substances, the signal from the active channel (A) is divided by the signal from the reference channel (R), and the resulting ratio is proportional to the intensity of light on the active channel. We can't know exact value of I_0, but above relation provide all necessary information. Therefore, Eq. (2) can be approximate in the form:

$$ABT = 1 - \frac{\frac{A}{R}}{\frac{A_0}{R_0}}; \qquad (6)$$

where A/R is the current measurement, while A_0/R_0 is the ratio of the signals from the active and reference channels in clean air, referred to as the sensor $zero$. Therefore, Eq. (6) can be expressed as:

$$ABT = 1 - \frac{A}{zero \cdot R}. \qquad (7)$$

ABT cannot be directly applied to Eq. (5). The active-channel filters in NDIR sensors are broad and cover many absorption lines with different absorption coefficients, as well as regions between these lines where no absorption occurs [3]. For this reason, the measurement A contains "background" light, so the value of A cannot reach 0, and thus ABT cannot reach 1.

Knowing the contribution of the background to the measured signal, we can normalize it. The maximum achievable value of absorption (light loss) for a given gas and sensor unit is called the $span$. We then obtain the calibrated absorbance:

$$ABT_C = \frac{1 - \frac{A}{zero \cdot R}}{span}. \qquad (8)$$

In Eq. (5), the product kL remains unknown. It is constant for a given sensor and substance, and from the model's point of view there is no need to separate it into individual factors. For the purposes of the static characteristic model, we can replace it with a single coefficient: $kL = \frac{1}{W}$. Due to imperfections of the measurement method, such as the presence of multiple optical paths (modes) between the source and the detector, it is necessary to introduce a coefficient P that corrects the curvature of the sensor characteristic. The value of P is usually close to 1. Equation (5) then takes the form:

$$C = [-\ln(1 - ABT_C) \cdot W]^P. \qquad (9)$$

The obtained mathematical model of the static characteristic of an NDIR sensor has four parameters: P, W, $zero$, and $span$. The $zero$ is determined directly for each individual sensor unit; the coefficients P and W are fitted numerically by minimizing the mean squared error between the model and the experimentally obtained results; while the span is fitted for each sensor unit by solving a linear equation at a point sufficiently close to the sensor's full-scale range.

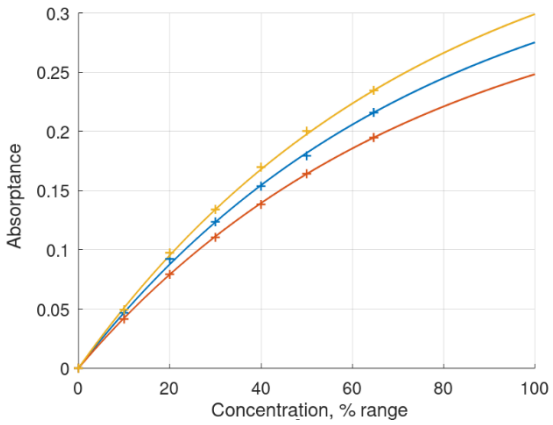

Fig. 2. Measured absorptances (crosses) and model response (lines).

Model fitting and verification were performed for propane in the range of 0–65% LEL, as shown in Fig. 2. The obtained error for three sensors did not exceed 1.3% of the full-scale range, which is considered a good result. The full error profiles are shown in Fig. 3. Table 1 presents the maximum errors for other tested substances.

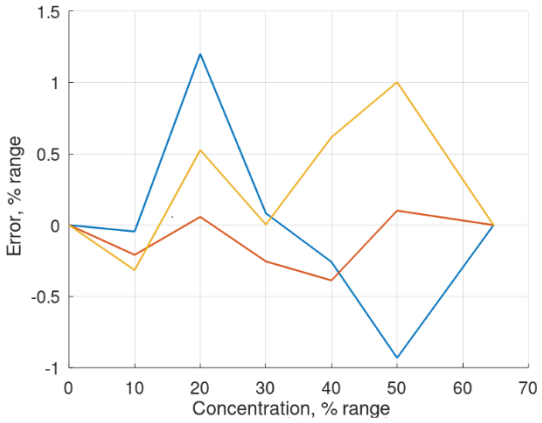

Fig. 3. Errors between model response and measurements.

Tab. 1. Errors obtained with other substances at 100% LEL range.

Substance	Range, % vol.	Maximum error, % range
Ethylene Oxide	2.6	2.0
Hexane	1.1	0.4
Pentane	1.5	0.6
Xylene	1.1	1.1
Acetone	2.5	1.1
Toluene	1.2	3.8
Ethyl Acetate	2.0	0.8
Styrene	0.9	3.0

Acknowledgments: This work was supported by European Regional Development Fund as part of the "Ulepszone metrologicznie optoelektroniczne czujniki gazu do przemysłowych systemów bezpieczeństwa" project.

References:

[1] Mayerhöfer, T. G., Mutschke, H., & Popp, J. (2016). Employing theories far beyond their limits—the case of the (Boguer-) beer–lambert law. ChemPhysChem, 17(13), 1948-1955.

[2] Jha, R. K. (2021). Non-dispersive infrared gas sensing technology: A review. IEEE Sensors Journal, 22(1), 6-15.

[3] Klingbeil, A. E., Jeffries, J. B., & Hanson, R. K. (2007). Temperature-dependent mid-IR absorption spectra of gaseous hydrocarbons. Journal of Quantitative Spectroscopy and Radiative Transfer, 107(3), 407-420

Biophotonic Fiber Optic Measurement System as an Advanced Medical Diagnostic Tool Increasing the Safety of Urological Procedures

M. SŁADEK [1], M. PROCEK [1], K. BARCZAK [1], E. MACIAK[1]

[1] Silesian University of Technology, Akademicka 2A, 44-100, Gliwice, Poland

e-mail address: michal.sladek@polsl.pl

Modern medicine is constantly searching for innovative solutions that will improve patient treatment standards. In the field of urology, one of the most important factors is the safety of endoscopic procedures in the treatment of kidney stones. There are two minimally invasive methods of breaking up kidney stones. These are ureterorenoscopic lithotripsy (URSL) and retrograde intrarenal lithotripsy (RIRS). Both methods are the gold standard for the treatment of kidney stones, with the difference that URSL is a procedure involving the insertion of a rigid ureterorenoscope into the ureter, while RIRS involves the insertion of a flexible ureterorenoscope into the kidney itself. The stones are broken up using a holmium laser [1].

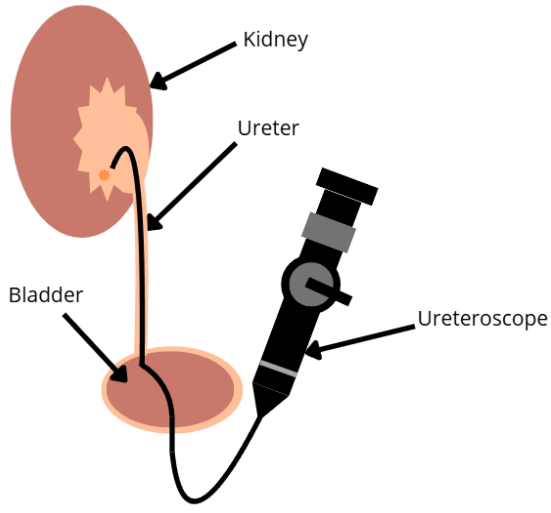

Fig. 1. Simplified diagram of the RIRS procedure

The research problem is how to measure physical parameters during procedures. As a result of laser operation and the procedure itself, the intrarenal temperature (IRT) increases, and the intrarenal pressure (IRP) rises due to the supply of irrigation fluid [3 - 4], which poses a risk of damage to the kidneys or urinary tract.

One solution to this problem is the development of miniature measuring transducers using fiber optic pressure and temperature sensors.

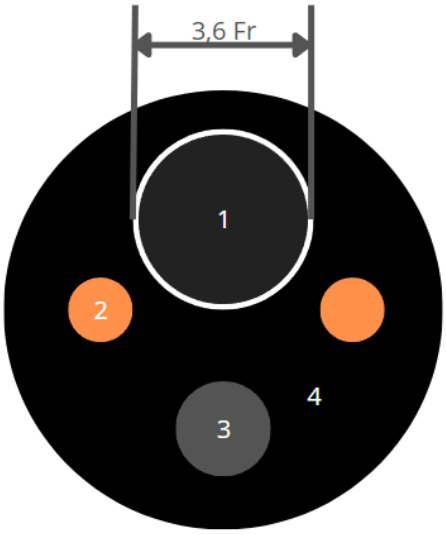

Fig. 2. Simplified front of the ureterorenoscope, 1 – working channel (diameter 3.6 Fr), 2 – dual light source, 3 – camera, 4 – sheath

The paper will present the application potential in IRP and IRT measurements of fiber optic sensors with Bragg gratings (FBG) and interferometric Fabry-Pérot structures (FO-FPI). These sensors should enable the determination of IRP and IRT parameters in situ during the surgical procedure. In order to develop a solution, challenges such as miniaturization and flexibility resulting from the design of the tools used in the procedures must be addressed. Various approaches to solving this problem can be found in the literature. Research on miniature fiber optic sensors with the potential for technological integration with ureterorenoscopes leads to increased safety in urological procedures such as RIRS and URSL.

Acknowledgments: This research was financially supported by the Silesian University of Technology research subvention (SUBB) under Grant No. 05/040/BK_26/2044

References:

[1] Pauchard, F.; Ventimiglia, E.; Corrales, M.; Traxer, O. A Practical Guide for Intra-Renal Temperature and Pressure Management during Rirs: What Is the Evidence Telling Us. J. Clin. Med. 2022, 11, 3429.

[2] lukasza.pl, access 22.11.2025

[3] Patel, Anuj U. et al., Development and Testing of an Anatomic in vitro Kidney Model for Measuring Intrapelvic Pressure During Ureteroscopy, Urology, Volume 154, 83 – 88

[4] Sierra, A.; Corrales, M.; Kolvatzis, M.; Doizi, S.; Traxer, O. Real Time Intrarenal Pressure Control during Flexible Ureterorrenscopy Using a Vascular PressureWire: Pilot Study. J. Clin. Med. 2023, 12, 147

Fabrication and Applications of Nonlinear Soft-Glass Fiber and Nanostructured Elements Based on 3D-Printed Preforms

P. WIENCŁAW [1,3], P. GOŁĘBIEWSKI [1,2], G. STĘPNIEWSKI[2], B. PAŁUBA[2], P. SOCHA[2], A. FILIPKOWSKI[2], D. PYSZ[2], W. LIU[4], A. BURGS[3], R. KASZTELANIC[1,2], R. BUCZYŃSKI[1,2]

[1] Faculty of Physics, University of Warsaw, Pasteura 5, 02–093 Warsaw, Poland.
[2] Lukasiewicz Research Network – Institute of Microelectronics and Photonics, al. Lotników 32/46, 02–668 Warsaw, Poland.
[3] Sygnis S.A., al. Grunwaldzka 472, 80–309 Gdansk, Poland.
[4] China-Poland Joint Laboratory on Measurement and Control Technology, Huazhong University of Science and Technology, Wuhan 430074, China.

e-mail address: p.wienclaw@uw.edu.pl

Abstract: Traditional manual assembly techniques for microstructured optical fibers, such as the stack-and-draw method, are often limited by non-scalability and the risk of human error. This work explores the application of Glass Direct Ink Writing approach, to automate the fabrication of complex glass preforms. Using a pressure-controlled extrusion system, we demonstrate the horizontal deposition of fused soft glass directly from bulk blocks of lead borate glass with a high nonlinear refractive index ($n_2 = 39 \times 10^{-20}\ m^2/W$).

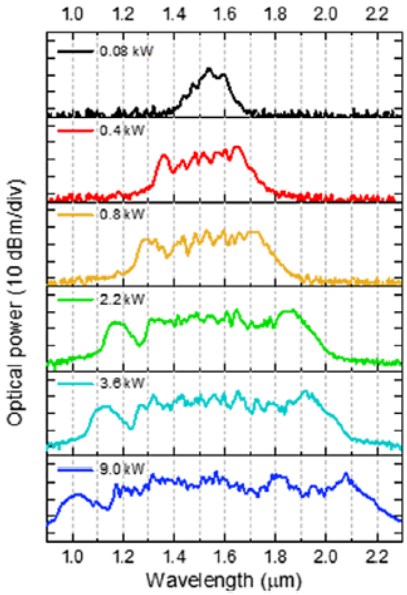

Fig. 1. Comparison of measured supercontinuum spectra for selected peak powers of the input pulse.

The viability of the 3D-printed method was validated through its application in nonlinear optics, where we achieved octave-spanning supercontinuum generation (940–2230 nm) in a 21 cm-long section of photonic cristal fibre (PCF) produced from 3D printed preform (fig 1 and fig 2).

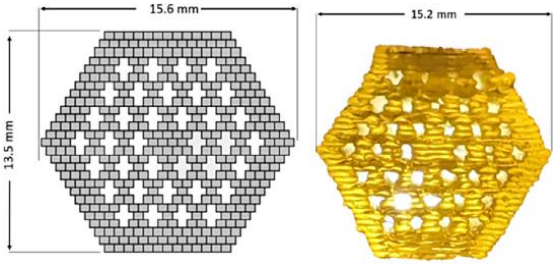

Figure 2. PCF preform core CAD model cross-section and the resulting 3D-printed glass structure.

The versatility of this additive method enables integrating two distinct types of soft glass within a single process. This capability has been utilized to manufacture nanostructured elements with specific refractive index distributions, including top-hat, vortex, zebra, PCF, as well as passive flat lenses.

Furthermore, the longitudinal control, allows for the integration of multiple design iterations within a single preform. This is demonstrated by structural transitions, such as a core geometry shifting from a square to a circular profile, providing a unique platform for producing different fiber designs in one manufacturing cycle.

Acknowledgments: This work was supported by the MAESTRO UMO-2022/46/A/ST7/00238 grant (National Science Centre, Poland), POIR.01.01.01-00-1326/17 grant (the European Regional Development Fund), and DWD/6/0464/2022 grant (The “Industrial Doctoral Program” of the Minister of Education and Science, Poland).

References:

[1] P. Wienclaw et al., Advanced Science 2025, 10.1002/advs.202511930.
[2] P. Golebiewski et al., Additive Manufacturing 2024, 79, 103899

A Process Design Kit for Mid-Infrared Photonic Pilot Line

S. STOPIŃSKI[1,2,3], J. OLSZEWSKI[1,2,4], A. ŚLIPEK[1,2], A. POŁATYŃSKI[1,5], M. LELIT[1,6], K. ANDERS[1,2,3], R. PIRAMIDOWICZ[1,2,3]

[1]Warsaw University of Technology, Institute of Microelectronics and Optoelectronics, Koszykowa 75, 00-662 Warsaw, Poland
[2]VIGO Photonics, Poznańska 129/133, 05-850 Ożarów Mazowiecki, Poland
[3]LightHouse sp. z o.o., Stefczyka 34, 20-151 Lublin, Poland
[4]Wrocław University of Science and Technology, Department of Optics and Photonics, Wyb. Wyspiańskiego 27, 50-370 Wrocław, Poland
[5]VPIphotonics GmbH, Carnotstr. 6, 10587 Berlin, Germany
[6]Warsaw University of Technology, Centre for Advanced Materials and Technologies CEZAMAT, Poleczki 19, 02-822 Warsaw, Poland

e-mail address: stanislaw.stopinski@pw.edu.pl

Photonic integration technologies are continuously maturing [1]. Today, the most advanced platforms are already deployed commercially, particularly in telecommunications and datacom applications, where they enable advanced multi-channel, high-speed transmitters and receivers. Significant progress has also been made in the fiber-optic sensing market, where integrated interrogator systems are increasingly commercialized.

However, several challenges remain to further accelerate the development of integrated technologies [2]. These vary with the targeted spectral operating range. Classical near-infrared platforms (InP, SOI, and SiN), operating in the telecom wavelength windows, require scalable manufacturing methods, versatile heterogeneous integration technologies, high-throughput, high-port-count generic packaging solutions, and entirely new classes of devices for optical communication based on quantum technologies.

In contrast, the challenges in the visible (VIS) and mid-infrared (MIR) spectral ranges are markedly different. This is primarily due to the relatively low technology and manufacturing readiness levels of platforms suitable for these wavelengths. As a result, there is a strong need for the efficient development of manufacturing technologies of light sources, detectors, modulators, and passive waveguiding circuits. The level of complexity is further increased by the fact that fully monolithic approaches are currently not viable, while heterogeneous integration techniques still require substantial advancement. Consequently, several European R&D institutions have joined forces and are currently working on a new distributed photonic pilot line, PIXEurope [3].

In this work, we present and discuss the development of a new process design kit (PDK) comprising a set of advanced software tools for modeling, simulation, and design of photonic integrated components and circuits. The PDK is being developed within the PIXEurope project for a mid-infrared (3.0 to 8.0 µm) photonic integration technology based on the Ge-on-Si material platform, MIRPIC [4]. The platform, developed by Warsaw University of Technology, provides a range of waveguiding components, including low-loss passive waveguides (attenuation coefficient below 3 dB/cm), multi-mode interference couplers, arrayed waveguide grating demultiplexers, and grating couplers. Furthermore, it offers the potential for hybrid or heterogeneous integration with active devices, such as quantum and interband cascade lasers and type-II superlattice photodetectors. The latest achievements of the MIRPC PDK and the remaining challenges are presented and discussed.

Acknowledgments: This work received support from the National Center for Research and Development through projects MIRPIC (TECHMATSTRATEG-III/0026/2019-00) and HyperPIC (FENG.02.10-IP.01-0005/23, IPCEI ME/CT). This work has received funding from the European Union's Horizon Europe under Grant Agreement #101213727, Chips Joint Undertaking.

References:

[1] S. Shekhar et al., "Roadmapping the next generation of silicon photonics", Nat. Commun 15, 751 (2024).
[2] C. Zhang et al., "Integrated photonics beyond communications" Appl. Phys. Lett. 4 December 2023; 123 (23): 230501.
[3] https://pixeurope.eu/#about
[4] R. Piramidowicz et al., "HyperPIC: on the road to mid-infrared photonic integrated circuits", Proc. SPIE 13369 133690

Use of Broadband Propagation in the Metrology of Waveguide Layers

K. GUT[1]

[1] Silesian University of Technology, Department of Optoelectronics,
2 Krzywoustego St.,44-100 Gliwice, Poland

e-mail address: kazimierz.gut@polsl.pl

Optical characterization techniques have always been a fascinating tool for researchers, allowing them to discover and study fundamental properties of materials. Because waveguides are fundamental components of integrated optical devices, characterizing such light-guiding structures plays a crucial role in the design and manufacturing processes. One of the crucial waveguide properties that must be determined is the effective refractive index. Methods for determining this parameter for a single wavelength have been described in the literature. A commercial device for determining this parameter is also available. This paper demonstrates how to determine the effective refractive index for the entire spectral range in a waveguide.

The paper presents experimental investigations of a planar waveguides The white light emitted by the LED diode was fed into a multimode optical fiber terminated with a collimator. Then, the light, after passing through the polarizer, falls on the input prism and is introduced into the planar waveguide. The propagating light after traveling a distance l in the waveguide is output through the output prism [1-3].

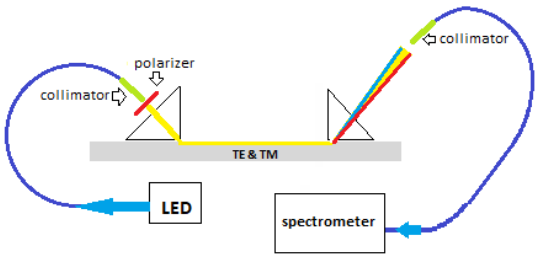

Fig. 1. Test stand for introducing white light into a planar waveguide and measuring the spectral distribution at the output.

The output beam, falls on the collimator connected to the spectrometer with a multimode optical fiber (Figure1).

The polarizer at the input of the system enables (by rotating around the axis) an even division of the optical power between the orthogonal basic modes TE0 and TM0. The rotation of the output polarizer enables recording of the following modes spectrum: TE0 (transmission axis of the polarizer is parallel to the surface of the waveguide - 0°) and TM0 (transmission axis of the polarizer is rotated by 90°). The collimator that records the output light can move perpendicularly to the beam. Knowing the spatial spectral distribution and the distance of the collimator from the output point, the dependence of the effective refractive index on wavelength can be determined. Subsequent calculations can be used to determine the refractive index dispersion of the waveguide layer. An example image of the output spectrum for both TE and TM polarizations is shown in Figure 2.

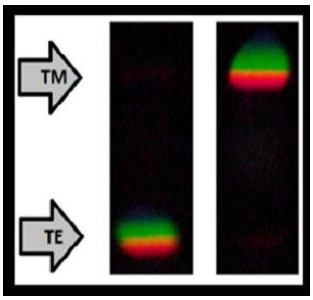

Fig. 2. Widmo wyjściowe dla obu polaryzacji TE i TM.

References:

[1] K. Gut, Opt. Express, 25, 3111 (2017)
[2] K. Gut, Nanomaterials, 9, 729 (2019)
[3] K. Gut, M. Błahut, Sensors, 23, 6092 (2023)

Design of a Mid-IR Suspended GaAs/AlGaAs Membrane Waveguide Gas Sensor for CO_2 Detection

A. ŚLIPEK[1,2], J. OLSZEWSKI [1,2,3], T. MARTYNKIEN[2,3], J. JUREŃCZYK[2], K. ANDERS[1,2], S. STOPIŃSKI[1,2], R. PIRAMIDOWICZ[1,2]

[1]Warsaw University of Technology, Institute of Microelectronics and Optoelectronics, Koszykowa 75, 00-662 Warsaw, Poland
[2]VIGO Photonics S.A., Poznańska 129/133, 05-850, Ożarów Mazowiecki, Poland
[3]Wrocław University of Science and Technology, Department of Optics and Photonics, Wybrzeże Wyspiańskiego 27, 50-370 Wrocław, Poland

e-mail address: adrian.slipek@pw.edu.pl

The mid-infrared (MIR) spectral range (3-50 µm [1]) plays a key role in sensing applications, enabling the identification of trace amounts of gas analytes through their characteristic absorption bands [2, 3]. Although bulk systems still dominate this area, there is an increasing trend toward miniaturization using integrated photonics technologies.

In this work, we present and discuss the design of a mid-infrared integrated gas sensor based on a new GaAs/AlGaAs material platform. It enables monolithic integration of interconnects and sensing waveguides, and input/output grating couplers, providing an efficient fiber-optic or free-space optical interface [4]. The cross-section of the proposed sensing waveguide, shown in Fig. 1, is based on a suspended GaAs/AlGaAs membrane rib architecture [4-6].

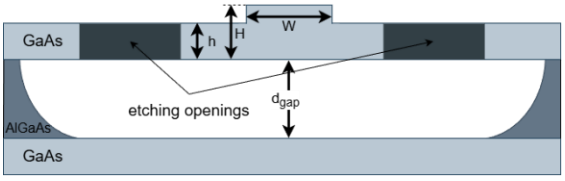

Fig. 1. Schematic geometry of suspended GaAs on AlGaAs waveguide with etch openings. Calculated confinement factor and propagation loss for H = 500 nm, W = 1.95 µm, h = 400 nm, dgap > 4.5 µm, and wavelength 4.26 µm are about 125% and <3dB/cm, respectively

The design is optimized for CO_2 detection at 4.26 µm, a key absorption line in the MIR "fingerprint" region, relevant for environmental monitoring, industrial, and digital health applications.

To maximize sensitivity, the design employs a suspended GaAs membrane that maximizes overlap between the guided mode and the target gas. This configuration leverages the slow-light characteristics of the fundamental TM-like mode to increase the effective interaction path length. Consequently, this results in an interaction level that exceeds that of conventional free-space propagation, as quantified by the confinement factor defined as [8,9]:

$$\Gamma = \frac{N_g \int_a \varepsilon_a |E|^2 \, dxdy}{n_a \int_{-\infty}^{+\infty} \varepsilon |E|^2 \, dxdy} [\%],$$

where N_g is the group effective refractive index of the mode, n_a – the refractive index of the region in which the analyte is located, E – the distribution of the electric field intensity, and ε – the distribution of dielectric permittivity (ε_a – in the region of the analyte presence).

In numerical simulations, material models refined by experimental spectroscopic ellipsometry measurements (Fig. 2) are used, thus ensuring high predictive accuracy. For a waveguide height of H = 500 nm, we report a confinement factor of approximately 125%, propagation losses below 3 dB/cm, and a grating-coupling efficiency of 18% for TM polarization. Initial experimental trials on the GaAs-on-AlGaAs substrate have been conducted, confirming the platform's feasibility for subsequent prototype fabrication.

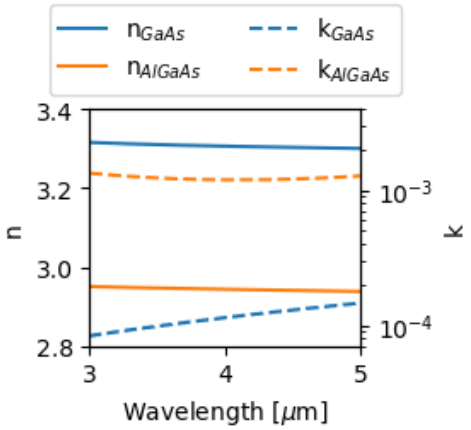

Fig. 2. Results of ellipsometry measurements of fabricated GaAs and AlGaAs samples.

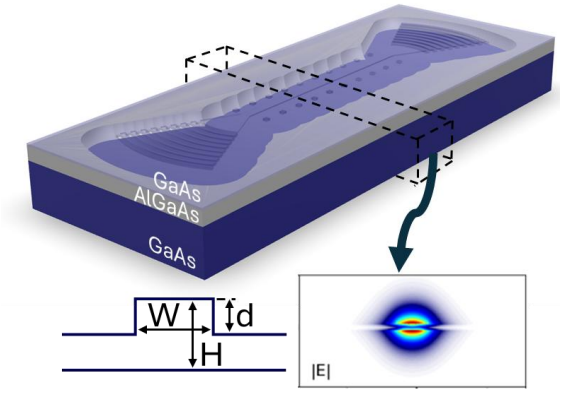

Fig. 3. Visualisation of the proposed integrated sensor architecture. The plot in the lower-right corner shows the electric field profile of the guided TM-polarized fundamental mode. Partial transparency of the top GaAs layer was added for visualisation purposes.

To ensure practical device viability, we implemented a design framework that optimizes the positions of etching openings to reduce footprint and losses introduced by their presence. Finally, we demonstrate that with an optimized waveguide geometry, the system reaches the theoretical limit of detection [9, 10] for an optimized waveguide length [10] in the sub-ppm range.

This design provides a robust solution for miniaturized, high-performance environmental and industrial gas sensing in the MIR fingerprint region.

This approach provides substantial advantages over conventional SOI-based MIR photonics, which are limited by SiO_2 absorption above ~4 µm, as well as over bulk optics, offering miniaturization, reduced power requirements, and enhanced interaction per unit length.

Acknowledgments: This work received support from the National Center for Research and Development through projects MIRPIC (TECHMATSTRATEG-III/0026/2019-00) and HyperPIC (FENG.02.10-IP.01-0005/23, IPCEI ME/CT). This work has received funding from the European Union's Horizon Europe under Grant Agreement #101213727, Chips Joint Undertaking (Chips JU).

References:

[1] ISO 20473:2007, Optics and Photonics – Spectral Bands
[2] Q. Liu, J.M. Ramirez, V. Vakarin et al., Light Sci. Appl. 7, 17138 (2018)
[3] C. Mitchell, T. Hu, S. Sun et al., APL Photonics 9, 031101 (2024)
[4] T.H Stievater, M. W. Pruessner et al., Appl. Opt. 54, 31 (2015)
[5] T.H Stievater, R. Mahon et al., Opt. Lett. 39, 945-948 (2014)
[6] H. Cong, B. Yang, W. Wei et al., Appl. Phys. Lett.; 119, 13 (2021)
[7] S. E. Hansen, G. Arregui et al., Opt. Express 31, 17424 (2023)
[8] M. Vlk, A. Datta et al., Light Sci. Appl. 10, 26 (2021)
[9] J. Lim, J. Shim et al., ASC Photonics 11.10.1021 (2024)
[10] J. Shim, J. Lim et. al., Opt. Express 21, 18037-18058 (2021)

Optical Transducers for Measuring Small Temperature Changes in Aqueous Environment Caused by the Absorption of High-Energy Radiation

C. TYSZKIEWICZ [1], M. ZIĘBA [1], P. KARASIŃSKI [1], Z. OPILSKI [1], K. BARCZAK [1]

[1] Silesian University of Technology, Department of Optoelectronics, ul. B. Krzywoustego 2 44-100 Gliwice

e-mail address: cuma.tyszkiewicz@polsl.pl

One of the most common methods of cancer treatment is the irradiation of tumours with high-energy radiation. Part of this energy is absorbed by cancer cells and converted into heat, raising the local temperature. The success of radiotherapy depends on the precise and uniform delivery of the dose to the treated area. An optimally planned dose distribution is designed to damage cancer cells while sparing the healthy cells surrounding the treated area. Too low a dose leads to the survival of cancer cells and recurrence of the disease. Too high a dose leads to damage to healthy tissue. The doses that cause local cancer cure without a strong reaction in healthy tissues fall within a narrow range. It is estimated that a 5% change in dose can affect the probability of cure by up to 25%. Maintaining precision at 3.5% is difficult. The fundamental issue in such cancer therapy is to determine a safe dose of high-energy radiation for the patient. To this end, the dose absorbed in water must be reproduced and transferred to the therapeutic dosimeter during calibration. In practice, research is conducted on so-called phantoms to resolve these issues. The absorbed dose of high-energy radiation can be determined based on the temperature increase at the irradiation site. The radiation doses used in practice cause slight temperature increases, hence it is necessary to use a temperature meter with a very high resolution, at the level of 10^{-3} K. This requirement can be met by optical measurement methods.

The presentation will show the results of modelling three types of optical interferometers used to measure temperature changes. The first one uses an interferometer with ring resonators made using SOI (silicon-on-insulator) technology. The second type of modelled interferometer takes the form of a photonic mirror produced on the front of an optical fibre. The photonic mirror is constructed from periodically occurring pairs of layers with high and low refractive indices, Si and TiO_2, respectively. Photonic structures with defects were also analyzed. The third type of transducer uses a Fabry-Perot interferometer with an air cavity created between the ends of optical fibres.

Acknowledgments: The work was supported by the project PM-II/SP/0042/2024/02, founded by the state budget through the Polish Minister of Science and Higher Education under the Polish Metrology II program.

Ministry of Science and Higher Education
Republic of Poland

Concept to Produce Next-Generation Low-Loss ZBLAN Optical Fibers

A. DJORDJEVIC [1,2,3], T. UNGER [3], S. LEYER [2], H. A. MOSER [3], R. BUCZYŃSKI [1]

[1]Faculty of Physics, University of Warsaw, ul. Pasteura 5, 02-093, Warsaw, Poland
[2]Faculty of Science, Technology and Medicine, University of Luxembourg, rue Richard Coudenhove-Kalergi 6, 4365, Luxembourg, Luxembourg
[3] Flawless Photonics S.à r.l., rue du Fort Wallis 4, 2714, Luxembourg, Luxembourg

e-mail address: a.djordjevic@uw.edu.pl

Currently, there are two promising research areas with the potential to produce next-generation optical fibers for telecommunication applications, solving the exorbitant energy consumption problem of the telecommunication network and replacing solid-core SiO_2. Research on SiO_2 hollow-core optical fibers is advancing, but there are still challenges lying ahead [1, 2]. Another potential solution is to produce optical fibers from ZBLAN glass. This material has a, relative to SiO_2, 100 times lower theoretical attenuation in the mid-infrared range [3, 4]. The production of pristine ZBLAN optical fibers is challenging and currently the lowest loss achieved for ZBLAN optical fibers at the telecommunication wavelength of 1.5 µm is still 10 times higher than the best solid-core silica fibers, see Fig. 1.

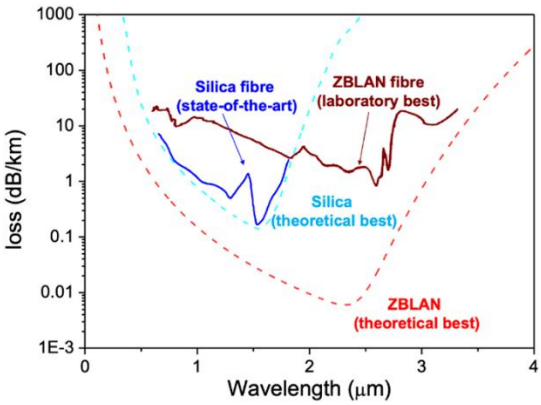

Fig. 1. Attenuation of SiO_2 and ZBLAN optical fibers [5, 6]

This is mainly due to ZBLAN's tendency to crystallize. One way to solve this problem is the elimination of impurities in the ZBLAN raw materials. There is another way to avoid crystallization. A study from 2018 has revealed the cooling rate needed, when cooling down ZBLAN from the melt to solid state, to produce amorphous ZBLAN glass [7]. This critical cooling rate is difficult to achieve for state-of-the-art production methods, like the rotational casting process, see Fig. 2, where first a glass preform needs to be produced, and then in a second step softened at one end to be drawn to fiber.

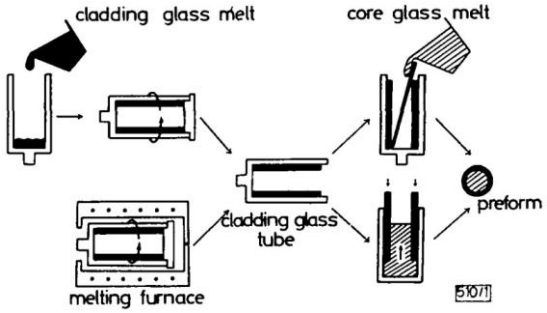

Fig. 2. Rotational casting method [8]

Another challenge for these methods is producing longer lengths of fiber needed for telecommunication applications.

Other alternative glass production methods, like crucible-drawing and extrusion, that can potentially be adapted to fulfill both targeted criteria, i.e. producing amorphous low-loss ZBLAN glass and drawing longer lengths of optical fibers, exist.

In this research, we present, based on these methods, a novel concept for a ZBLAN fiber drawing prototype. A numerical model was designed to support the most crucial process step of the concept.

Acknowledgments: This work was supported by the Luxembourg National Research Fund under the Industrial Fellowship Grant (N° 18038303).

References:

[1] S. Gao, H. Chen, Y. Xiong, Y. Sun, W. Ding, and Y. Wang, 2025 European Conference on Optical Communications (ECOC), pp. 1–4, (2025)
[2] B. Debord, F. Amrani, L. Vincetti, F. Gérôme, and F. Benabid, Fibers, vol. 7, no. 2, (2019)
[3] A. Torres, J. Ganley, and A. Maji, J Mater Sci, vol. 49, no. 22, pp. 7770–7781, (2014)
[4] S. Varma, S. E. Prasad, I. Murley, and T. A. Wheat, in Infrared Fiber Optics III, J. A. Harrington and A. Katzir, Eds., SPIE, (1992)

[5] I. Cozmuta, S. Cozic, M. Poulain, S. Poulain, and J. R. Martini, in Optical Components and Materials XVII, M. J. Digonnet and S. Jiang, Eds., SPIE, Mar. 2020, p. 25, (2020)
[6] https://www.laserfocusworld.com/test-measurement/research/article/16556282/optical-fiber-manufacturing-gravity-free-optical-fiber-manufacturing-breaks-earthly-limitations.
[7 T.-C. Ong, Queensland University of Technology, (2018)
[8] D. C. Tran, C. F. Fisher, and G. H. Sigel, Electron Lett, vol. 18, no. 15, pp. 657–658, (1982)

Design and Performance of a Home-Built Scalable Projection Microstereolithography Platform

M. PTASZEK [1], S. ERTMAN [1]

[1] Faculty of Physics, Warsaw University of Technology, Koszykowa 75, 00-662, Warsaw, Poland

e-mail address: michal.ptaszek.dokt@pw.edu.pl

3D microprinting has emerged as a powerful and versatile technique for the rapid fabrication of complex three-dimensional microstructures with a wide variety of applications, such as beam splitters [1] or lens arrays [2]. Nevertheless, most commercially available systems impose significant limitations on optical configuration, experimental flexibility, and the ability to implement custom exposure strategies, which restrict their applicability in advanced photonic and sensor research.

Projection microstereolithography is an advanced additive manufacturing technique that enables the fabrication of three-dimensional microstructures through the spatially controlled photopolymerization of photosensitive resins. The polymerization process is initiated by ultraviolet light, whose spatial distribution is precisely modulated using a micromirror array combined with projection optics, in a manner analogous to that of a digital optical projector. The structure is formed in a layer-by-layer fashion, with each newly exposed layer being sequentially stacked upon the previously cured one, allowing for the realization of complex geometries with high spatial resolution.

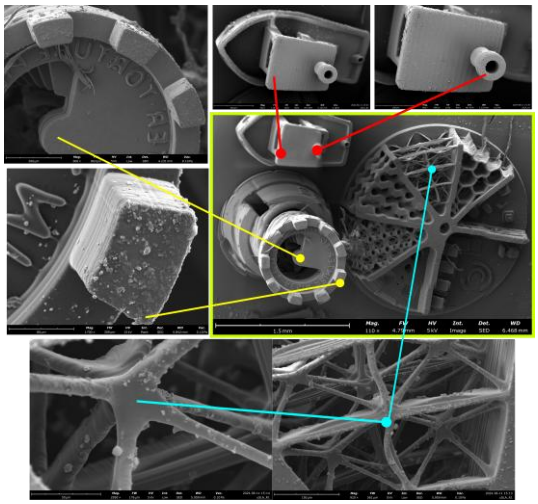

Fig. 1. *Example benchmark microprints fabricated using the developed system: 3D Benchy (FDM benchmark), 3D Rook (resin printing benchmark), and Opticon Test Geometry (universal additive manufacturing benchmark).*

In this work, we present a fully custom-designed projection-based 3D microprinting platform together with its complete development cycle, from the initial proof-of-concept prototype to a refined, high-fidelity system. The platform was developed entirely in-house, encompassing optical design, mechanical construction, electronic control, and software-based exposure management. The system employs a digital light projection (DLP) approach for high-resolution, layer-by-layer photopolymerization of photosensitive resins. A key feature of the proposed architecture is a modular and easily reconfigurable optical path that enables continuous scaling of the projected pixel size from 2 µm to 20 µm (where state-of-the-art commercial projection microstereolithography systems typically provide fixed pixel sizes on the order of several micrometers, most commonly in the ~5–10 µm range). This capability allows for precise control over printing resolution and build area, providing an optimal balance between feature fidelity and fabrication throughput that is tailored to specific applications.

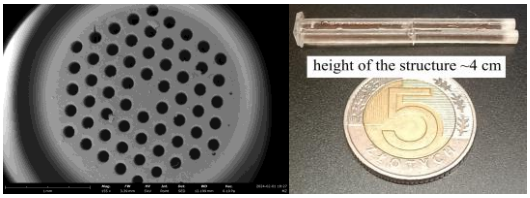

Fig. 2 *Photonic crystal fiber preform fabricated as a proof of concept for additive manufacturing using silica-based materials.*

The platform was intentionally optimized to provide a high degree of experimental freedom, facilitating rapid prototyping, systematic parameter exploration, and the investigation of novel microfabrication strategies. The open system architecture, based on readily available off-the-shelf components, enables straightforward maintenance, repair, and future expansion, including the integration of additional optical elements or motion stages. Using the developed setup, a wide range of three-dimensional microstructures was successfully fabricated,

including standard benchmark geometries for additive manufacturing (Fig.1), as well as periodic (Fig.3) and aperiodic architectures of particular relevance to integrated photonics and optical sensing. The resulting photonic microstructures exhibit high structural fidelity, excellent repeatability, and well-defined feature resolution, confirming the robustness and reliability of the proposed approach. Additionally, polymer-based preforms of photonic crystal fibers were fabricated (Fig 2) [3], as a proof of concept for further work with silica based resins, providing the capability of printing arbitrary sintered silica preforms.

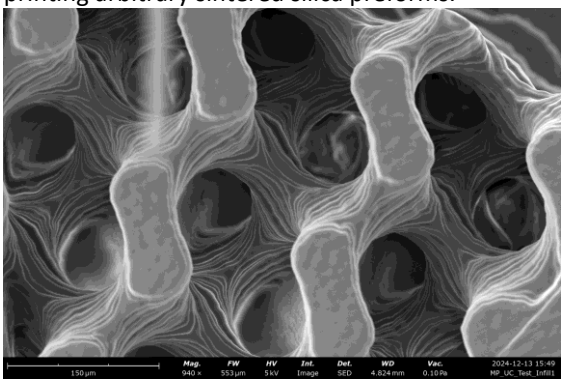

Fig. 3 *Gyroid-type periodic infill structure, as a part of benchmark structure*

Beyond single-material fabrication, the presented system establishes a foundation for future development of multimaterial microprinting capabilities. Such an extension would enable the fabrication of highly complex functional microdevices, including mechanically compliant MEMS components with integrated flexible linkages, structures incorporating functional materials, such as piezoelectric-loaded resins , as well as directly printed optical waveguides with spatially engineered refractive index profiles for core–cladding structures. The results demonstrate that custom projection-based microprinting platforms constitute powerful and flexible research tools for the development of next-generation photonic microstructures and advanced sensor technologies.

References:

[1] G. Stella et. al. Micro 3, 338-352, (2023)
[2] I.-B. Park et. al. Int. J. Precis. Eng. Manuf. 11, 483–490, (2010)
[3] L. Yanhua et. al. Appl. Phys. 12, 011322, (2025)

Silica Fiber with Nd:YAG Nanocrystals: the Influence of Fiber Drawing Process on Structure and Emission Properties of Nd^{3+} Cations

M. ADAMOWSKA [1,2], B. PAŁUBA [1], A. MARKOVSKYI [3], L. SOJKA [4], A. FILIPKOWSKI [3], K. OLSZEWSKA [5], D. PYSZ [1], T. RUNKA [5], G. STĘPNIEWSKI [3], R. KASZTELANIC [1], S. SUJECKI [4,6], R. BUCZYŃSKI [1]

[1] University of Warsaw, Faculty of Physics, Pasteura 5, 02-093, Warsaw, Poland
[2] University of Warsaw, Faculty of Chemistry, Pasteura 1, 02-093, Warsaw, Poland
[3] Lukasiewicz Research Network, Institute of Microelectronics and Photonics, Wolczynska 133, 01-919, Warsaw, Poland
[4] Wroclaw University of Science and Technology, Department of Telecommunications and Teleinformatics, Faculty of Electronics, Wybrzeze Wyspianskiego 27, 50-370, Wroclaw, Poland
[5] Poznan University of Technology, Institute of Materials Research and Quantum Engineering, Faculty of Technical Physics, Piotrowo 3, 60-965, Poznan, Poland
[6] Military University of Technology, Faculty of Electronics, gen. Sylwestra Kaliskiego 2, 00-908, Warsaw, Poland

e-mail address: m.adamowska2@uw.edu.pl

Nanotechnology is a big part of our daily lives. Nanomaterials, such as nanocrystals (NCs) and nanoparticles (NPs) are used in various fields including medicine, cosmetology, catalysis, agriculture, electronics, optical physics and much more [1, 2]. The reason behind such broad applications of these materials is their enhanced properties compared to bulk materials, due to significant quantum effects (e.g. surface plasmon resonance) and possibility of surface functionalization using diverse chemical compounds.

Recently, intense research have been conducted on designing optical fibers containing nanocrystals with active ions (e.g. Nd^{3+}, Tm^{3+}, Er^{3+}) inside of their core. Then, one can fabricate a fiber laser or amplifier combining properties of both glass matrix (obtaining long and flexible gain media) and crystals (a.o. narrow emission bands, no laser quenching caused by ion clusters formation).

In the case of optical fibers, there are few main ways to introduce the nanocrystals to the glass matrix, namely: direct introduction of crystals to the glass, formation of crystals during fiber drawing or crystallization after fiber fabrication [3]. Recently, the alternative and simple method of dip-coating was proposed to incorporate the microcrystals with active ions into the tellurite glass [4]. However, the aim of this research was not to obtain an optical fiber but a glass fiber with preserved microcrystals.

The aim of our project was to examine the structure and emission properties of Nd:YAG nanocrystals introduced to the silica optical fiber via dip-coating approach followed by nanostructuring method. During the preform fabrication, 37 glass rods made of GeO_2 doped silica (10% mol) were coated with Nd:YAG (1% mol) nanocrystals and stacked in hexagonal lattice along with pure silica glass rods (Fig. 1.).

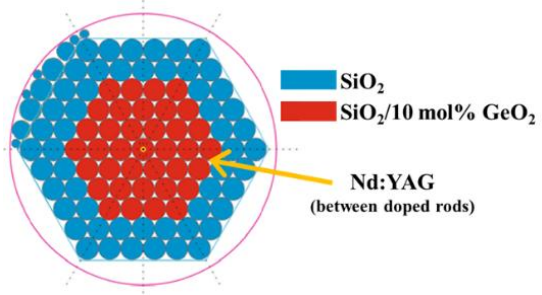

Fig. 1. Design of the Nd:YAG fiber core preform.

Then, the preform was drawn once and obtained subpreform was examined using a Raman microscope in order to determine whether the crystals survived the heat treatment during fiber drawing. Moreover, the emission lifetime of Nd^{3+} was examined with the 808 nm laser source and was equal to 457 µs (Fig. 2.). Obtained results indicated that the Nd:YAG NCs dissolved the in surrounding silica glass.

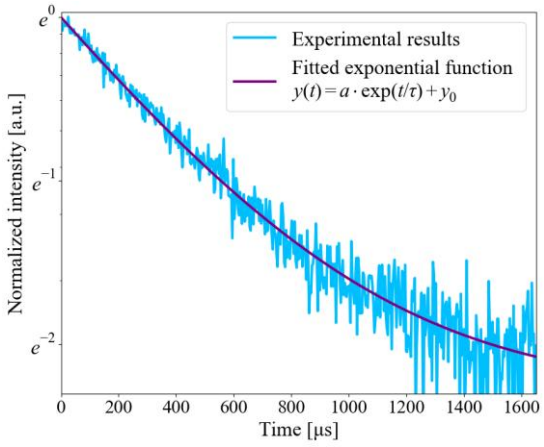

Fig. 2. Emission lifetime of Nd^{3+} obtained for Nd:YAG silica preform measured with 808 nm laser pump.

Afterwards, the subpreform was drawn again to obtain the final fiber, which was characterized with scanning electron microscopy (SEM). The diameters of the fiber and its core were equal to 127 µm and 10.3 µm, respectively.

Furthermore, optical properties of the developed fiber, such as attenuation, numerical aperture, chromatic dispersion, luminescence spectra and emission lifetime were determined. Obtained optical parameters are gathered in Tab. 1.

Tab. 1. Results of attenuation (α) in the range of 750 – 2050 nm, numerical aperture (NA), cut-off wavelength (λ_c), wavelength of zero dispersion (ZDW) and emission lifetime (τ) obtained for silica fiber doped with Nd:YAG nanocrystals.

Parameter	Value
α (750 – 2050 nm)	< 1.1 dB/m
NA	0.159
λ_c	1670 nm
ZDW	1280 nm
τ	468 µs

Due to low effective concentration of neodymium, the lasing action was not achieved, but broadened emission bands with maxima at ca. 905 and 1064 nm were observed.

All things considered, in this work, we successfully used dip-coating to incorporate Nd:YAG into the silica optical fiber. A proof-of-concept few-mode Nd:YAG fiber was fabricated in-house using nanostructuring method [5, 6] and was examined in terms of nanocrystals preservation and optical properties. Even though the crystals did not survive the thermal treatment associated with fiber drawing process, we verified experimentally that neodymium luminescence can be detected. Emission lifetimes of 457 µs (subpreform) and 468 µs (final fiber) suggested lack of Nd^{3+} ions clustering despite NCs dissolution. It is a promising result for future research on similar systems with higher dopants concentration to develop all-fiber laser setup.

Acknowledgments: This work was financially supported by the National Science Centre, Poland, grant Maestro 14, no. 2022/46/A/ST7/00238

References:

[1] S.S. Chakraborty, et al., Discover Materials 4, 17 (2024)
[2] M. Lu, et al., Photonic Sensors 14, 240202 (2024)
[3] D. Dorosz, et al., Scientific Reports, 14, 7404 (2024)
[4] J. Lee, et al., Advanced Optical Materials, 2401536 (2024)
[5] G. Stepniewski, et al., Carbon, 215, 118465 (2023)
[6] R. Kasztelanic, et al., Advanced Science, 11, 2402886 (2024)

POSTERS

Heart Rate Variability Monitoring Using a Photonic Integrated Interrogator of Fiber Bragg Grating Sensors

A. BIENIEK-KACZOREK[1], S. STOPIŃSKI[1,2,3], A. JUSZA[1,3], K. ANDERS[1,2,3], R. PIRAMIDOWICZ[1,2,3]

[1] Warsaw University of Technology, Institute of Microelectronics and Optoelectronics, Koszykowa 75, 00-662 Warsaw, Poland
[2] VIGO Photonics S.A., Poznańska 129/133, 05-850 Ożarów Mazowiecki, Poland
[3] LightHouse Sp. z o.o., Stefczyka 34, 20-151 Lublin, Poland

e-mail address: aleksandra.bieniek@pw.edu.pl

Heart Rate Variability (HRV) is a vital physiological marker used to assess autonomic nervous system function and cardiovascular health. In healthy individuals, the heartbeat duration naturally fluctuates in synchrony with respiration, a phenomenon known as respiratory sinus arrhythmia (RSA) [1]. Beyond this normal modulation, detecting and analyzing anomalous variations is critical for identifying potential pathophysiological conditions.

Conventionally, HRV is monitored using electrocardiography (ECG), however, alternative modalities such as ballistocardiography (BCG), which capture the heart's mechanical activity, are increasingly utilized. Fiber Bragg grating (FBG) sensors offer a robust solution for such mechanical sensing due to their many advantages, including immunity to electromagnetic interference, high reliability, and low production and maintenance costs. However, traditional readout systems remain bulky and expensive. The miniaturization of optical interrogation units, enabled by photonic integrated circuits (PICs), is a critical step towards the deployment of wearable and point-of-care fiber optic sensing devices.

To address this need, a photonic integrated interrogator based on asymmetric Mach-Zehnder interferometers (AMZIs) for vital signs monitoring is presented in this work (Fig. 1). The photonic chip was manufactured on a generic indium phosphide (InP) technology platform, enabling the monolithic integration of active and passive components. Selected experimental results obtained from interrogation of FBG sensors are presented. The obtained data were validated against simultaneous ECG measurements, which served as the reference.

For the experimental setup, FBG sensors were integrated into a medical mattress. The subject was positioned on the mattress in the supine position, while five ECG electrodes were attached to the chest.

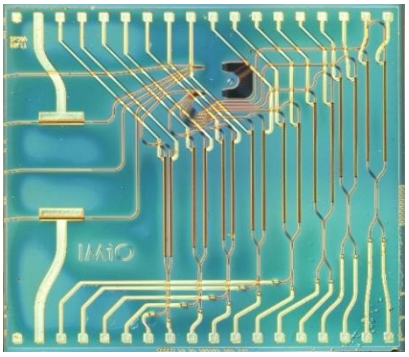

Fig. 1. Micrograph of the integrated interrogator based on AMZI structures.

The optical signal, sampled at 1 kHz, was digitally post-processed using a dedicated Python script. First, a 2nd-order Butterworth bandpass filter (4–10 Hz) was applied to isolate the cardiac component and eliminate respiratory artifacts, followed by Savitzky-Golay smoothing and Z-score normalization. Heartbeats were identified using a custom adaptive thresholding algorithm incorporating a 600 ms refractory period to prevent false detections. This method was based on the approach described in [2]. All detected peaks were visually verified and manually corrected if needed to ensure precision before calculating time-domain HRV metrics. The respiratory signal was extracted directly from the raw optical FBG data by applying a 2nd-order Butterworth bandpass filter (0.1-0.6 Hz), which isolated the low-frequency baseline modulation induced by breathing mechanics. The reference ECG signal was synchronized with the FBG data and processed using the NeuroKit2 library, employing standard algorithms for noise removal and automated R-peak detection.

A representative excerpt of the results obtained from the on-chip AMZI with an optical path imbalance of ΔL = 187.8 µm is presented in Fig. 2. An FBG sensor with a Bragg wavelength of λ_B = 1535 nm was used in the experiment. In the figure, the raw signal and the extracted respiratory and cardiac components are shown.

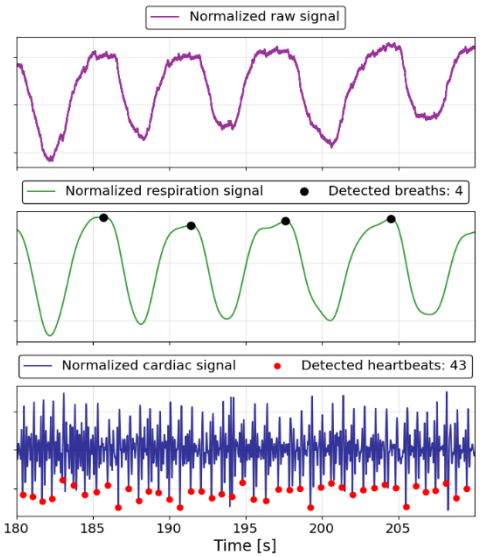

Fig. 2. Analyzed results from FBG interrogation – raw signal (purple), extracted respiration signal (green), extracted cardiac signal (blue).

A comparison of the reference ECG and the proposed photonic sensing system shows a high degree of concordance. In the presented sample, the number of detected heartbeats was identical – 43 beats (Fig. 3).

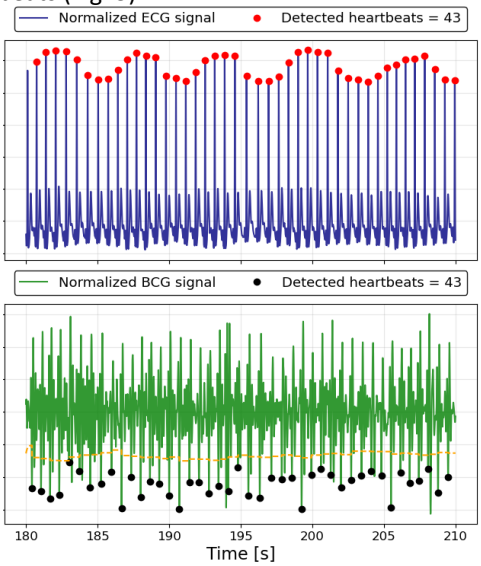

Fig. 3. Comparison between ECG (blue) and BCG obtained from FBG interrogation (green).

The mean heart rate (HR) differed by only 0.4 BPM (86.3 BPM for ECG vs. 86.7 BPM for the photonic system), confirming robust peak detection capabilities. Furthermore, the average heartbeat duration (695 ms vs. 692 ms) and the shape of the HRV waveform show high agreement (Fig. 4).

Collectively, these results demonstrate that the developed system based on a photonic integrated circuit is capable of robustly detecting respiration and heartbeats, and of capturing the subtle beat-to-beat variations essential for reliable assessment of the autonomic nervous system.

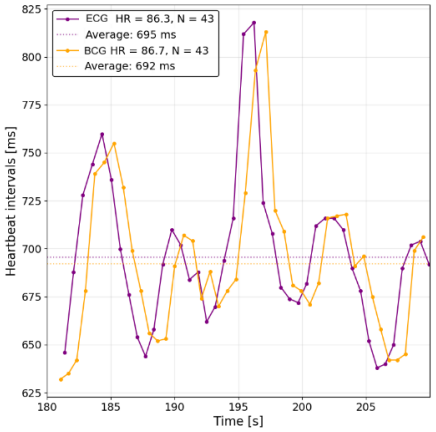

Fig. 4. Calculated heartbeat intervals from ECG (purple) and BCG obtained from FBG interrogation (yellow).

The signals obtained from the interrogator exhibit a slight time shift relative to the ECG due to the fundamental difference between the measurement modalities. While the ECG records the electrical excitation (R-peak) of the heart, the FBG sensor detects the subsequent mechanical response (Fig. 5). This results in a physiological delay – R-J intervals, typically around 100-300 ms [3].

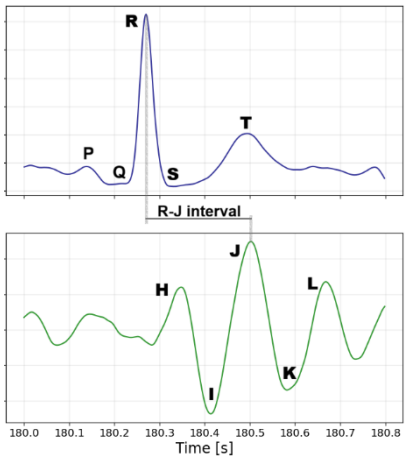

Fig. 5. Difference in waveform shape between ECG (blue) and BCG (green) signals, along with the temporal offset of their maxima (R-J interval).

Future work will focus on developing a portable demonstration system equipped with dedicated electronics and optimized peak detection algorithms.

Acknowledgments: The research was funded by the Warsaw University of Technology under the Initiative of Excellence: Research University, project title: “Miniature interrogators in integrated photonics technologies”.

References:

[1] F. Yasuma *et al.*, *Chest*, vol. 125, no. 2, pp. 683–690, 2004.

[2] J. Nedoma *et al.*, *IEEE Access*, vol. 8, pp. 181205–181223, 2020.

[3] C. S. Kim *et al.*, *IEEE Trans. Biomed. Eng.*, vol. 62, no. 11, pp. 2657–2664, 2015.

Nanodiamond- Decorated Optical Fiber Interferometric Probes: Dual-Domain Sensing With Improved Sensitivity

M. JANIK[1], T. GABLER[1], M. FICEK[2], M. PIERPAOLI[2], M. SAWCZAK[3], P. NIEDZIAŁKOWSKI[4], M. KOBA[1,5], M. ŚMIETANA[1,6], R. BOGDANOWICZ[2]*

[1 1]Institute of Microelectronics and Optoelectronics, Warsaw University of Technology, 75 Koszykowa St., 00-662 Warsaw, Poland
[2]Department of Optoelectronics, Faculty of Electronics, Telecommunications and Informatics, Gdańsk University of Technology, 11/12 Gabriela Narutowicza St., 80-233 Gdańsk, Poland
[3]The Centre for Plasma and Laser Engineering, The Szewalski Institute of Fluid-Flow Machinery, Polish Academy of Sciences, 14 Fiszera St., 80-231 Gdańsk, Poland
[4]Department of Analytical Chemistry, Faculty of Chemistry, University of Gdańsk, 63 Wita Stwosza St., 80-308 Gdańsk, Poland
[5]National Institute of Telecommunications, 1 Szachowa St., 04-894 Warsaw, Poland
[6]Łukasiewicz Research Network – Institute of Microelectronics and Photonics, Department of Glass, al. Lotników 32/46, 02-668 Warsaw, Poland

e-mail address: robbogda@pg.edu.pl

This work presents the first integration of nanostructured diamond layers with microcavity in-line Mach-Zehnder interferometers (μIMZI), enabling simultaneous interferometric and nitrogen-vacancy (NV) center-based fluorescence detection in a fiber-optic platform. Nanodiamond surface modification resulted in enhanced surface sensitivity for low-molecular-weight protein detection, achieving a limit of detection of 0.14 μg/mL for 27 kDa protein—approximately 100-fold improvement compared to conventional silanized sensors. The demonstrated picoliter-volume analysis capability and dual-domain sensing functionality establish this approach as a viable strategy for addressing current limitations in label-free biomolecular detection using optical fiber interferometric sensors [].

Label-free optical biosensors constitute important analytical platforms for clinical diagnostics, environmental monitoring, and biomedical research. Detection of low-molecular-weight biomolecules (< 30 kDa) remains challenging due to minimal refractive index perturbations induced upon molecular binding. Optical fiber-based interferometric sensors exhibit volume sensitivities of 10^4–10^5 nm/RIU but demonstrate limited surface sensitivity, restricting applications primarily to larger biological targets. Nanodiamonds present relevant physicochemical properties: biocompatibility, tunable surface chemistry with oxygen-containing functional groups, high refractive index (n ≈ 2.38 at 1550 nm), photostable nitrogen-vacancy centers, and nanostructured morphology providing increased surface area [2]. However, integration with in-fiber microcavity interferometric architectures has not been previously reported.

Microcavity in-line Mach-Zehnder interferometers were fabricated via femtosecond laser micromachining (λ = 1030 nm, 400 fs pulse duration, 8 nJ pulse energy) in standard SMF28e fiber, producing cylindrical cavities (64 μm diameter, 62.5 μm depth) that partially expose the fiber core. Nanodiamond layers with varied particle sizes (40, 140, 250 nm mean diameter) were deposited via aqueous suspension (0.1 mg/mL, overnight incubation, Fig. 1.).

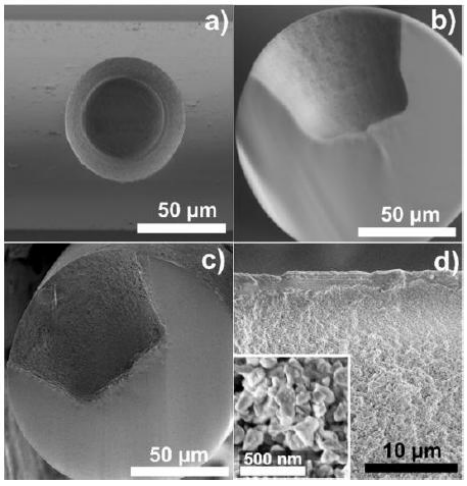

Fig. 1. SEM images of the microcavity before (a), (b), and after (c), (d) the integration with NDs: (a) top view, (b) cross-section, (c) cross-section with a rectangular marker indicating magnified area shown in (d).

Finite-difference time-domain simulations quantified NDL thickness effects on evanescent

field distribution, revealing that the 250 nm configuration provided optimal balance: field confinement within the high-index layer extended laterally across broader cavity surface while maintaining interferometric behavior, increasing bulk refractive index sensitivity from 14,998 to 15,300 nm/RIU while enhancing surface responsiveness through extended evanescent field penetration.

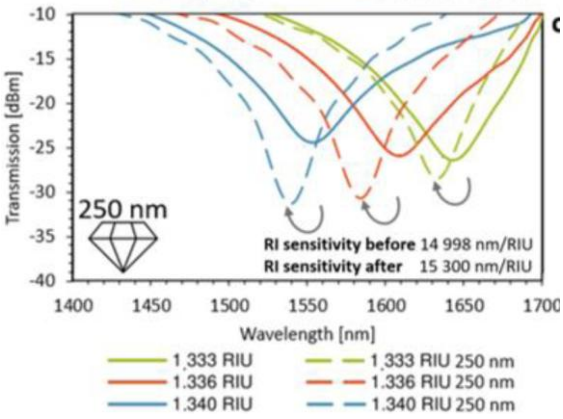

Fig. 2. Transmission spectra of the µIMZI - 250 nm nanodiamond deposition and their response to RI.

Surface sensitivity was assessed through biorecognition targeting enhanced green fluorescent protein with Strep-tag II (eGFP-StrepTag, 27 kDa). Following sequential surface functionalization with APTES silanization, NDL-poly-L-lysine-peptide conjugates, and streptavidin (60 kDa), spectroscopic interrogation (1100–1700 nm, 0.5 nm resolution) across 0.35–350 µg/mL eGFP-StrepTag concentration range revealed monotonic response. The NDL-modified µIMZI achieved lowest detected concentration of 0.35 µg/mL (wavelength shift: 1.3 ± 0.10 nm) and calculated limit of detection of 0.14 µg/mL. Receptor loading efficiency showed 6.35 nm shift for streptavidin versus 0.35 nm for conventional silanized surfaces (18-fold difference). Reference measurements without NDL modification showed no detectable response at 0.35 or 3.5 µg/mL, indicating approximately 100-fold improvement with nanodiamond modification.

Proof-of-concept experiments demonstrated dual-domain detection using NV color centers within 140 nm nanodiamonds (~3 ppm NV concentration). Optical excitation via 532 nm laser (0.5 mW) coupled through fiber core enabled NV center excitation, producing characteristic fluorescence with zero-phonon lines at 575 nm (NV^0) and 637 nm (NV^-). Bovine serum albumin exposure (0.1 mg/mL) produced measurable fluorescence intensity modulation, confirming complementary readout capability: interferometric detection of molecular binding and fluorescence-based environmental parameter monitoring (temperature, pH, magnetic field) via NV photophysics.

The observed enhancement derives from synergistic optical, morphological, and chemical contributions. Evanescent field redistribution by high-index NDL increased penetration depth from ~200 nm to >400 nm, with lateral extension beyond fiber core increasing active sensing area by factor of 3-5. Nanostructured topology provided 5-10× geometric surface area increase versus planar surfaces, with interparticle spaces accommodating protein molecules in three-dimensional matrix. Surface carboxyl groups (estimated ~10^{14}-10^{15} groups/cm²) enabled high-density receptor immobilization while maintaining biocompatible interface. The picoliter cavity volume (≈ 200 pL) enables precious sample conservation, with integration within standard 125 µm diameter fiber providing remote sensing capability and electromagnetic interference immunity. Batch-to-batch reproducibility was confirmed across 12 sensors with consistent spectral characteristics.

This work demonstrates nanodiamond surface modification as an approach for enhancing optical fiber interferometric biosensor performance for low-molecular-weight biomolecule detection. The measured 100-fold detection limit improvement, picoliter-volume analysis, and dual-domain sensing combining interferometric and fluorescence modalities provide a foundation for multifunctional miniaturized diagnostic devices exploiting diamond's optical properties and surface chemistry.

Acknowledgments: This research was supported by the Foundation for Polish Science within the TEAM-NET program (grant POIR.04.04.00-00-1644/18) co-financed by the European Union under the European Regional Development Fund. M.F. acknowledges the funding from the National Science Centre, Poland, under the OPUS call in the Weave program (Project number: 2021/43/I/ST7/03205; GACR project no. 23-04322L).

References:

[1] Janik, Monika, et al. Journal of Lightwave Technology (2025).

[2] Głowacki, Maciej J., et al. Journal of Colloid and Interface Science 675 (2024): 236-250.

Photonic System for Monitoring Nitrite and Nitrate Content in Water

P. BORTNOWSKI[1], J. KALWAS[1,2], M. KOZUBAL[1], A. JUSZA[1,3], F. ŁABAJ[1,2], E. KIEDRZYŃSKA[4], R. PIRAMIDOWICZ[1,2,3]

[1]Warsaw University of Technology, Institute of Microelectronics and Optoelectronics, Koszykowa 75, 00-662 Warsaw, Poland
[2]VIGO Photonics S.A., Poznańska 129/133, 05-850 Ożarów Mazowiecki, Poland
[3]LightHouse Sp. z o.o., Stefczyka 34, 20-151 Lublin, Poland
[4]European Regional Centre for Ecohydrology of the Polish Academy of Sciences, Tylna 3, 90-364 Łódź, Poland

e-mail address: pawel.bortnowski@pw.edu.pl

Water contamination remains a critical global challenge, with anthropogenic pollutants severely degrading aquatic ecosystems. Currently, monitoring in Poland relies on manual sampling and laboratory analysis. While accurate, this approach suffers from significant time lags and logistical constraints. Consequently, the lack of real-time capability prevents the detection of dynamic changes in water quality or immediate pollution spikes.

The FoSMoWater project aims to bridge this technological gap by shifting the paradigm from periodic lab analysis to continuous in-situ monitoring. The project focuses on developing a prototype system based on advanced photonic probes. This innovative technology is designed for the remote, real-time detection of key pollution indicators, specifically nitrite, nitrate, phosphate, and ammonium ions. By enabling instant data acquisition, FoSMoWater aims to create a responsive early-warning system that can significantly improve water resource management and environmental protection.

This study addresses the precise detection and quantitative determination of nitrite (NO_2^-) and nitrate (NO_3^-) concentrations in aqueous environments. The detection methodology is based on a comprehensive analysis of the ultraviolet spectrum, examining both characteristic absorption bands and spectral regions where the analytes are optically transparent. Specifically, the research investigates the absorption windows at 330-370 nm for nitrite and 280-320 nm for nitrate, as well as the deep-UV region (200-240 nm), which is characteristic of both ions. Figure 1 illustrates the UV-VIS absorption spectra for nitrite concentrations spanning the range of 0.1–250 mg/l. All spectra were baseline-corrected by subtracting the absorbance of deionized water to isolate the specific contribution of the nitrite ions.

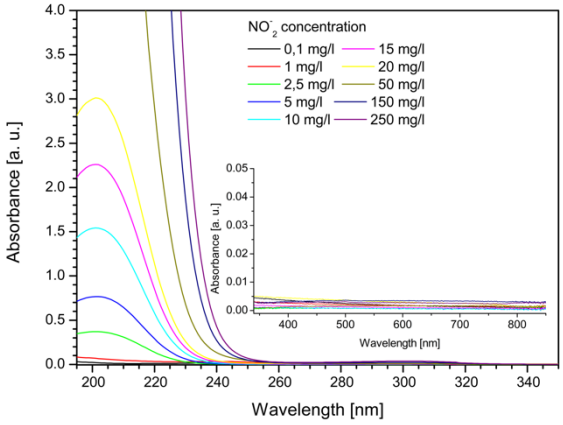

Fig. 1. Absorption spectra of nitrite samples

Analysis of the obtained UV spectra reveals a significant disparity in absorption intensity across spectral regions. Absorption in the deep UV range (200–240 nm) is orders of magnitude higher than in the 280–320 nm band, which remains barely discernible and becomes visible only at high nitrite concentrations. The 260-280 nm band and the visible region are optically transparent to nitrite ions. Consequently, these regions provide suitable reference windows for single- or multi-wavelength baseline correction in the developed demonstrator.

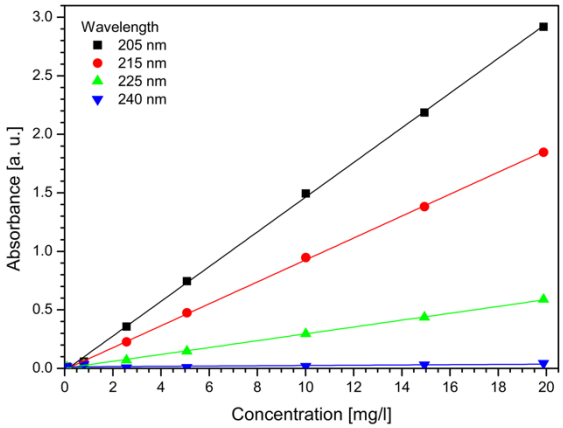

Fig. 2. Dependence of absorbance on nitrite concentration

Figure 2 shows the dependence of absorbance on nitrite concentration at four selected wavelengths (205, 215, 225, and 240 nm).
The measured dependencies show a linear response across all selected wavelengths, as predicted by Beer-Lambert's Law. The slope of the calibration curve increases with decreasing wavelength, directly translating into enhanced sensitivity for the designed sensor. However, the scarcity of cost-effective light sources emitting at approximately 210 nm presents a significant practical challenge.

The design of the functional demonstrator addresses three primary challenges: selecting an optimal light source and wavelength, determining the sampling geometry, and choosing a detection scheme. The paper presents a comparative analysis of Light Emitting Diodes (LEDs) and excimer sources, evaluating their spectral characteristics and suitability for the target application.

Regarding the measurement methodology, two distinct configurations are discussed. The first is a direct transmission mode, in which the light propagates through both the aqueous sample and the cuvette walls. A significant limitation of this approach is the strict requirement for high optical transparency of the cuvette material in the deep UV region. The alternative approach uses reflective geometry with a mirror at the bottom of the cell. While this eliminates the need for UV-transparent cuvette walls, it necessitates precise mechanical control to ensure a reproducible optical path length for every measurement.

Concerning signal acquisition, the study focuses on silicon-based technology, explicitly contrasting a single-silicon photodetector configuration with a balanced silicon detection circuit. The latter is analyzed for its efficacy in suppressing noise and compensating for source fluctuations. Finally, the research evaluates the optical architecture, weighing the trade-offs between a fiber-optic coupled system and a free-space optical arrangement.

This paper presents a comprehensive spectroscopic analysis of the target analytes, followed by a detailed discussion of the device construction and system architecture. The outcome of this research is a fully functional photonic sensing system demonstrator, validated for the effective detection of water contaminants.

Acknowledgments: This work has received support from the National Centre for Research and Development through project FOSMO (HYDROSTRATEG1/000E/2022).

Correlation Between Deposition Conditions and Structural Properties of Palladium Thin Films

L. CZYŻEWSKA, M. GRZESIAK, M. GIL-KOWALCZYK, P. MERGO

Laboratory of Optical Fibers Technology, Maria Curie-Sklodowska University,
Maria Curie-Sklodowska Sq. 5, 20-031 Lublin, Poland

e-mail address: lidia.czyzewska@mail.umcs.pl

Abstract: The aim of this study is to investigate the influence of deposition conditions on the structural properties of palladium (Pd) layers deposited on optical fibers. Prior to palladium coating, silica optical fiber samples were subjected to a surface activation process in order to enhance metal adhesion to the glass substrate. The preparation procedure included removal of the protective layers followed by thorough surface cleaning using isopropyl alcohol and an acetone/chloroform mixture.

Subsequently, a two-step chemical activation of the lateral surface of the optical fibers was carried out using aqueous solutions of tin(II) chloride ($SnCl_2$) and palladium(II) chloride ($PdCl_2$). In the first step, the fibers were immersed in a $SnCl_2$ solution for 30 minutes and then rinsed with deionized water. In the second step, the samples were treated with a $PdCl_2$ solution for an additional 30 minutes, followed by rinsing with deionized water [1].

After the activation process, a 200 nm thick palladium layer was deposited onto the optical fiber surface by magnetron sputtering. The deposition was performed using an EM SCD500 sputtering system at three different deposition rates: 0.10 nm/s, 0.20 nm/s, and 0.34 nm/s. The Pd-coated fibers were characterized using optical profilometry and atomic force microscopy (AFM) to evaluate the morphology, uniformity, topography, and structural features of the deposited films.

The obtained results constitute a basis for the development of an optical hydrogen sensor based on palladium-coated optical fibers, exploiting the unique interaction between palladium and gaseous hydrogen. Upon hydrogen exposure, palladium forms palladium hydride (PdH_x), accompanied by changes in its crystal structure depending on the hydrogen partial pressure. This process leads to lattice expansion of palladium, resulting in a modification of the optical response of the fiber. The presence of a palladium coating enables direct transduction of metal volume changes into optical signal variations, allowing effective hydrogen detection.

References:

[1] X. Wei et al., Journal of The Electrochemical Society 161, (2014).

Modeling the Effect of UV Degradation on the Raman Spectrum of Microplastics Detected in Drinking Water

Ł. DREWNIAK [1], S. DREWNIAK [1], I. ZIMOCH [2], E. ŁOBOS-MOYSA [2], E. MACIAK [1]

[1] Department of Optoelectronics, Faculty of Electrical Engineering,
Silesian University of Technology, Gliwice, Poland
[2] Department of Water And Wastewater Engineering , Faculty of Energy And Environmental Engineering,
Silesian University of Technology, Gliwice, Poland

e-mail address: lukasz.drewniak@polsl.pl

Microplastics generated by the environmental degradation of common polymers increasingly accumulate in aquatic systems, posing significant analytical challenges for their identification and quantification. Polyethylene (PE) and polypropylene (PP), due to their widespread use and high environmental persistence, are among the most prevalent materials detected. Raman spectroscopy is commonly applied for polymer identification in microplastic analysis, its quantitative applicability is limited by spectral variability related to particle heterogeneity, fluorescence background, instrumental effects, and environmental aging.

In particular, UV-induced photo-oxidation alters polymer chemical structure, leading to the formation of carbonyl groups and changes in Raman peak intensity, linewidth, and baseline characteristics. Although the Carbonyl Index is commonly used to assess oxidative degradation, its interpretation is complicated by non-linear intensity scaling and baseline growth, which may obscure purely chemical effects.

In this study, simplified Raman spectral simulations are employed to isolate the influence of UV-induced aging from geometric and instrumental factors. The proposed model focuses on characteristic PE Raman bands and enables systematic evaluation of degradation-related spectral changes independent of particle size and concentration variability. This approach improves the interpretation of Raman spectra of aged microplastics.

Modeling the Effect of UV Degradation on the Raman Spectrum of Microplastics Detected in Drinking Water

S. DREWNIAK [1], Ł. DREWNIAK [1], E. MACIAK [1], K. MORACZEWSKA-MAJKU [2], W. K. NOCOŃ [2]

[1] Department of Optoelectronics, Faculty of Electrical Engineering,
Silesian University of Technology, Gliwice, Poland
[2] Department of Water And Wastewater Engineering , Faculty of Energy And Environmental Engineering,
Silesian University of Technology, Gliwice, Poland

e-mail address: sabina.drewniak@polsl.pl

Microplastics generated through the environmental degradation of common polymers are increasingly detected in aquatic systems, including drinking water, creating significant analytical challenges for their reliable identification and interpretation [1,2]. Polyethylene (PE) and polypropylene (PP), owing to their extensive use, chemical stability, and resistance to biodegradation, represent the most frequently reported polymer types in environmental microplastic studies [1]. Raman spectroscopy is widely applied for polymer identification due to its chemical specificity; however, quantitative interpretation of Raman spectra remains limited by spectral variability arising from particle heterogeneity, fluorescence background, instrumental effects, and environmental aging processes [3].

Among environmental stressors, UV-induced photo-oxidative aging plays a key role in modifying the chemical structure of polymer surfaces [2,4]. This process leads to the formation of carbonyl-containing functional groups and induces systematic changes in spectroscopic features, including attenuation of C–H vibrational bands, emergence and growth of carbonyl-related peaks, peak broadening, and increasing background signals — phenomena that can complicate interpretation [4]. Although the Carbonyl Index is commonly employed as a proxy for oxidative degradation, its interpretation is complicated by non-linear intensity scaling, baseline contributions, and noise amplification, which may mask purely chemical aging effects [2,4].

In this study, simplified Raman spectral simulations are used to examine the effect of UV-induced aging on polymer Raman spectra. Instead of relying on experimental spectra influenced by particle size, concentration, or measurement conditions, the model generates synthetic Raman spectra in which only aging-related spectral changes are controlled and varied. Raman spectra are described as a sum of individual vibrational bands characteristic of the polymer. UV aging is simulated by introducing a gradual increase of carbonyl-related bands, accompanied by a systematic decrease of C–H band intensities, peak broadening, baseline growth, and increasing noise with UV dose. This approach helps distinguish spectral changes caused by UV aging from those arising from geometric or instrumental factors.

The proposed simulation approach helps interpret how UV-induced aging alters Raman spectra of microplastics detected in drinking water. It distinguishes degradation-related spectral features from changes caused by non-chemical spectral effects, supporting more reliable spectroscopic interpretation of environmental microplastic samples.

[1] A. A. Koelmans, et al., Water Research 2019, 155, 410–422; https://doi.org/10.1016/j.watres.2019.02.054
[2] Y. Shi, Environmental Chemistry Letters 2024, 22, 1861–1888; https://doi.org/10.1007/s10311-024-01731-5
[3] S. Rytelewska, A. Dąbrowska, Microplastics 2022, 1(2), 263-281; https://doi.org/10.3390/microplastics1020019
[4] C. Campanale, et al., Polymers 2023, 15(4), 911; https://doi.org/10.3390/polym15040911

Periodically Patterned Boron-Doped Diamond Nanostructures for Enhanced Opto-Electrochemical Transduction

M. FICEK [1], A. OLEJNIK[1], M. BABIŃSKA[1], B. STONIO[2,3], M. PIERPAOLI[1], R. BOGDANOWICZ[1]

[1] Gdańsk University of Technology, 11/12 Gabriela Narutowicza Street, 80-233 Gdańsk, Poland
[2] Warsaw University of Technology, Institute of Microelectronics and Optoelectronics, Koszykowa 75, 00-662 Warsaw, Poland
[3] University of Technology, Centre for Advanced Materials and Technologies, Poleczki 19, 02-822 Warsaw, Poland

e-mail address: robbogda@pg.edu.pl

Boron-doped diamond (BDD) nanostructures have attracted considerable attention in recent years due to their unique combination of structural robustness and excellent electrochemical (EC) performance. These materials possess a wide potential window, superior chemical and thermal stability, very low background currents, and minimal double-layer capacitance, which distinguishes them from conventional electrode materials such as gold, platinum, or glassy carbon. As a result, BDD-based electrodes have found extensive use in a broad spectrum of applications ranging from environmental sensing and electroanalytical chemistry to biosensing and energy conversion. In particular, the possibility to tailor the morphology and doping level of diamond films enables the design of high-performance electrode surfaces optimized for specific electrochemical and optical responses.

This study introduces a novel and effective approach for the fabrication of ordered diamond nanostructures through the growth of boron-doped diamond on periodically patterned surfaces. The proposed method allows precise control of diamond morphology and doping distribution, leading to the formation of periodic boron-doped diamond (PBDD) electrodes with highly uniform structural features. The nanostructures were grown on etched and nanodiamond-seeded fused silica substrates with various pattern periodicities, allowing systematic investigation of the relationship between geometric order and electrochemical behavior. The synthesis process employed microwave plasma-enhanced chemical vapor deposition (MWPECVD) using methane and hydrogen as the main reactive gases, with diborane introduced as the boron source. A boron-to-carbon ratio of 10,000 ppm in the gas phase was maintained to achieve highly conductive, p-type BDD layers while preserving excellent crystalline quality. The resulting films exhibited sharp, edge-defined morphologies forming periodic surface patterns with remarkable reproducibility. In addition to their electrochemical advantages, these ordered surfaces exhibited distinctive diffraction features visible in optical reflection measurements, revealing their potential for multifunctional optoelectronic applications.

Comprehensive characterization was performed to assess the structural, spectroscopic, and electrochemical properties of the fabricated electrodes. Scanning electron microscopy (SEM) provided insight into the surface topography, pattern uniformity, and grain structure of the diamond layer, while Raman spectroscopy confirmed the high crystalline quality, sp^3 carbon bonding, and the successful incorporation of boron atoms through characteristic peak shifts and broadening. The electrochemical performance was evaluated using cyclic voltammetry (CV) and electrochemical impedance spectroscopy (EIS) in a three-electrode configuration with aqueous electrolytes. The CV measurements demonstrated stable and reproducible current responses over a wide potential range, confirming the high stability and low background current typical of BDD electrodes. EIS analysis revealed a notable reduction in charge transfer resistance for electrodes with shorter periodicities, indicating improved electron transfer kinetics and modified diffusion dynamics at the electrode–electrolyte interface.

Furthermore, simultaneous optical and electrochemical measurements were recorded to investigate the correlation between structural periodicity and dual-mode responses. The optical characterization, carried out through reflectance spectroscopy, confirmed measurable spectral modulations associated with the periodic surface geometry and revealed changes induced by electrochemical processes at the electrode

surface. The complementary optical and electrochemical datasets provided mutual validation of the observed effects, confirming that the periodic BDD surfaces can couple EC activity with measurable optical responses. These findings demonstrate the feasibility of using periodic BDD electrodes not only for efficient and stable electrochemical sensing but also for integrated optoelectronic biosensing platforms capable of real-time cross-modal signal analysis.

Acknowledgments: This research work is supported by the National Science Centre, Poland under the OPUS call in the Weave program (no.: 2021/43/I/ST7/03205; GACR no.23-04322L).

References:

[1] Bogdanowicz, Robert, and Jacek Ryl, Current Opinion in Electrochemistry 31 (2022): 100876.
[2] Brodowski, Mateusz, et al., Sensors and Actuators B: Chemical 370 (2022): 132427.
[3] Ficek, Mateusz, et al., Microchimica Acta 190 (2023):410.

Lithography Methods in the Fabrication of Integrated Photonics Circuits

M. JUCHNIEWICZ, M. SŁOWIKOWSKI, D. DRECKA, M. JAROSIK

Warsaw University of Technology, CEZAMAT Centre for Advanced Materials and Technologies
ul. Poleczki 19, Warsaw 02-822, Poland

e-mail address: marcin.juchniewicz@pw.edu.pl

The work presents an overview of lithographic processes used for the fabrication of integrated photonic circuits (PICs) at CEZAMAT. Currently, the research conducted at CEZAMAT covers several photonic platforms that differ in the materials used, the geometry of the fabricated structures, and their target spectral range, and thus in their potential areas of application.

The study focuses on two selected platforms: a platform designed for operation in the visible spectral range, based on silicon nitride (SiN), and a platform intended for mid-infrared (MIR) operation, based on a germanium-on-silicon (Ge-on-Si). The differences in the spectral range of these platforms define the potential applications for each of them. The visible range platform offers promising capabilities in biochemical and chemical analysis, e.g. in lab-on-a-chip systems. In contrast, the MIR platform is of particular interest for modern communication technologies, LIDAR systems, as well as for precise gas detection and identification, where the characteristic absorption features in this wavelength region play a key role.

The optimization of integrated photonic circuit fabrication processes focuses primarily on optimizing waveguide geometry, as this directly affects propagation losses, which is a critical performance parameter of photonic devices. The fabrication of low-loss PICs is not possible without the appropriate selection of lithographic techniques.

The work compares three lithography techniques currently used at CEZAMAT for PIC fabrication: UV light lithography, laser lithography , and electron-beam lithography (EBL). UV lithography, despite its limited resolution, remains a fundamental method for structures with critical dimensions above 1 µm, offering the highest process throughput. Laser lithography is a highly flexible method for rapid maskless prototyping, which is invaluable during the research phase of new photonic circuit topologies. The highest precision (essential for defining submicron features such as photonic crystals or grating couplers) is delivered by EBL.

Additionally, the study discusses the nanoimprint lithography (NIL) technique, which will become available at CEZAMAT in the next few months. The introduction of NIL represents an important step toward scalable production, combining nanometer-level resolution with significantly lower costs compared to electron-beam lithography.

The possibilities of combining different lithography techniques will also be discussed, as this approach enables achieving high process throughput without compromising the quality of the fabricated structures.

Acknowledgments: The research work presented in this paper was carried out within the framework of the PIXEurope Pilot Line. PIXEurope is co-funded by the Chips Joint Undertaking and national funding authorities of the Participating States: Austria, Belgium, Finland, France, Ireland, Italy, The Netherlands, Poland, Portugal, Spain, United Kingdom.

Dye-Assisted Optical Detection of Trace Water in Diesel Fuel

M. GIL-KOWALCZYK, M. JÓZWICKI, P. MERGO

Laboratory of Optical Fibers Technology, Maria Curie-Sklodowska University,
Maria Curie-Sklodowska Sq. 5, 20-031 Lublin, Poland

e-mail address: malgorzata.gil-kowalczyk@mail.umcs.pl

Abstract: The presence of water in diesel fuel is a well-known factor adversely affecting fuel quality, engine performance, and storage stability. Even trace amounts of water may lead to corrosion of fuel system components, degradation of fuel additives and bio-components, and microbial growth. Conventional methods for water determination in fuels, such as Karl Fischer titration or infrared spectroscopy, provide high accuracy but often require specialized equipment, time-consuming procedures, and controlled laboratory conditions. Therefore, the development of rapid, simple, and cost-effective alternative approaches remains an important analytical challenge, particularly for routine quality control [1-6].

In this work, a dye-assisted optical method for trace water detection in diesel fuel is proposed. The approach is based on the use of Rhodamine 6G as a polarity-sensitive indicator dye, whose optical response is strongly influenced by changes in the local solvent environment. UV–Vis spectrophotometric measurements revealed clear and reproducible changes in the transmission spectra with increasing water content in the hydrophobic diesel fuel matrix, enabling indirect detection of water through optical signal variations.

The spectrophotometric response showed a clear linear dependence on water concentration in the range from 0.004% to at least 0.024%, corresponding to the limits defined by diesel fuel quality standards. An optimal dye concentration of 5.92×10^{-5}% provided a well-defined transmission minimum, a broad linear response range, and low signal noise, ensuring good sensitivity and measurement repeatability.

The proposed method offers a simple, rapid, and cost-effective optical tool for preliminary quantitative detection of water contamination in diesel fuel and may serve as a practical alternative to more complex analytical techniques. Owing to its simplicity and low instrumental requirements, the method shows potential for routine fuel quality monitoring and on-site screening applications.

References:

[1] F. J. Passman, International Biodeterioration & Biodegradation 81, (2013)
[2] M. T. Ghannam et, Petroleum Science and Technology 27, (2009)
[3] E. Scholz, Karl Fischer Titration: Determination of Water, Springer, Berlin, (1984).
[4] P. Felizardo et al., Analytica Chimica Acta 595, (2007)
[5] J. R. Lakowicz, Principles of Fluorescence Spectroscopy, Springer, New York, (2006)
[6] V. Pujari et al., IOP Conference Series: Materials Science and Engineering 1221, (2022).

When Light Prints More Than Objects: Nanoscale Waste, Environmental Persistence, and Cytotoxicity in Photopolymer Manufacturing

P. KAŁUŻYŃSKI [1], D. KAŁUŻYŃSKA [1,2]

[1] Department of Optoelectronics, Silesian University of Technology, 44-100 Gliwice, Poland
[2] Biotechnology Center, Silesian University of Technology, 44-100 Gliwice, Poland,

e-mail address: pkaluzynski@polsl.pl

The rapid integration of 3D printing – particularly photopolymer-based methods like Digital Light Processing (DLP) – has revolutionized nanostructured device prototyping and fabrication in optoelectronics. The accelerating adoption of these additive manufacturing techniques has unlocked innovative capabilities in photonic device engineering, yet our investigations reveal an overlooked hazard: routine processing of resin-printed parts can generate nanoscale plastic debris. We found that common post-print workflows (e.g., immersion in isopropanol or ethanol followed by UV curing) induce spontaneous polymer precipitation from residual, partially polymerized resin. Analytical characterization (optical profilometry, Fourier-transform infrared spectroscopy, scanning electron microscopy, and energy-dispersive X-ray analysis) confirmed that the resulting waste contains both visible sediment and colloidal suspensions of polymeric nanoparticles, with dimensions on the order of 10÷100 nanometers, up to 1 µm. Such nanoscopic polymeric contaminants can adhere to surfaces or remain suspended in solution, threatening the optical clarity and performance of photonic components.

In parallel, we assessed the biological impact of these particulate wastes. Wash effluents from DLP prints of common resins (basic, ABS-like, and glow-in-the-dark formulations) were introduced into different aqueous media – deionized water, tap water, and artificial seawater at marine salinity – to simulate realistic exposure conditions. MTT viability assays on human keratinocyte (HaCaT) cultures revealed significant cytotoxicity associated with certain resin wash residues, even after standard UV post-curing protocols. Notably, cytotoxic effects varied with medium composition, underscoring how environmental factors modulate the toxicity of resin leachates. Fluorescence microscopy demonstrated that the smallest particulate fraction indeed enters cells, corroborating their measured 10÷1000 nm size range and raising concerns about transcellular transport of plastic nanoparticles. These results indicate that photopolymer printing wastes can act as both environmental pollutants and biologically active xenobiotics.

To mitigate these risks, we explored post-print surface engineering. Applying an SU-8 epoxy photoresist coating – a strategy drawn from established microfabrication techniques – effectively immobilized residual monomers and nanoparticles on printed surfaces. This barrier layer preserved optical transparency while significantly reducing monomer leaching and nanoparticle release, thereby enhancing surface biocompatibility. Taken together, our findings expose two interlinked challenges in photopolymer additive manufacturing: the inadvertent generation of nano- and microplastic (NMP) contaminants and the inadequacy of current post-processing to ensure environmental and human safety. A holistic approach – integrating material reformulation, process optimization, and surface passivation – is therefore essential to realize the full promise of 3D printing in sensitive optoelectronic and biomedical applications.

Funding and acknowledgements. This work was supported by IDUB Programme (Program Inicjatywa Doskonałości - Uczelnia Badawcza) – Silesian University of Technology, Student Chapters Scientific Projects.

Raman Spectroscopy in Water Quality Monitoring

Ł. KOZŁOWSKI[1], A. BIENIEK-KACZOREK[1], P. BORTNOWSKI[1], M. ZIELIŃSKA[1], K. ANDERS[1,2,3], S. STOPIŃSKI[1,2,3], A. JUSZA[1,2], J. KALWAS[1,3], R. PIRAMIDOWICZ [1,2,3]

[1] Warsaw University of Technology, Institute of Microelectronics and Optoelectronics, Koszykowa 75, 00-662 Warsaw, Poland
[2] LightHouse Sp. z o.o., Stefczyka 34, 20-151 Lublin, Poland
[3] VIGO Photonics S.A., Poznańska 129/133, 05-850 Ożarów Mazowiecki, Poland

e-mail address: lukasz.kozlowski@pw.edu.pl

In the context of anthropogenic climate change and intensifying industrial activity, protecting freshwater resources has become a strategic priority for public health and the global economy. Surface waters are increasingly threatened by agricultural runoff and wastewater, leading to dangerous concentrations of nitrites (NO_2^-), nitrates (NO_3^-), phosphates (PO_4^{3-}), and ammonium ions (NH_4^+), which contribute to eutrophication and toxic algal blooms. Furthermore, the pervasive presence of microplastics in both standing and flowing water poses a growing environmental hazard that requires immediate attention. Current quality testing methods rely heavily on laboratory techniques that often require sample transport and the use of chemical reagents, preventing real-time threat identification.

To address these limitations, this work, supported by the FoSMoWater project, presents the development of innovative, reagent-free photonic methods for water quality monitoring. While various optical methods have been explored as alternatives to standard FTIR techniques, Raman spectroscopy can also be used to detect water contaminants and offers distinct advantages for detecting polymer types in aqueous environments. This study focuses on a comparative analysis of Raman spectroscopy configurations to determine their effectiveness in detecting both dissolved contaminants and evaporated contaminant particles.

We present experimental measurements of concentrations of key pollutants, specifically NO_2^-, NO_3^-, PO_4^{3-}, and NH_4^+. Additionally, the research provides a detailed analysis of microplastic contamination, presenting detection results for polymer particles with diameters of 20 µm and 100 µm. Reference measurements were conducted using the ThermoScientific iS50 FT-Raman module, equipped with a 1064 nm excitation laser with adjustable power up to 500 mW and an InGaAs detector. The system features a spot size of <60 µm and an automated X-Y-Z stage, enabling precise sample positioning and point analysis, controlled via OMNIC software. Moreover, measurements were also conducted at a different excitation wavelength of 785 nm using a Thorlabs Raman Spectroscopy Kit.

A comparative experiment was conducted, involving measurements of powders containing NO_2^-, NO_3^-, PO_4^{3-}, and NH_4^+, as well as evaporated solutions containing these pollutants. The solutions were evaporated onto a reduced surface area of a microscopic slide, as shown in Fig. 1, and spectral acquisitions were subsequently performed.

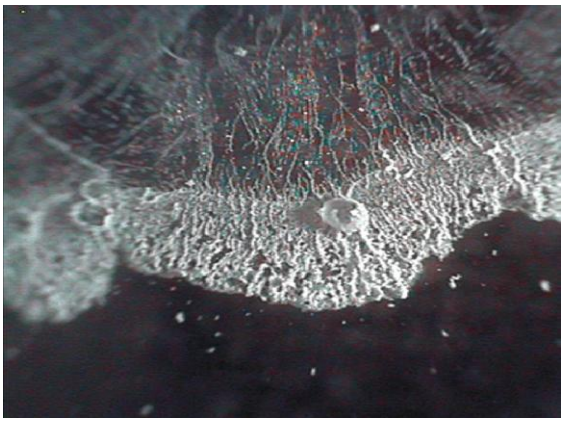

Fig. 1. Image of an evaporated aqueous sample containing NO_3^- ions.

Exemplary measurements demonstrating characteristic Raman spectra of NO_3^- are presented in Fig. 2. Although the spectral intensities observed for powder samples are higher than those for evaporated samples, the characteristic peaks are clearly distinguishable in both scenarios.

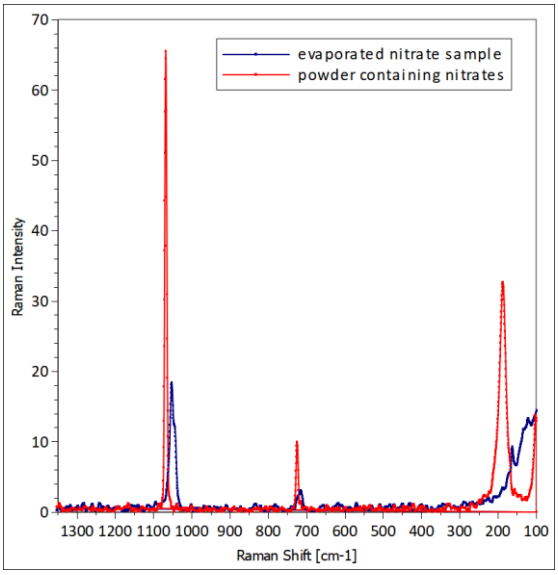

Fig. 2. Measurement results displaying characteristic Raman peaks for NO_3^- in powder and evaporated sample from an aqueous solution.

This work demonstrates that Raman spectroscopy is a versatile tool for the rapid identification of water contaminants. The successful detection of both dissolved ions and microplastics at distinct excitation wavelengths underscores the technique's adaptability across diverse environmental conditions. By eliminating reliance on consumable reagents and complex sample transport logistics, this approach significantly reduces operational costs and time delays associated with traditional monitoring. Consequently, this research validates the feasibility of deploying Raman-based sensor architectures for autonomous, real-time water quality assessment.

Acknowledgments:
This work was supported by the National Centre for Research and Development through the project FoSMoWater (HYDROSTRATEG1/000E/2022).

Application of N,N-Dimethyl-4,4’-azodianiline (DMADA) for UV Fiber Optic Sensing

K. KUCHTA[1], A. RYBCZYŃSKI[1], J. M. KUBICA[1]

[1] Central Institute for Labour Protection – National Research Institute, Czerniakowska 16, 00-701 Warsaw, Poland

e-mail address: jacek.kubica@ciop.pl

In this work, we investigate the application of N,N-Dimethyl-4,4’-azodianiline (DMADA) as a UV-responsive functional material integrated with a fiber Bragg grating (FBG) to enable UV radiation sensing. DMADA is an organic azo compound characterized by a conjugated aromatic structure and an azo (–N=N–) bond (Fig.1), which exhibits strong absorption in the UV region and undergoes reversible photo-induced trans–cis isomerization under UV irradiation. This leads to macroscopic dimensional changes of the DMADA-based coating, which generate axial stress transferred to the underlying fiber and the Bragg grating. As a result, the FBG experiences photo-induced strain, which is detected as a wavelength shift proportional to the UV irradiation intensity [1], [2].

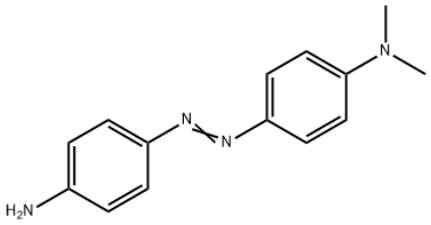

Fig. 1. Structure of N,N-Dimethyl-4,4’-azodianiline

The sensing element involved a fiber Bragg grating implemented in a single-mode telecommunication optical fiber (SMF-28). The nominal Bragg reflection wavelength was 1549.97 nm at room temperature in the absence of UV irradiation. The UV-sensitive photomechanical coating was prepared using DMADA at a concentration of 5 wt. % dispersed in a polymer cladding resin LS-2311HT. The components were mechanically stirred for up to 20 hours at room temperature to achieve uniform distribution of the azo compound within the polymer matrix. The resulting DMADA–polymer composite was deposited onto the fiber Bragg grating region and subsequently UV cured at room temperature under a nitrogen atmosphere to minimize oxygen-induced inhibition effects. The curing process was performed using a 80 W LED lamp of 395 nm emission wavelength and consisted of two consecutive stages of 3 and 2 min, respectively.

The fiber was coupled to a broadband superluminescent diode (SLED) source with an optical circulator (DL-BP1 1501A), which ensured efficient separation of the incident broadband radiation and the reflected Bragg signal (Fig.2). The fiber Bragg grating response was monitored by using a fiber-optic interrogator Ibsen Photonics I-MON 512 USB, operating in the 1550 nm wavelength range. The system allowed spectral acquisition of the FBG reflection peak with a resolution of 5 pm at sampling rates of up to 3 kHz, enabling high-speed tracking of Bragg wavelength shifts induced by UV-driven mechanical strain.

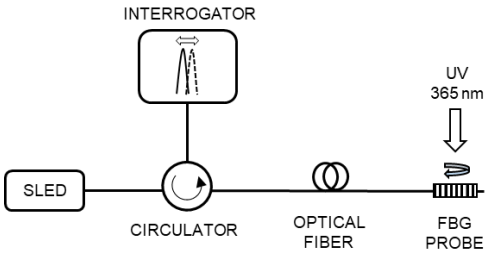

Fig. 2. Measurement setup

UV exposure of the DMADA-coated fiber Bragg grating was conducted using a 25 W UV LED lamp emitting at 365 nm. Measurements revealed a fast Bragg wavelength shift of up to 0.5 nm. The magnitude and dynamics of the observed shift are consistent with the photomechanical response of the DMADA-coated FBG, rather than purely thermal expansion of the DMADA coating.

Acknowledgments: This work was supported by the II-43 project funded by CIOP-PIB.

References:

[1] H.-K. Kim et. al, „UV sensor based on photo-mechanically functional polymer-coated FBG”, IEEE Photonics Technol. Lett., 22, 1404, (2010)

[2] I.-S. Song et. al, „Sensitivity enhancement of a UV photo-sensor based on a fiber Bragg grating coated by a photomechanical functional polymer”, Sens. Actuators Phys., 232, 223, (2015)

Flotation Froth Pattern Recognition for the Ore Content Estimation

J. GALAS[1], D. LITWIN[1], K. RADZIAK[1], W. MAŁKIŃSKI[1], M. KARLIŃSKI[1], N. BŁOCKI[1], A. CZYŻEWSKI[1], M. KOZIELSKI[2], D. FOSZCZ[3], D. SARAMAK[3], S. LENCZOWSKI[4], E. KASIŃSKA-PILUT[5], R. PĘPKOWSKI[5], Ł. PAŁKA[5]

[1]Łukasiewicz Research Network – Tele and Radio Research Institute,
11 Ratuszowa St., 03-450 Warsaw, Poland
[2] Łukasiewicz Research Network – Institute of Innovative Technologies EMAG,
31 Leopolda St., 40-189 Katowice, Poland
[3] AGH University of Cracow, 30 Mickiewicza Ave., 30-059 Cracow, Poland
[4] AGH University of Cracow, 30 Mickiewicza Ave., 30-059 Cracow, Poland (Emeritus)
[5] KGHM Polska Miedź S.A., Division of Concentrators,
1 Kopalniana St, 59-100 Polkowice, Poland

e-mail address: dariusz.litwin@itr.lukasiewicz.gov.pl

The paper is focused at Artificial Intelligence algorithms applied to flotation process at a mineral processing plant.

The approach utilizes the froth pattern recorded by a collection of imaging sensors[1]. The flotation process is the dominant technology in extracting minerals from the ore. The precise assessment of the metal content in the flotation froth, especially performed on-line, is crucial for the efficiency of metal extraction industrial process[2]. Other technologies, like X-ray-based measurement systems are more expensive and time consuming. The presented approach has the ability to quick, on-line froth content estimation on the basis of the Machine Learning process[3]. The key element consists in the classification process of the flotation froth images acquired during the flotation process, which enables significant improvement of the accuracy and efficiency of the extraction technology as a whole.

Acknowledgments: The project has been funded by the European Commission, Call: HORIZON-CL4-2022-RESILIENCE-01 (A DIGITIZED, RESOURCE-EFFICIENT AND RESILIENT INDUSTRY 2022), Topic: HORIZON-CL4-2022 RESILIENCE-01-06. Type of Action: HORIZON-IA, Project number: 101091885, Project acronym: Mine.io.

References:

[1] S. Lenczowski, , J. Galas, "Optical Analysis of Metal Content in the Column Complex Ore Flotation Froth," Proc of the XIX IMPC, San Francisco, 1995, pp. 257-260, (E. Forssberg, ed)

[2] J. Galas, D. Litwin, "Machine Learning technique for recognition of flotation froth images in a non-stable flotation process," Minerals 2022, 12, 1052, pp. 1-11, https://doi.org/10.3390/min12081052

[3] J. Galas, D. Litwin, M. Kozielski, D. Foszcz, D. Saramak, S. Lenczowski, E. Kasińska-Pilut, J. Prętki, „Flotation froth content estimation on the basis of a Machine Learning process", 23rd Slovak-Czech-Polish Optical Conference on Wave and Quantum Aspects of Contemporary Optics, edited by Dušan Pudiš, Daniel Jandura, Ivana Lettrichová, Proc. of SPIE Vol. 13508, 1350818.

Analysis of FBG Signal Transmission in Optical Fiber Telecom Networks

J. ŁYŻWA, M. MIKA, M. ŻUK, B. SUDOŁ, A. AUGUSTOWSKI, A. OLSZEWSKI, K. BARCZAK, A. OLSZEWSKA

Department of Optoelectronics, Faculty of Electrical Engineering, Silesian University of Technology, 2 Krzywoustego Str., 44-100 Gliwice, POLAND

e-mail address: kamil.barczak@polsl.pl

Introduction and Motivation

Fiber Bragg Grating (FBG) sensors enable remote distributed measurement of physical parameters such as temperature, strain, and pressure in optical fiber networks. This work investigates the feasibility of integrating FBG sensors into existing fiber-optic telecommunications networks (FTTH/GPON) originally designed for data transmission, enabling simultaneous monitoring of network infrastructure and service delivery while reducing deployment costs and improving system scalability.

Methodology

System Design: The project evaluated three optical path configurations (K1, K2, K3) integrated with FTTH/GPON infrastructure, incorporating passive optical components including PLC (Planar Lightwave Circuit) splitters (1×2, 1×8), optical filters, and an FBG temperature sensor operating at 1548.9 nm wavelength. Selected configuration (K2) is shown in Figure 1.

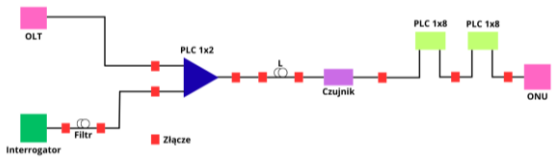

Fig. 1 Diagram showing Configuration K2

Experimental setup: A comprehensive testbed was constructed at the Department of Optoelectronics, Silesian University of Technology using an FTTH laboratory platform enabling network distances of L1 (0.769 km), L2 (2.158 km), and L3 (3.513 km). Signal detection utilized a Scan-400 interrogator (SYLEX) for FBG signal readout and OTDR (Optical Time-Domain Reflectometry) measurements for assessing optical path quality (fig. 2)

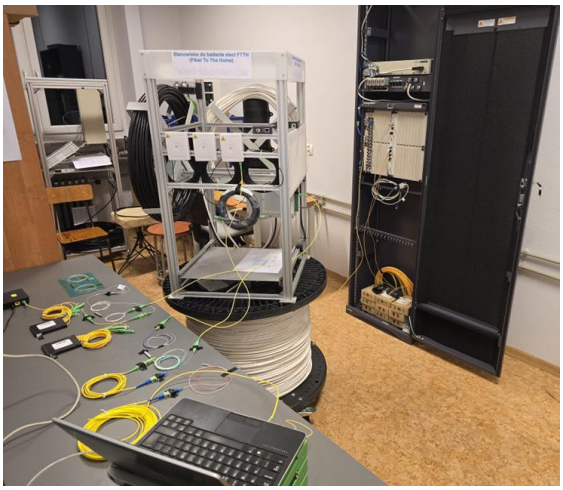

Fig. 2 Experimental setup

Measurement Protocol: Each configuration was tested with variable PLC splitter quantities, including data transmission speed tests (Mbps), FBG peak detection capability and optical loss analysis via OTDR reflectograms.

Results

Experimental validation confirmed successful FBG measurement signal transmission through FTTH telecommunications infrastructure across two of three configurations tested at network distances L1–L3 (0.769–3.513 km).

Configuration K1 (signal combining/splitting) achieved reliable FBG peak detection with stable data rates (938–945 Mbps) and OTDR attenuation of 0.426–2.166 dB/km. Configuration K2 (FBG sensor in main transmission line) delivered superior performance with high-intensity FBG peaks (907–940 Mbps). Configuration K3 (FBG within distribution network) failed due to signal attenuation.

Optical Fiber-Based Remote Powering (PoF) and Sensing Platform for Environmental Applications

P. RADEK, K. RATAJCZYK, T. WOJNAR, K. PAŁUCHOWSKI, A. GARGULA, N. TOMANEK, E. MACIAK

Department of Optoelectronics, Faculty of Electrical Engineering, Silesian University of Technology, 2 Krzywoustego Str., 44-100 Gliwice, POLAND

e-mail address: erwin.maciak@polsl.pl

This paper presents the design and commissioning of a laboratory demonstrator of Power-over-Fiber (PoF) for remote powering of environmental sensing nodes, where optical energy is delivered through a telecom single-mode fiber (SMF) and converted into electrical power at the receiver side. The system was developed to verify feasibility in applications requiring galvanic isolation, high immunity to electromagnetic interference, and potential intrinsic safety. A complete chain was integrated, including an optical source based on an SFP transceiver, an SMF transmission path, and an optical-to-electrical conversion stage using InGaAs photovoltaic devices. It was observed that the average optical output of an SFP operating in a media converter may depend on link activity, which reduces the available harvested power; therefore, direct powering of the laser module was implemented, yielding an approximately six-fold increase in optical power. Measurements of a single InGaAs device confirmed an open-circuit voltage of approximately 0.38 V, while a series connection of four devices provided about 1.31 V, enabling start-up of an ultra-low-power energy management circuit (ADP5091) and charging of a supercapacitor energy store. The sensing subsystem was built around an MSP430 microcontroller operating in an ultra-low-power mode, performing cyclic temperature and humidity measurements (SHT40) every 60 s and transmitting data via UART. The demonstrator confirmed functional viability of the PoF-powered node while revealing power-budget limitations (slow supercapacitor charging), indicating further optimization paths in optical coupling, conversion efficiency, and storage sizing.

Keywords: Power-over-Fiber; optical-to-electrical conversion; InGaAs; energy harvesting; ultra-low-power; MSP430; SHT40; environmental monitoring.

Use of Low Bend-Loss Optical Fibers in Distributed Sensing

M. MAKARA [1], M. GRZESIAK [1], K. POTURAJ [1], G. WÓJCIK [1], A. WALEWSKI [1], M. JÓZWICKI [1], L. CZYŻEWSKA [1], Ł. BEDNARSKI [2], P. MERGO [1]

[1] Laboratory of Optical Fiber Technology, Institute of Chemical Sciences, Faculty of Chemistry, Maria-Curie Skłodowska University in Lublin, 3 Maria Curie-Skłodowska Sq., 20-031 Lublin, Poland
[2] SHM System Sp. z o.o., 82A Jana Pawła II St., 30-444 Kraków

e-mail address: pawel.mergo@mail.umcs.pl

Distributed Fiber Optic Sensing (DFOS) systems have become, in recent years, one of the key technologies for monitoring civil infrastructure, engineering structures, and the natural environment. Their principal advantage lies in the ability to perform continuous measurements of physical parameters—such as strain, temperature, and vibration—along the entire length of an optical fiber, which simultaneously serves as both the transmission medium and the sensing element. Depending on the underlying light scattering mechanism, DFOS systems primarily rely on Rayleigh, Brillouin, or Raman scattering, each providing complementary metrological information.

Rayleigh scattering forms the basis of techniques offering very high spatial resolution, widely used for vibration and dynamic strain sensing (e.g., ϕ-OTDR, OFDR). Brillouin scattering, in turn, enables absolute measurements of strain and temperature over long distances (BOTDR, BOTDA), owing to the dependence of the Brillouin frequency shift on the mechanical and thermal state of the fiber. Raman scattering is commonly employed in distributed temperature sensing (ROTDR/DTS), exploiting the strong temperature dependence of the intensity ratio between the Stokes and anti-Stokes components. Increasingly, efforts are being made to integrate these methods within a single sensing fiber, enabling simultaneous multi-parameter monitoring of the operational environment of the monitored structure.

In practical DFOS deployments, optical fibers rarely operate under ideal conditions. Industrial, energy, and geotechnical installations often require routing fibers through confined spaces with numerous bends of small radii. In standard single-mode fibers, this leads to increased macrobending losses and local perturbations of propagation properties, resulting in degradation of the system power budget, reduced signal-to-noise ratio, and a shortened maximum sensing range. These issues are particularly critical in systems based on weak backscattered signals, where any additional attenuation mechanism directly increases measurement uncertainty.

A promising approach to mitigate these limitations involves the use of bend-insensitive optical fibers, in which a properly engineered refractive index profile enhances modal confinement within the core. However, the performance of such fibers in advanced distributed sensing applications has not yet been fully explored, particularly when multiple scattering mechanisms are exploited simultaneously. Modification of the modal field distribution affects not only bending loss, but also the efficiency of nonlinear processes responsible for Brillouin and Raman scattering. This may result in variations of the Brillouin gain coefficient, Brillouin linewidth, and the efficiency of Stokes and anti-Stokes generation in Raman scattering. Furthermore, stronger confinement of the optical mode near the core center can alter the fiber's sensitivity to microbending and localized transverse stresses, which directly impacts the stability and repeatability of temperature and strain measurements.

This work presents an investigation of the suitability of ultra-low bend-loss optical fibers for multi-parameter distributed sensing systems employing simultaneous Rayleigh and Brillouin scattering. The obtained results confirm that fibers with very low bending sensitivity constitute a promising platform for next-generation multi-parameter DFOS systems, enabling reliable operation under demanding installation conditions.

Acknowledgments: This work was supported by the project 'Distributed Temperature, Elongation and Shape Sensor – DTES Sensor' (FENG.01.01-IP.01-A0FZ/24) financed by the The National Centre for Research and Development.

3D-Printed Structured Optical Fibers for Terahertz Applications

A. ORFINGER[1], B. FORTUNA[1], M. WINKOWSKI[1,2], P. KOMOROWSKI[3], R. KASZTELANIC[1,2], N. PAŁKA[3], R. BUCZYŃSKI[1,2]

[1] Faculty of Physics University of Warsaw, Ludwika Pasteura 5, 02-093, Warsaw, Poland
[2] Łukasiewicz Research Network - Institute of Microeletronics and Photonics, Wólczyńska 133, 01-919 Warsaw, Poland
[3] Military University of Technology, 2 Kaliski Str., 00-908 Warsaw, Poland

e-mail address: a.orfinger@student.uw.edu.pl

Polymer terahertz (THz) waveguides were fabricated using fused deposition modeling (FDM) 3D printing with cyclic olefin copolymer (COC) filament. One anti-resonant fiber (ARF) and three photonic crystal fibers (PCFs) with different geometries were produced for experimental comparison of THz guiding properties. Photographs of the fabricated ARF and PCF structures, together with their characteristic geometric dimensions, are shown in Fig. 1.

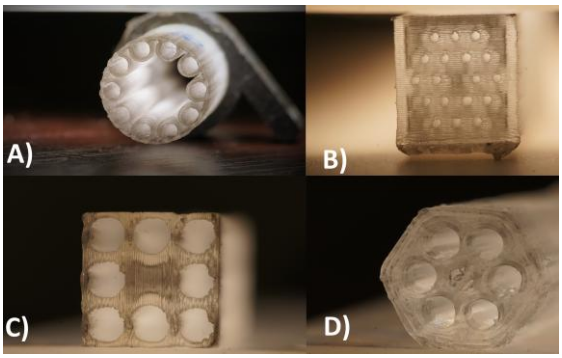

Fig. 1. Fabricated 3D-printed polymer THz waveguides: A) ARF 2: air-core radius 12.12, capillary radius 1.75, wall thickness 0.52, B) PCF 1: hexagon flat-to flat 14.6 – 15.0, C) PCF 2: 12.82 × 11.89, D) PCF3: 12.13 × 12.15. All dimensions are given in millimeters (mm).

Transmission properties were investigated in the 70–120 GHz frequency range. Output intensity distributions recorded with a THz camera confirm that radiation is guided predominantly in the fiber core for both ARF and selected PCF structures. Representative camera images for the ARF and best performing PCF (PCF1) at 90 GHz and 95 GHz are presented in Fig. 2.

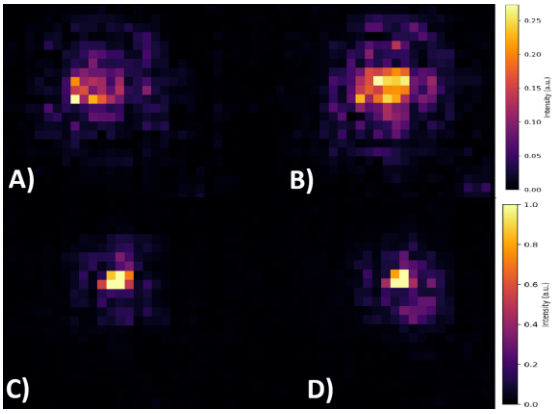

Fig. 2. Output intensity distributions recorded with a THz camera: A) ARF at 90 GHz, B) ARF at 95 GHz, C) PCF1 at 90 GHz, D) PCF1 at 95 GHz. The presented images are heatmaps reconstructed from measured 32 × 32 pixel intensity matrices.

The fabricated PCF and ARF waveguides are capable of guiding THz radiation, with transmission efficiency reaching up to approximately 45% in selected frequency ranges. Further experimental and numerical studies are required to assess the observed behavior and improve the fiber designs.

Acknowledgments:
This work was supported by the National Science Centre, Poland, grant Maestro-14, No. ***UMO-2022/46/A/ST7/00238*** *„Free-form optical fibers for information systems”*

References:

[1] M. Kałuża et al., Materials 17, 5104 (2024).
[2] J. Sultana et al., Fibers 8, 14 (2020).

NATIONAL SCIENCE CENTRE POLAND

Photonic Two-Qubit System for Generation and Characterization of Entangled Photon States

Z. OPILSKI [1], K. WERESZCZYŃSKI [2], A. DANIŁOWICZ [1], K. CYRAN [2], E. MACIAK [1]

[1] Silesian University of Technology, Department of Optoelectronics, Krzywoustego 2, 44-100 Gliwice, Poland
[2] Silesian University of Technology, Department of Computer Graphics, Vision and Digital Systems, Akademicka 2A, 44-100 Gliwice, Poland.

e-mail address: zbigniew.opilski@polsl.pl

Photonic entanglement is a fundamental resource for quantum information processing and experimental studies of non-classical correlations. In this work, we present a photonic two-qubit experimental system for generation, detection, data acquisition, and quantitative characterization of polarization-entangled photon states. The aim of the developed platform is to provide a stable and reconfigurable setup for laboratory investigations of entangled photon pairs. As part of the OptiQ project at the Department of Optoelectronics, in collaboration with the Department of Computer Graphics, Computer Vision, and Digital Systems of the Silesian University of Technology, a laboratory setup was designed and constructed that enables the generation of entangled photons, their detection, and the assessment of entanglement quality through quantum state tomography, as shown on Fig. 1

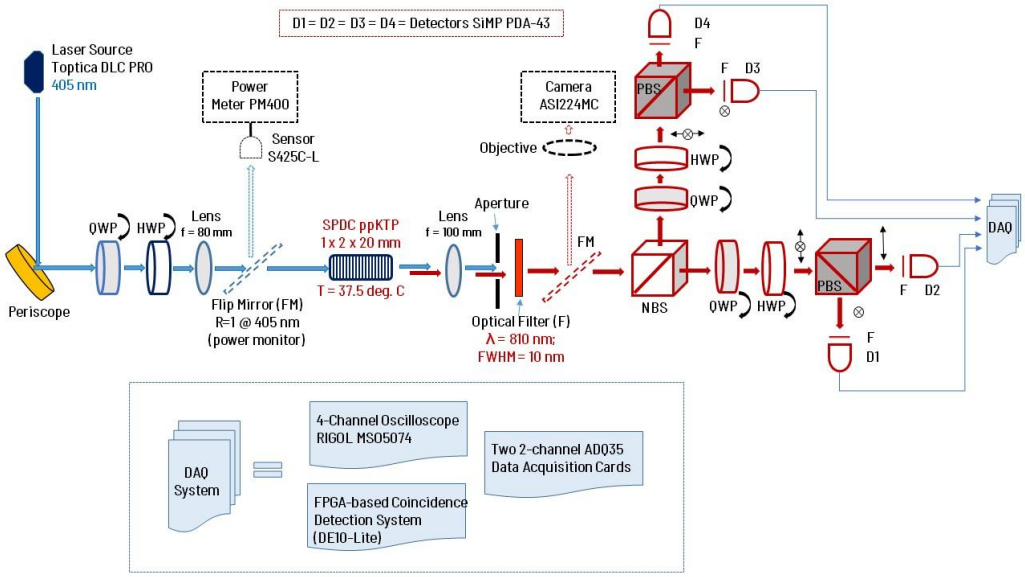

Fig. 1. Experimental setup for detection, analysis and detection of polarization-entangled photon pairs

Photon pairs are generated via type-II spontaneous parametric down-conversion in a periodically poled potassium titanyl phosphate (ppKTP) crystal with dimensions of 1 × 2 × 20 mm, pumped by a continuous-wave diode laser at 405 nm[1],[3]. The down-converted photons are produced at a central wavelength of 810 nm and are spectrally filtered to suppress residual pump radiation and background noise.

The optical layout consists of a beam-splitting stage that separates the photon pairs into two spatially distinct paths, defining the two qubits encoded in photon polarization. Each arm is equipped with a set of wave plates (half-wave and quarter-wave plates) followed by a polarizing beam splitter, enabling projective measurements in arbitrary polarization bases. This configuration allows independent control and analysis of both qubits.

Single-photon detection is performed using up to four silicon avalanche photomultipliers (SiPMs) placed at the outputs of the polarization analysis stage. The detector signals are processed by a custom-built FPGA (Field-Programmable Gate Array)-based coincidence module implemented on a DE10-Lite platform. Alternatively, a four-channel oscilloscope with a sampling time of 0.5 ns and 8-bit resolution is used for full waveform recording

with acquisition times of up to approximately 1 ms. The FPGA-based system also enables pulse counting in individual channels and the determination of signal coincidences within a specified time window. In addition, the system has been extended with two high-speed data acquisition cards offering 12-bit resolution and a sampling rate of 5 GS/s per channel, enabling parallel feature extraction from the signals and extended continuous data acquisition. This arrangement enables time-correlated photon counting and real-time monitoring of coincidence events. The modular electronics architecture allows flexible adjustment of coincidence windows and supports further extension toward advanced timing and correlation analysis.

The generated two-photon states are characterized using polarization correlation measurements and quantum state tomography. By performing projective measurements in multiple polarization bases, the density matrix of the two-qubit system can be reconstructed[2]. This enables quantitative evaluation of entanglement properties and assessment of the quality of the generated photonic states. The applied characterization procedure is compatible with standard polarization-encoded qubit protocols and can be readily extended to more complex measurement schemes.

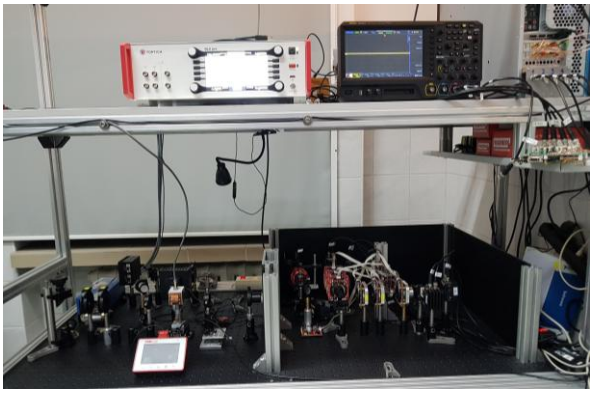

Fig. 2. Experimental setup for detection, analysis and detection of polarization-entangled photon pairs – real photo

The experimental system has been fully assembled and aligned. Initial measurements demonstrate stable generation of photon pairs and reproducible coincidence statistics over extended acquisition times. The recorded polarization correlations confirm the proper operation of the source and analysis stages, providing a basis for quantitative state characterization.

The presented system constitutes a modular experimental platform for investigations of photonic entanglement. Ongoing work is aimed at further optimizing the setup and expansion of its measurement capabilities. The illustration on Fig. 2 depicts the real measurement setup described above.

Literature:

[1]. Omshankar, Vivek Venkataraman, Joyee Ghosh, “Bright source of narrowband polarization-entangled photons from a thick type-II ppKTP crystal”, Optics Express, vol.32. No. 3/29 Jan 2024, 3470-3479.

[2]. Daniel F. V. James, Paul G. Kwiat, William J. Munro, Andrew G. White, “Measutement of qubits”, Physical Review A, vol. 64, 2001, 052312-1 - 052312-15.

[3]. Ali Motazedifard, S. A. Madani, J. J. Dashkasan, N. S. Vayaghan, “ Nonlocal realism test and quantum state tomography in Sagniac-based type-II polarization-entanglement SPDC-source”, Heliyon, vol. 7, 2021, 1-8.

Acknowledgments: This research was financially supported (partially) by the Silesian University of Technology research subvention (SUBB) under Grant No. 05/040/BK_26/2044.

Acknowledgments: This research was financially supported (partially) by the Silesian University of Technology research subvention (SUBB) under Grant No. 05/040/BK_26/2044.

Applicability of Commercial Optical Backscatter Reflectometer LUNA OBR4600 to Strain Measurements in Presence of Vibrations

A. PAŹDZIOR [1], J. RZECZKOWSKI [2], P. MACIĄG [2], P. MERGO [1]

[1] Laboratory of Optical Fiber Technology, Institute of Chemical Sciences, Faculty of Chemistry, Maria-Curie Skłodowska University in Lublin, 3 Maria Curie-Skłodowska Sq., 20-031 Lublin, Poland
[2] WaveFlow System Sp. z o.o., 1 Ignacy Mościcki St., 24-110, Puławy, Poland

e-mail address: adam.pazdzior@mail.umcs.pl

Rayleigh-scattering-based methods of fiber-optic distributed sensing are sensitive to even miniscule strain changes caused by vibration of sensing optical fiber. This sensitivity is used for constructing distributed acoustic sensors (DAS) based on phase-sensitive optical time-domain reflectometers that interrogate sensing fibers with light pulses sent into optical fiber at high-frequency rates (kilohertz). One of the factors limiting usability of distributed acoustic sensors in some applications is their spatial resolution of the order of one meter, or more. Thus, in many applications that do not require long sensing ranges optical frequency-domain reflectometry (OFDR) is a go-to solution for distributed strain sensing, as it readily enables measurements with spatial resolution of the order of centimeters, or even millimeters. In order to achieve such resolutions, the internal laser of OFDR interrogator must be swept over a broad wavelength range, which takes some time and ultimately limits interrogation rates of such devices because of the finite bandwidths of photodetectors and sampling rates of data acquisition devices—necessary sampling rate is proportional to laser sweep rate and characteristic trigger delay of the internal trigger/clock interferometer, which in turn poses a limit on sensing range due to the Nyquist–Shannon sampling theorem.

Although there are ODFR interrogators capable of operation at some dynamic rates (for example, LUNA ODiSI performance ranges from 250 Hz with short sensing range of 2.5 m down to 10 Hz with sensing range of 100 m), often in laboratory practice LUNA OBR4600 that has measurement rates below 1 Hz is used. In this work, based on actual experimental results from an aerodynamic tunnel, we discuss how vibration of a sensing fiber affects measurements made with LUNA OBR4600 and how its performance in presence of vibrations can be improved by adjustment of measurement hardware settings (sweep rate) and data processing settings (gauge length).

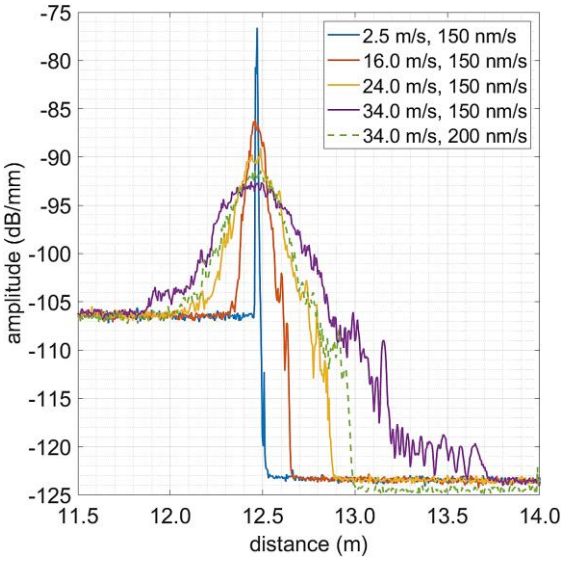

Fig. 1. Sensing optical fiber end reflection peak at various air flow speeds related to various set frequencies of turbine of aerodynamic tunnel. For the air flow speed of 34 m/s results for two sweep rates of LUNA OBR4600 internal laser are presented.

Acknowledgments: The measurements have been performed with the use of the infrastructure (aerodynamic tunnel) of Lublin University of Technology and with help of Konrad Pietrykowski and Paweł Magryta from Department of Thermodynamics, Fluid Mechanics and Aviation Propulsion Systems, Faculty of Mechanical Engineering, Lublin University of Technology.

The purchase of LUNA OBR4600 used in the experiments has been funded by the project „National Laboratory for Photonics and Quantum technologies" (Acronym: NLPQT; POIR.04.02.00-00-B003/18-00).

From Electronic Sensor to Optical Sensor – Concept of SPR Hydrogen Sensor Based on Polycarbazole Receptor Film

M. PROCEK[1], K. GŁOSZ[2], Ł. DREWNIAK[1], Z. OPILSKI[1], E. MACIAK[1], A. STOLARCZYK[2], T. JAROSZ[2]

[1] Department of Optoelectronics, Silesian University of Technology, 2 Krzywoustego Str., 44-100 Gliwice, Poland
[2] Department of Physical Chemistry and Technology of Polymers, Silesian University of Technology, Strzody 9, 44-100 Gliwice, Poland

e-mail address: marcin.procek@polsl.pl

Hydrogen sensors have become a crucial part of safety systems due to the increasing use of hydrogen as a fuel in the automotive and energy industries. The main concern is the risk associated with hydrogen's flammability and explosiveness over a wide concentration range in air. For this reason, hydrogen sensors must meet the safety requirements of the ATEX directives. Consequently, the optimal sensing solution should operate at room or ambient temperature and require minimal energy at the sensing head.

Our group has proposed a microelectronic, room-temperature hydrogen sensor based on polycarbazole deposited on Pt electrodes [1,2]. This method demonstrated high sensitivity across a wide range of hydrogen concentrations (from tens of ppm up to several percent). However, an optical hydrogen sensor would be even more advantageous, as it would eliminate the need for electrical power at the sensing transducer.

In the present work, we introduce the concept of an optical sensor based on sensing phenomena observed in polycarbazole films. The design relies on surface plasmon resonance (SPR) in the Kretschmann configuration, utilizing a gold thin film combined with an electropolymerized PCz layer. Both experimental studies and computer simulations are presented to demonstrate system performance. Experimentally, we describe the fabrication of the SPR transducer, deposition of the PCz thin film, and optical characterization using spectral ellipsometry. The optical modeling, performed using the STACK solver in Ansys Lumerical, provides calculations of the angular–spectral characteristics of the SPR sensor structure. These calculations show good agreement with the experimental results. The results (Fig. 1) demonstrate that the SPR effect can be observed in an Au/PCz structure on a glass substrate, providing a proof of concept for a future sensing system.

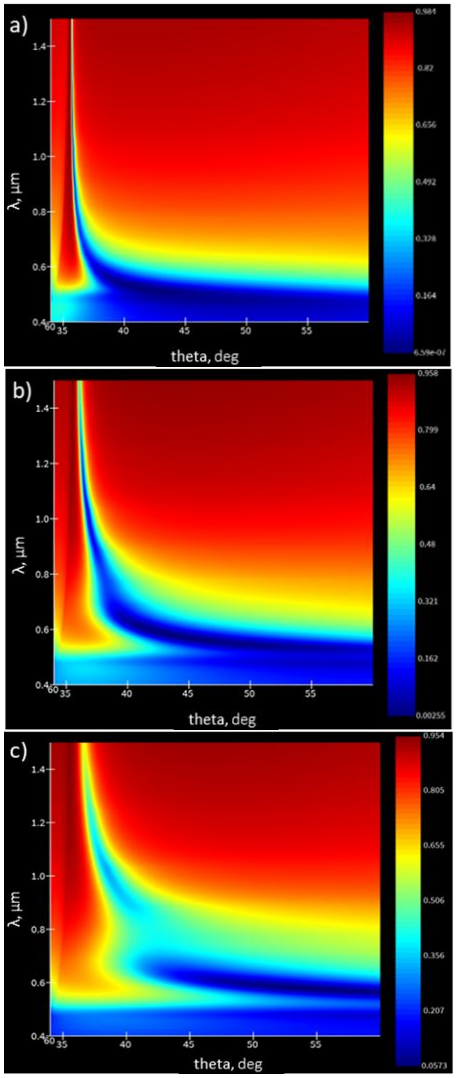

Fig.1. Calculated spectral and angular characteristics of structures with SPR films on glass substrates: a) Cr 1.4 nm/Au 37 nm; b) Cr 1.4 nm/Au 37 nm/PCz 20 nm; c) Cr 1.4 nm/Au 37 nm/PCz 40 nm

Acknowledgments: This work was supported by the research subsidy provided by the Polish Ministry of Education and Science, Grant No. 05/040/BK_26/2044; M.P. acknowledges the scientific and innovative merit grant no. 05/040/RGJ25/2032 of the Rector of Silesian

University of Technology. Publication supported by the Rector's habilitation grant implemented under the Excellence Initiative – Research University program. Silesian University of Technology, grant no. 05/040/SDU/10-07-01.

References:

[1] A. Stolarczyk, T. Jarosz, M. Procek, Patent PL (2022), No. 242011, (2022)
[2] A. Stolarczyk, , T. Jarosz, M. Procek, Sensors 19(5), 1098 (2019);

Polymer Receptor for PFAS: Material Rationale and Fiber-Optic Sensing Implications

P. RADEK, K. BARCZAK, A. OLSZEWSKA

Department of Optoelectronics, Faculty of Electrical Engineering, Silesian University of Technology,
2 Krzywoustego Str., 44-100 Gliwice, POLAND

e-mail address: patryk.radek@polsl.pl

This work presents material-driven premises and a preliminary validation of using poly(vinylidene fluoride) (PVDF) as a durable receptor layer for optical detection of PFAS in water under (quasi-)continuous operation. A fiber-optic Fabry–Pérot interferometric (FPI) sensor is proposed, where a PVDF coating deposited on the fiber end-face plays a dual role: (i) it sorbs the analyte (PFOS) and (ii) it forms the interferometric cavity. The sensing response is quantified as a shift of reflection-spectrum extrema caused by changes in the optical path length n·L (effective refractive index and coating thickness), associated with pore filling by water and PFOS sorption. FTIR characterization confirms a multiphase PVDF structure (α and β phases, with a possible γ contribution), while SEM reveals a porous, sponge-like morphology that increases the effective active surface area. Tests in the 1550 nm band (SLD source + circulator + OSA) show a small baseline drift in pure water (~0.0002 nm/s; ~0.2 nm/1000 s), whereas exposure to PFOS produces a markedly stronger response (e.g., for 0.001 ng/mL: ~0.0037 nm/s; ~1.67 nm/450 s) and enables separation of λ_max(t) trajectories for different concentrations. Practical calibration metrics are suggested (Δλ after a fixed exposure time or dλ/dt within a defined time window), along with the need for signal stabilization and drift compensation. The results support the potential of PVDF/FPI as a platform for miniature in-situ sensors and for integration into distributed PFAS monitoring networks.

Keywords: PVDF; PFAS; PFOS; fiber-optic sensor; Fabry–Pérot interferometer (FPI); optical detection; in-situ monitoring.

Advances in Sensor Technologies and Machine Learning for Glyphosate and Pesticide Detection in Water

A. PALECZEK[1] , D. GROCHALA[1], S. KARCZ[1], M. KOCOŃ[1], A. RYDOSZ[1]

[1] AGH University of Krakow, Faculty of Computer Science Electronics and Telecommunications, Institute of Electronics, al. A. Mickiewicza 30 Krakow, 30-059, Poland

e-mail address: rydosz@agh.edu.pl

Detection of glyphosate and other pesticides in water increasingly relies on sensor technologies that produce complex, multidimensional signals, including Raman/SERS spectra, voltametric waveforms, image data from vision-based systems, and microwave responses [1, 2, 3]. Because of their structural complexity and sensitivity to environmental disturbances, these signals are often difficult to interpret using classical univariate analysis methods, which frequently prove inadequate.

To overcome these limitations, machine learning (ML) and artificial intelligence (AI) techniques are now widely employed to efficiently analyze multivariate sensor data. Commonly used approaches include dimensionality reduction and data visualization methods (e.g., Principal Components Analysis (PCA)) classification algorithms for identifying individual compounds or mixtures (such as k-Nearest Neighbors (KNN), Support Vector Machines (SVM), Linear Discriminant Analysis (LDA), and Random Forest) [1], and regression models for the quantitative estimation of contaminant concentrations (including Partial Least Squares Regression (PLSR) and neural networks) [3]. In addition, integrating sensor platforms with IoT technologies and wireless sensor networks enables continuous water-quality monitoring and supports the development of intelligent early-warning systems for anthropogenic pollution at a low cost and with high effectiveness [4].

This paper reviews recent sensor-based strategies for glyphosate and pesticide detection in water that employ machine-learning analysis. Most reported studies exploit high-dimensional sensor outputs, where ML methods play a crucial role in both compound discrimination and accurate quantification at trace concentration levels.

The paper published by Gómez *et al.* presents an electronic tongue-type system based on screen-printed carbon electrodes for the detection of pesticides in water. The electrochemical responses of the sensors were analyzed using machine learning and multivariate analysis methods, including PCA, LDA, SVM, and KNN. The algorithms used enabled unambiguous classification of the pesticide type and estimation of its concentration, achieving very high discrimination efficiency between the tested compounds and high quantitative prediction accuracy. The techniques achieved over 90% accuracy in determining pesticide concentrations. Moreover, compound-type classification was achieved with a 100% success rate. The results confirm the potential of combining low-cost electrochemical sensors with machine learning methods for effective water pollution monitoring [1].

Wang *et al.* presented a dual-mode sensor for glyphosate detection that combines photoelectrochemical and fluorescent signals generated by a CdTe/$Bi_4O_5Br_2$ heterostructure. A key element of the work is the application of machine learning to fuse and analyze data from both sensor channels. The authors utilized dimensionality reduction and classification methods (including PCA, LDA, and KNN) to extract significant signal features and precisely distinguish analyte concentrations. ML-assisted fusion of photocurrent and fluorescence signals reduced the glyphosate detection limit to 1.27 fM, ~3.4× and ~5.4× lower than PEC or fluorescence alone. Integrating dual-mode transduction with ML algorithms significantly improved the sensitivity, selectivity, and reliability of detection, confirming the potential of ML as a tool for developing intelligent chemical sensors [2].

Aira *et al.* present SpectroGLY, a low-cost, portable IoT system for detecting glyphosate residues in water that combines VIS–NIR spectral sensing, data analytics, and cloud infrastructure into a coherent measurement ecosystem. At the core of the device is the AS7265X multispectral sensor (410–940 nm, 18 channels), used for colorimetric analysis of the glyphosate-ninhydrin reaction, which generates an absorption peak around 570 nm. Based on this, a linear regression model (calibrated to 10–2000 mg/L) was developed, enabling automatic classification of samples using traffic-light indicators (none, warning, high

contamination). The system supports Wi-Fi, LoRaWAN, and BLE connectivity and integrates a mobile app and an IoT platform (ThingsBoard) to provide geolocation, measurement history, and environmental condition validation, enabling applications in both the field and the laboratory. Validation results show high agreement with the reference laboratory spectrometer, no false classifications, and the ability to obtain a result in approximately 10 minutes, with a device cost of approx. 250 USD, making SpectroGLY a promising alternative to expensive and time-consuming laboratory analyses and a solid base for further development towards more advanced ML methods [4].

The system proposed by Ranbir *et al.* utilizes a portable array of azo dyes that react with various pesticides and herbicides. Machine learning and multivariate analysis play a key role in data analysis. Methods such as PCA, LDA, and PLSR enable the extraction of characteristic signal patterns, the differentiation of analytes even in mixtures, and the accurate estimation of their concentrations. The use of ML enabled the achievement of high correlation between predicted and actual pesticide concentrations (R^2 = 0.89–0.96) and the effective classification of various compounds, including mixtures, with detection limits of 5–12 ppm. Integrating ML with sensor arrays not only increases detection sensitivity and selectivity but also enables automatic sample classification in the field, significantly enhancing the system's practical utility for monitoring water, soil, and agricultural products [3].

Overall, these studies show that machine learning is a key enabling technology for sensor-based detection of glyphosate and pesticides in water. The reviewed studies show that modern approaches to detecting glyphosate and other pesticides in water increasingly depend on sensor platforms that generate complex, multivariate signals. Interpreting this type of data reliably is difficult without MI/AL and chemometric methods. In electrochemical electronic tongues and microwave sensors, ML is primarily applied to pattern recognition and regression tasks, providing detection limits sufficient for rapid screening applications. Overall, ML and AI have evolved from supportive tools into key enabling components, effectively narrowing the gap between low-cost sensing platforms and laboratory-grade analytical techniques, and facilitating the development of fast, selective, and field-deployable systems for monitoring pesticide contamination in water.

Acknowledgments: This work was supported by NCBR HYDROSTRATEG1/0006/2022 “An integrated intelligent monitoring system limiting the migration of compounds of anthropogenic origin in rainwater retention systems”.

References:

[1] Gómez et al., Water, 2023, 15(4), 624;
[2] Wang et al., Chemical Engineering Journal, 2025, 525, 170337;
[3] Ranbir et al. Anal. Chem. 2023, 95, 39, 14533–14540
[4] Aira et al. IEEE Transactions on Instrumentation and Measurement, 71, 2022, 600561

Holographically Designed Diffractive Optical Element for Efficient Coupling into Multicore Fibers

M. KAŁUŻA, K. POGORZELEC, A. SIEMION, P. LESIAK

Faculty of Physics, Warsaw University of Technology, Koszykowa 75, 00-662, Warsaw, Poland

e-mail address: agnieszka.siemion@pw.edu.pl

Fiber-optic–based solutions, particularly those employing multicore fibers (MCFs), have found numerous applications in areas such as biosensing [1] and optical communications [2]. However, their practical implementation requires efficient fiber-optic coupling solutions. Conventional coupling approaches typically rely on concepts such as used biconical tapering techniques [3] or planar lightwave circuit (PLC) splitters [4]; nevertheless, these methods suffer from several inherent limitations. Consequently, alternative approaches are being actively explored, among which fan-in/fan-out couplers have emerged as particularly promising solutions.

Fan-in/fan-out couplers enable selective excitation of individual MCF cores by appropriately shaping the optical beam in free space such that it fits within the numerical aperture (NA) of the fiber. Moreover, such functionality can be implemented using a single diffractive optical element (DOE), resulting in a compact and mechanically robust architecture.

The rapidly advancing field of additive manufacturing, in particular two-photon polymerization (TPP), enables the fabrication of DOEs directly on the facet of an MCF [5]. A printing resolution reaching 100 nm ensures high fabrication precision [6], allowing the realization of phase-encoded DOE structures with continuous surface profiles, which theoretically can achieve diffraction efficiencies approaching 100% [7].

In this study, we present a fan-in fiber-optic coupler based on a holographically designed DOE to simultaneously excite all cores of a four-core optical fiber. The proposed coupler is applicable to both optical communication systems and biosensing platforms.

The DOE was designed using an iterative algorithm based on a modified Gerchberg–Saxton method [8], resulting in a diffractive optical element designed as a hologram. The phase delay map of the proposed structure is shown in Fig. 1a. Subsequently, the structure was fabricated on a glass substrate using TPP; a microscope image of the printed DOE is presented in Fig. 1b.

The structure shown in Fig. 1 was designed for an operating wavelength of 1550 nm and has a diameter of 150 µm. It redirects an incident Gaussian beam emerging from a single-mode fiber (SMF) into the four cores of a four-core fiber at a distance of 310 µm. In this study, the input SMF was Corning SMF-28, while the four-core fiber was Fibercore SM-4C1500(8.0/125)/001, featuring a core-to-core spacing of 50 µm. During the slicing process, the three-dimensional model of the structure was discretized into 15 phase levels, yielding a theoretical diffraction efficiency of approximately 99%.

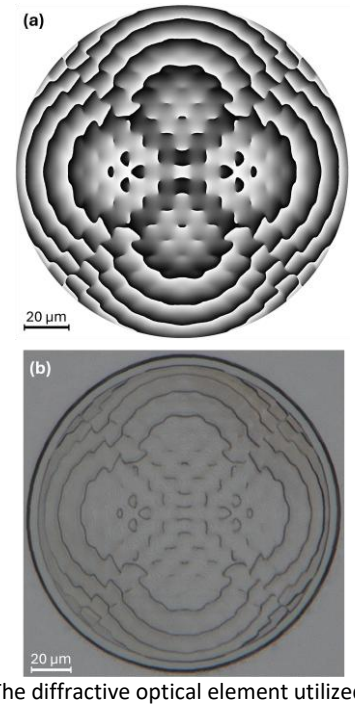

Fig. 1. The diffractive optical element utilized for the coupler implementation: (a) phase map of the structure; (b) microscope image of the 3D-printed structure.

Numerical simulations were carried out to verify the correct operation of the structure shown in Fig. 1 using LightSword 6.0 software, based on the modified convolution method [9]. The resulting intensity distribution in the plane of the four-core fiber facet is presented in Fig. 2. The positions of the fiber cores and the cladding are marked in white in Fig. 2.

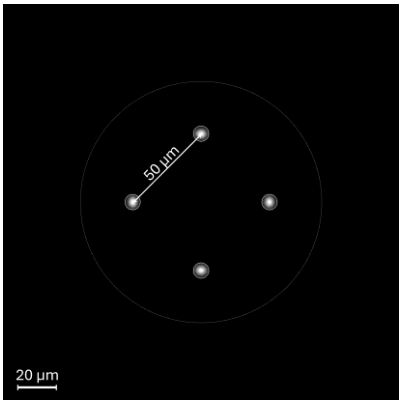

Fig. 2. Numerical simulation results of the intensity distribution in the four-core fiber facet plane.

The obtained results clearly demonstrate the correct operation of the proposed structure. The incident radiation is successfully redirected into the regions corresponding to the four cores of the four-core optical fiber. Importantly, the focal spots are well confined within the individual fiber cores and simultaneously remain within the numerical aperture (NA) of the fiber. Moreover, no significant signal losses were observed within the analyzed region, which could otherwise arise, for example, from improperly diffracted radiation caused by imperfections in the structure. Therefore, at the stage of numerical simulations, the designed structure demonstrates correct and efficient operation.

Subsequently, the structure was fabricated directly on the facet of the four-core optical fiber using TPP. For this purpose, a dedicated scaffold was employed, enabling precise positioning of the structure at a distance of 310 µm from the fiber facet, as well as accurate alignment with respect to the fiber cores. A microscope image of the printed structure on the fiber facet is shown in Fig. 3. The fabricated structure constitutes the final fan-in optical coupler.

Preliminary experimental results obtained for the printed coupler on the fiber facet are presented in Fig. 4, which shows the intensity distribution recorded using an infrared (IR) camera (Xenics Xeva 17437) behind the end facet of the four-core fiber.

The preliminary experimental result presented in Fig. 4 indicates correct operation of the fan-in coupler. All four cores of the multicore fiber were successfully excited. Moreover, the recorded intensity distributions emerging from each core exhibited comparable intensity levels, demonstrating that the structure evenly distributed the optical power among the cores of the four-core fiber.

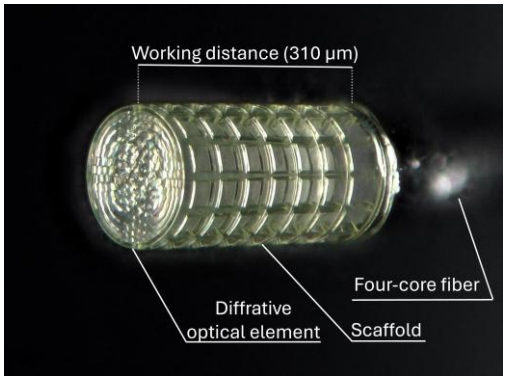

Fig. 3. Structure fabricated on the facet of the four-core optical fiber using two-photon polymerization.

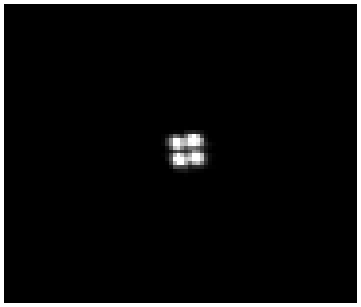

Fig. 4. Experimental result showing the intensity distribution at the output of the four-core optical fiber.

To summarize, this study demonstrated a compact fiber-optic fan-in coupler based on a single DOE fabricated via TPP directly on the facet of a four-core fiber. Numerical simulations and preliminary experiments confirmed efficient and uniform excitation of all fiber cores, highlighting the potential of the proposed approach for MCF applications in optical communications and biosensing.

Funding: Research was funded by Warsaw University of Technology within the Excellence Initiative: Research University (IDUB) programme.

References:

[1] Z. Zhao et. al., Opto-Electron. Adv. 3, 2, (2020)
[2] W. Chen et. al., Photonics 11, 3, (2024)
[3] F. Anell et. al., J. Lightwave Technol. 42, 7, (2024)
[4] Y. Xu et. al., Adv. Quantum Technol. 6, 8, (2023)
[5] C. Xiong et. al., Front. Mater. 7, (2020)
[6] K. Bornillo et. al., Prog. Addit. Manuf. 10, 9, (2025)
[7] A. Siemion, J. Infrared Millim. Terahertz Waves 40, 9, (2019)
[8] M. Kaluza et. al., Opt. Lasers Eng. 184, (2025)
[9] M. Sypek, Opt. Comm., 116, 1–,3 (1995)

Passive Integrated Photonics Platform for VIS Spectral Range

M. SŁOWIKOWSKI [1], D. DRECKA [1], M. JUCHNIEWICZ [1], B. STONIO [1],
M. GOLAS [1], M. FILIPIAK [1], M. LELIT [1,2], M. JAROSIK [1,2]

[1] Warsaw University of Technology, Centre for Advanced Materials and Technologies CEZAMAT, Poleczki 19, 02-822, Warsaw, Poland
[2] Warsaw University of Technology, Institute of Microelectronics and Optoelectronics, Koszykowa 75, 00-662, Warsaw, Poland

e-mail address: mateusz.slowikowski@pw.edu.pl

Silicon nitride (SiN), alongside silicon-on-insulator (SOI) and indium phosphide, constitutes the third major material platform for photonics. Its key advantages include a broad transparency window extending from the visible to the mid-infrared range, compatibility with CMOS fabrication processes, low propagation losses, and a relatively high refractive index contrast between SiN and SiO_2, enabling compact photonic components. A distinguishing feature of this platform is the capability to realize circuits operating in the visible spectral range, which finds applications in areas such as sensing and life sciences.

In order to fully exploit the potential of integrated photonics, it is necessary not only to achieve the desired optical parameters of the system, but also to establish connections with the external environment, provide mechanical protection for the system and ensure temperature stabilisation. These issues fall within the scope of optoelectronic packaging.

The work currently being carried out is being conducted in two areas simultaneously: preparing photonic integrated circuits for photonic packaging and improving the lithography process.

In the area of packaging preparation, it is necessary to improve the quality of the interface between the photonic integrated circuit and the optical fibre. On the photonic integrated circuit side, in the case of edge coupling, this involves obtaining perpendicular side walls with low roughness in the waveguide area, a precise arrangement of waveguides at the edge and obtaining the largest possible mode field. In order to improve these aspects, waveguides have been arranged at the edge at fixed intervals equal to the spacing of optical fibres in a standard fibre array unit. Inverted tapers have been designed and tested in order to increase the mode field of the waveguides. As part of the work carried out, A dedicated lithography process for precisely defining the borders of photonic integrated circuits was developed. As next step optimization of the deep etching process (above 100 µm depth) was done in order to prepare the edges of photonic integrated circuits before saw dicing. Further work in this area is being carried out - it is planned to combine the fabrication of inverted tapers with a suitably prepared side edge of photonics integrated circuits.

As an intermediate step towards optoelectronic packaging, a photonic integrated circuit was mounted on a dedicated printed circuit board, with wire connections to the thermomodulator heaters. The result of the work is presented in Figure 1.

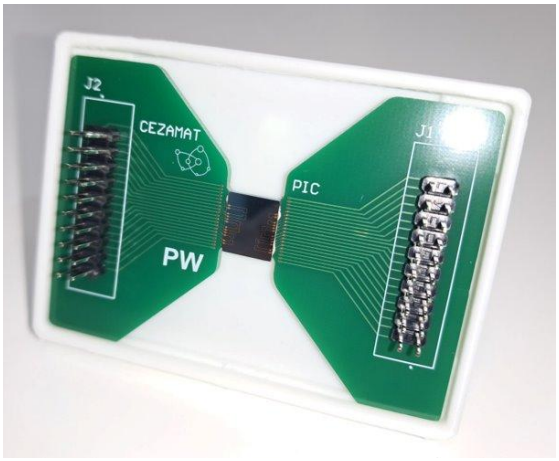

Fig. 1. Photonic integrated circuit mounted on a dedicated printed circuit board.

In parallel with the activities described above, work is underway on the development of technologies for fabrication of waveguides and other integrated photonic components. As part of the work carried out, a series of optimization of the electron beam lithography technique was completed. Lithography is the first stage of transferring the design layout to the material and, together with reactive ion etching, determines the quality of the pattern. During the research, issues related to the selection of the diameter and density of the electron beam spots were analysed in the context of exposure precision in nanometric range and process time duration. This was

followed by experiments aimed at calibrating the lithography process in terms of proximity effect correction for the final set of sample materials – silicon, silicon oxide and silicon nitride. As a result of the work carried out, a set of parameters for the electron beam lithography process was obtained, which will enable the precise transfer of the designed photonic topographies of integrated circuits to the intermediate layer and will be a suitable starting point for further technological processes.

Acknowledgments: This work has received support from The National Centre for Research and Development (Poland), through project SiNPIC (LIDER14/0068/2023).

Influence of Polarization on Demodulation Methods for Determining the SRI Value for a Single TFBG and an Orthogonal Grating System

S.CIĘSZCZYK, D. HARASIM, K. SKORUPSKI, P. PANAS, J. KLIMEK

Politechnika Lubelska, ul. Nadbystrzycka 38d, 20-618 Lublin

e-mail address: k.skorupski@pollub.

This paper presents a comparison of the spectra of single and cascade of two tilted fiber Bragg grating (TFBG) sensors. These sensors are characterized by high sensitivity to the refractive index. The disadvantage of a single TFBG is cross-sensitivity to changes in the polarization of the light introduced to the sensor, which is visible both when analyzing individual modes and when analyzing a wide spectral range with global demodulation algorithms. In response, a cascade structure was created consisting of a set of two TFBGs connected in series with 90 degrees of mutual rotation between them. This work presents a comparison of the polarization cross-sensitivity of sensor spectral demodulation algorithms for measuring the surrounding refractive index (SRI). While maintaining the high accuracy of the SRI measurement typical of TFBG gratings, a cascade of two such gratings properly oriented toward each other allows for a significant reduction in the sensitivity of the SRI measurement to polarization changes. Importantly, the reduction in the polarization cross-sensitivity is significantly greater for the demodulation methods that determine the cutoff wavelength shift; owing to this, a perpendicular TFBG(P-TFBG) measurement system without polarization control remains highly reliable. The application of the proposed P-TFBG system also allows greater SRI sensitivity to be obtained for a single tilted grating with the same tilt angle.

References:

1. B. Jiang, K. Zhou, C. Wang, et al., Opt. Express 25(21), 25910–25918 (2017).
2. C. Chen, C. Caucheteur, P. Mégret, et al., Meas. Sci. Technol. 18(10), 3117–3122 (2007).
3. J. Albert, L. Y. Shao, and C. Caucheteur, Laser Photonics Rev. 7(1), 83–108 (2013).
4. T. Guo, F. Liu, B. O. Guan, et al., Opt. Laser Technol. 78(B), 19–33 (2016).
5. T. Guo, Z. C. Zhang, F. Liu, et al., in 2013 6th IEEE/International Conference on Advanced Infocomm Technology (ICAIT) (2013), pp. 242–243.
6. K. Tomyshev, E. I. Dolzhenko, A. D. Vasilyeva, et al., Sens. Actuators, B 384, 133618 (2023).
7. C. Caucheteur, V. Voisin, and J. Albert, Opt. Express 21(3), 3055–3066 (2013).
8. P. Kisała, K. Skorupski, S. Ci ¸esczyk, et al., Metrol. Meas. Syst. 25(3), 429–440 (2018).
9. T. Guo, F. Liu, B. O. Guan, et al., Opt. Express 22(6), 7330–7336 (2014).
10. Y. C. Lu, R. Geng, C. Wang, et al., J. Lightwave Technol. 28(11), 1677–1684 (2010).

Multi-Pass Measurement Chamber as a Tool for Detection of Trace Substances in Aqueous Environment

P. WERAJTIS, J. IMAŃSKA, W. GILICKI, W. KOZŁOWSKI, V. STAWINOGA, K. BARCZAK, A. OLSZEWSKA

Department of Optoelectronics, Faculty of Electrical Engineering, Silesian University of Technology,
2 Krzywoustego Str., 44-100 Gliwice, POLAND

e-mail address: kamil.barczak@polsl.pl

Introduction

Water quality monitoring represents a critical challenge in environmental protection and public health. Current methods for detecting trace substances in aqueous environments often require high sensitivity combined with rapid measurement capabilities. Optical spectroscopy offers a promising approach for such applications; however, conventional single-pass absorption measurements are frequently limited by insufficient optical path lengths and weak absorption signals, particularly for dilute analyte concentrations.

Motivation and Objective

The primary motivation of this work is to develop a rapid and sensitive detection method for trace substances in water. We present a comprehensive study of a multi-pass measurement chamber designed to enhance the sensitivity of optical spectroscopy through the extension of the effective optical path length. The objective of this research is to design, fabricate, and experimentally validate a multi-pass cell capable of detecting analytes in aqueous samples with improved sensitivity.

Methodology

The project was realized through a systematic approach combining optical modeling, numerical simulation, prototype design, and experimental validation:

Optical Design and Simulation: We employed Zemax optical design software to optimize the chamber geometry and light propagation properties.

The simulations focused on analyzing the influence of chamber geometry and mirror materials on light propagation, effective optical path length, and optical losses. The simulation results were used to modify the mirror positions and select the input beam parameters (fig. 1).

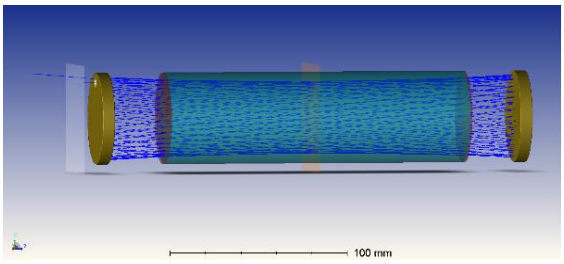

Fig. 1. Simulation of laser beam propagation in the chamber using Ansys Zemax software.

CAD Design and Fabrication: The optimized design was translated into a three-dimensional model using Fusion 360 CAD software, facilitating precise manufacturing of the measurement chamber prototype.

System Integration: The fabricated multi-pass cell was integrated with a complete optical measurement setup that included a light source operating at a wavelength of 635 nm powered by a laboratory power supply. The optical signal was delivered to the measurement chamber by an input optical fiber, where a dedicated mirror system implemented multiple reflections of the light beam. Inside the chamber, a measurement cuvette containing the analyte solution was precisely positioned along the optical path.

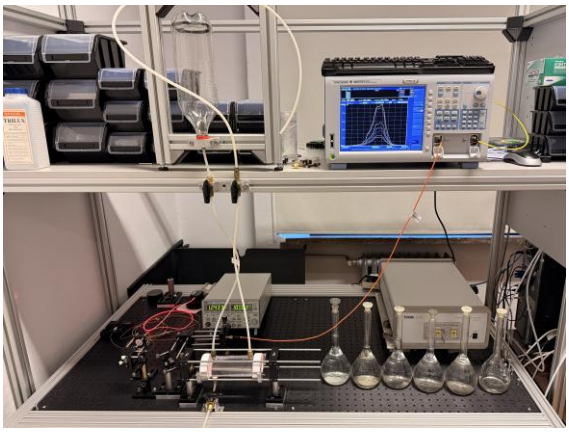

Fig. 2. Measurement setup with visible light source, mirror system, and measurement chamber equipped with a cuvette.

After passing through the chamber, the transmitted light was collected by an output optical fiber and directed to a Yokogawa AQ6370D Optical Spectrum Analyzer, which was used for signal detection and analysis. The measurement setup is shown in figure 2 and figure 3.

Fig. 3. Measurement chamber during calibration using a red laser (630 nm) – visible beam trajectory reflected between mirrors.

Experimental Validation

Absorption measurements were performed using aqueous solutions of potassium chloride (KCl) and sodium chloride (NaCl) at various concentrations (0–30 g/L for NaCl, 5 g/L for KCl) to verify the system's capability for detecting concentration-dependent changes in optical signal intensity.

Results

The experimental results conclusively demonstrate that the designed and fabricated multi-pass chamber prototype meets all specified requirements. The developed system enables:

1. Reliable Detection: Quantitative detection and discrimination of analyte concentration changes through analysis of optical signal variations at the chamber output.
2. Measurement Repeatability: High repeatability of absorption measurements across multiple test cycles, confirming the system's stability and consistency.
3. Concentration Sensitivity: Clear correlation between analyte concentration and detected optical signal intensity, with the system successfully discriminating between solutions of different salt concentrations.

The optical signal measurements exhibited strong concentration dependence, enabling qualitative assessment of analyte presence and quantitative determination of concentration levels. Repeated measurements for identical samples showed minimal variation, confirming system stability and measurement reliability.

Applications and Future Work

This research establishes a foundation for advanced optical sensing applications in water quality monitoring. The multi-pass cell technology demonstrates significant potential for deployment in rapid, portable water monitoring systems. Future development directions include:

• Minimization of optical losses and signal noise through optimized fiber coupling and light path design
• Enhancement of measurement signal stability through refined data acquisition and analysis methods
• Expansion of the system to detect a wider range of analytes and operating wavelengths
• Adaptation of the system for field deployment in environmental water quality monitoring applications
• Integration with portable optical detection systems for rapid on-site analysis

Conclusion

This project successfully demonstrates the feasibility of multi-pass optical detection chambers for sensitive analysis of trace substances in aqueous environments. The complete project cycle—encompassing optical modeling, numerical simulation, prototype fabrication, and experimental validation—confirms that the developed system meets design specifications and performs reliably for concentration detection. The work contributes to the broader field of integrated photonic sensors and represents an important step toward practical environmental monitoring applications. The interdisciplinary nature of the project has developed student competencies in optical modeling, CAD design, laboratory measurement techniques, and data analysis, demonstrating the educational value of research-based learning in photonics and sensor engineering.

Acknowledgments: This work was supported by the Research Excellence Initiative—Research University program, Silesian University of Technology

High Contrast Gratings for Highly Transparent and Conductive Mid-Infrared Electrodes

K. WIDAJ [1], T. SMOŁKA[1], M. RYGAŁA[1], W. GŁOWADZKA[2], K. BOGDANOWICZ[2], M. EKIELSKI[3], M. MARCINIAK[2], M. ZADURA[2], P. ŚPIEWAK[2], M. KOWALSKI[4], M. GĘBSKI[2], M. KAŁUŻA[2], O. SADOWSKI[3,5], M. WASIAK[2], A. SZERLING[3], T. CZYSZANOWSKI [2], M. MOTYKA[1]

[1] Wrocław University of Science and Technology, Wybrzeże Wyspiańskiego 27, 50-370 Wrocław, Poland
[2] Photonics Group, Institute of Physics, Łódz University of Technology, ul. Wólczańska 219, 90-924 Łódź, Poland
[3] Łukasiewicz Research Network – Institute of Microelectronics and Photonics, al. Lotników 32/46, 02-668 Warsaw, Poland
[4] Institute of Optoelectronics Military University of Technology Gen. S. Kaliskiego, 00-908 Warsaw, Poland
[5] Warsaw University of Technology – Institute of Microelectronics and Optoelectronics, , Koszykowa 75, 00-662 Warsaw Poland

e-mail address: konrad.widaj@pwr.edu.pl

The design of transparent conductive electrodes (TCEs) for optoelectronic devices is inherently constrained by a fundamental trade-off between high electrical conductivity and optical transmittance, which limits device efficiency. In this work, we report a major advance in TCE technology through the introduction of a novel fabrication strategy that substantially alleviates this trade-off: a monolithic, metal-integrated high-contrast grating, termed metalMHCG (Fig. 1).

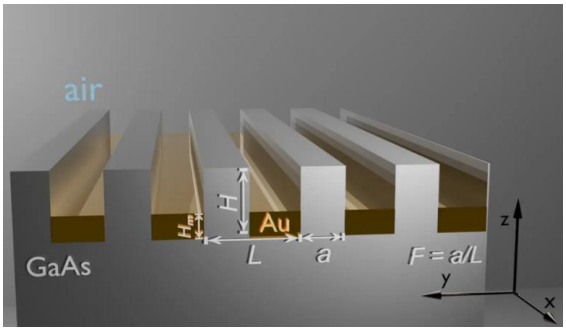

Fig. 1. Cross-section of the metalMHCG configuration with geometrical definitions of the grating parameters [1].

The metalMHCG architecture provides electrical conductivity superior to that of existing TCEs while simultaneously maintaining excellent optical transparency and strong antireflective performance. At a designed wavelength of 10 µm, the proposed metalMHCG achieves a record absolute transmittance of 75% for unpolarized infrared (IR) light, corresponding to a relative transmittance of 108% compared with a bare GaAs substrate. Remarkably, this exceptional optical performance is accompanied by an unprecedentedly low sheet resistance of 0.5 – 1 Ω/sq, several times lower than any previously reported TCE [1].

In addition, a second TCE design comprising gold stripes embedded within a GaAs grating exhibits 94% transmittance at a wavelength of 7 µm and a record high relative transmittance of 135%, while maintaining a low sheet resistance of 2.8 Ω/sq [2].

Together, these metalMHCG-based structures combine outstanding optical and electrical characteristics, establishing a new performance benchmark for mid- to far-infrared (M-FIR) TCEs. This platform holds significant promise for high-power optoelectronic applications, including quantum cascade lasers, infrared detectors, and transparent heaters.

Acknowledgments: We would like to acknowledge financial support from the Swiss Contribution to reducing economic and social disparities in the EU and from the state budget through the National Centre for Research and Development, Call 2024/90/2025, project entitled “Quantum-cascade vertical cavity surface emitting laser for gas sensing” (QCVCSEL).

References:

[1] M. Ekielski et al., Adv. Funct. Mater. 34, 2312392 (2023).
[2] K. Bogdanowicz et. al., Laser & Photonics Reviews, Submitted (2026).

Photocatalytic Properties of Oxide Films Obtained by the Sol–Gel Method

M. ZIĘBA, C. TYSZKIEWICZ, P. KARASIŃSKI

Silesian University of Technology, Department of Optoelectronics, ul. B. Krzywoustego 2 44-100 Gliwice

e-mail address: magdalena.zieba@polsl.pl

Over the past decades, water contamination by organic compounds has attracted significant attention worldwide. However, effective removal of these pollutants remains a challenge despite considerable progress in recent years [1-2].

Semiconductor photocatalysts, such as titanium dioxide (TiO_2), zinc oxide (ZnO), iron oxide (Fe_2O_3), and tungsten oxide (WO_3), offer a promising approach for degrading organic contaminants under UV light. These materials are cost-effective, chemically stable, strong oxidizing, and non-toxic under ambient conditions [1,3,4].

Among them, TiO_2 and ZnO have attracted particular attention owing to their favorable electronic structures, high photocatalytic efficiency, and broad environmental applications. TiO_2 occurs in three crystalline phases: rutile, anatase (both tetragonal), and brookite (orthorhombic) with band gap energies of 3.0 eV, 3.2 eV, and 3.4 eV, respectively. Anatase exhibits the highest photocatalytic activity due to its longer charge-carrier lifetimes and reduced recombination rates [3]. Similarly, ZnO, an *n*-type, water-insoluble semiconductor with a direct wide band gap of 3.37 eV, has attracted considerable interest in photocatalytic applications owing to its high electron mobility, large exciton binding energy (60 meV), excellent piezoelectric and luminescent properties, as well as high thermal, mechanical, and electrochemical stability [4].

Thin films can be prepared using various techniques, including vacuum evaporation, chemical vapor deposition (CVD), physical vapor deposition (PVD), hydrothermal synthesis, and sol–gel method [1,5]. Among these methods, the sol–gel method is particularly attractive due to its high process efficiency, broad tunability of material structure, low equipment requirements, and precise control over film thickness, which make it suitable for both laboratory and industrial applications [6]. The sol–gel method involves two main techniques for sol deposition on substrates: dip-coating and spin-coating [6,7].

In this work, thin films were fabricated by dip-coating. In this technique, a homogeneous liquid film forms on the substrate surface upon withdrawal from the sol solution, and subsequent solvent evaporation yields a thin solid film with controlled thickness and structure [6]. Examples of TiO_2 and ZnO films fabricated using the sol-gel method and the dip-coating technique are shown in Fig. 1.

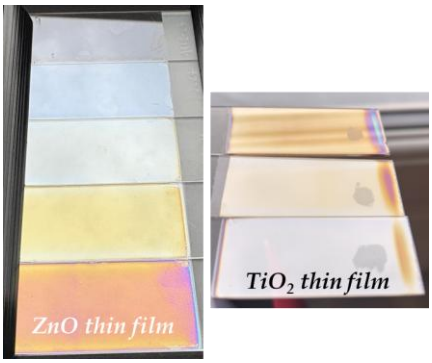

Fig. 1. Examples of TiO_2 and ZnO films fabricated using the sol-gel method and the dip-coating technique.

This work focuses on the fabrication of TiO_2 and ZnO thin films for the degradation of methylene blue under UV irradiation. It provides valuable information on their photocatalytic activity and the optical properties of the fabricated films.

Acknowledgments: This work was partially funded by a grant for young researchers from the Silesian University of Technology BKM-533/RE4/2025.

References:

[1] R.S. Pedanekar, et.al., *Curr. Appl. Phys***.** 20; 8, (2020), 931-952.

[2] N. Ahmadpour, et.al., *J. Water Process Eng.*, 57, (2024), 104597,

[3] A. Al Miad, et.al., *Nanoscale Adv.*, 6, (2024), 4781-4803.

[4] Wojtasik, et.al., *Materials, 16*, (2023),1898.

[5] M.A. Butt, Coatings, 12, (2022), 1115.

[6] M. Zięba, et.al., *Materials*, *14*, (2021)**,** 7125.

[7] E. Bindini, et.al, J. *Phys. Chem. C., 121,* 27, (2017) 14572–14580.

Table of contents

interFOS
światłowód jako ciągły czujnik **pomiarowy**

- Detekcja i lokalizacja wycieku z rurociągów i zbiorników
- Pomiary dla reaktorów i gazyfikatorów
- Monitoring konstrukcji on-line i z alarmem
- Ochrona perymetryczna obiektów i instalacji
- Badanie obciążalności kabli energetycznych
- Pomiary drgań maszyn z elementami wirującymi
- Wykrywanie i monitorowanie mikropęknięć
- Określanie cyklu życia elementów

INTERLAB®

www.INTERLAB.pl ■ TEL.: (+48) 22 840 81 80

OptaSense® LUNA DEFYING IMPOSSIBLE. LIOS TECHNOLOGY MICRON OPTICS

MONO SPEKTRA

Monospektra is a dedicated supplier of scientific equipment and industrial solutions in the Baltic states and Poland. We are supplier of Edmund Optics and an exclusive distributor of Attolight, Edmund Optics, Lightsource.tech, Ocean Optics and Physik Instrumente (PI) products in Poland.

Our Partners:

attolight™ Edmund optics | worldwide FEMTUM

lightsource.tech OceanOptics PI

UAB Monospektra

Tel. No.: +370 5 2196359
E-mail: sales@monospektra.com
Web: www.monospektra.com